FERRATE(VI), FERRATE(V), AND FERRATE(IV) OXIDATION OF MICROCYSTIN-LR, FLUMEQUINE, AND SULFADIAZINE: OXIDIZED PRODUCTS

A Thesis

by

LONG CHEN

Submitted to the Office of Graduate and Professional Studies of
Texas A&M University
in partial fulfillment of the requirements for the degree of

DOCTOR OF PUBLIC HEALTH

Chair of Committee,	Virender K. Sharma
Committee Members,	Leslie Cizmas
	Natalie Johnson
	Hongwei Zhao
Head of Department,	Mark Benden

May 2017

Major Subject: Epidemiology and Environmental Health

ABSTRACT

Microcystin (MC-LR) is a potent toxin and its presence in drinking water create a serious risk to human health. This paper presents the degradation of MC-LR in water by iron-based molecules, ferrates ($Fe^{VI}O_4^{2-}$, $Fe^{V}O_4^{3-}$, and $Fe^{IV}O_4^{4-}$) at pH 7.0. The oxidized products (OPs) were analyzed at various concentrations of ferrate species. Product studies showed the fragmentation of the cyclic MC-LR by all ferrates, which varied with the concentration and the oxidation state of ferrates. Three predominant degradation pathways are proposed, involving hydroxylation and breakage of peptide bond of MC-LR. The extent of hydroxylation of MC-LR by Fe^{VI} was more than by Fe^{V} and Fe^{IV}. Fe^{VI} oxidation has potential to generate OPs with low molecular weight. Additionally, three pH (4.0, 7.0 and 9.0) were investigated to learn their on three pathways of MC-LR by Fe^{VI}, Fe^{V}, and Fe^{IV}. Analysis of peak areas of OPs showed that acidic conditions greatly facilitated the hydroxylation by three ferrates compared with the neutral and basic pH.

Antibiotics have recently attracted increasing concern worldwide due to their ubiquitous occurrence and negative ecological effects on aquatic organisms. This paper investigated the oxidation kinetics and mechanisms of sulfadiazine (SDZ), a representative sulfonamide, by Fe^{VI}. The results showed that the reaction followed the second-order kinetics, and the rate constants decreased with the increasing pH from 4.0 to 10.0. Eleven OPs of SDZ were identified, and three initial pathways were proposed, including SO_2 extrusion, deamination, and hydroxylation, of which the involvement of SO_2 extrusion was first demonstrated during Fe^{VI} oxidation of SDZ.

In addition, the removal of flumequine (FLU), a representative fluoroquinolone antibiotic, by Fe^{VI}, Fe^{V}, and Fe^{IV} species and the effect of ammonia were studied. The results indicated that Fe^{VI} exhibited a higher capability for the elimination of FLU than Fe^{V} and Fe^{IV}. Furthermore, the presence of ammonia enhanced the removal efficiency of FLU by Fe^{VI} and Fe^{V}. The reason was proposed to be the formation of higher reactive Fe^{VI}-ammonia and Fe^{V}-ammonia complexes than un-complexed ferrate species. Mechanical analysis indicated that these complexes reacted faster at the double bond moiety of the quinolone ring of FLU.

DEDICATION

I dedicate my dissertation research to my parents, Zhen Chen and Teng Huang who emotionally and financially supported me throughout my academic endeavors. A special my uncle, Hui Chen and aunt, Juan Kang. I truly appreciate my grandmother, Xiuzhen Zhang, who supported me to excel in education and guided me to be a nice human being.

A great appreciation to Puja for giving me homely environment in the United States throughout my education, first in Florida and then in Texas.

I am very grateful for the support of all of the mentioned individuals. Without their support, this dissertation would not have been possible.

ACKNOWLEDGMENTS

I would like to extend thanks to my committee chair, Dr. Virender Sharma, for his support, encouragement, and guidance throughout my DrPH work. Dr. Sharma provided me a great opportunity to develop my skills in research on the topic of environmental chemistry and health. I sincerely thank my committee members, Dr. Leslie Cizmas, Dr. Natalie Johnson, and Dr. Hongwei Zhao, for their guidance and support throughout my pursuance to obtain my degree.

I also thank my many friends who have guided me throughout this program. Special thanks and gratitude go to Dr. Mingbao Feng. Technical and analytical help from Dr. Piero R. Gardinali, Dr. Kevin E. O'Shea, and Dr. Dionysios D. Dionysiou are greatly appreciated.

CONTRIBUTORS AND FUNDING SOURCES

Contributors

This work was supported by a thesis committee consisting of Professor Virender Sharma (advisor and chair), Professor Leslie Cizmas, Professor Natalie Johnson of the Department of Environmental and Occupational Health, and Professor Hongwei Zhao of the Department of Epidemiology and Biostatistics.

The analyzation of samples for Chapter two and Chapter three was supported by Professor Piero R. Gardinali (Florida International University), Professor Kevin E. O'Shea (Florida International University) and Professor Dionysios D. Dionysiou (University of Cincinnati). The data analysis in Chapter four and Chapter five was supported by Dr. Mingbao Feng.

All other work conducted for the thesis was completed by the student independently.

Funding Sources

This ferrate project was supported by the National Science Foundation (NSF – CBET 1439314).

TABLE OF CONTENTS

Page

LIST OF FIGURES

Page

LIST OF TABLES

Page

1. INTRODUCTION

1.1. Micropollutants in the water environment

During the past few decades, the research focus in the environmental field has been partly transferred from the traditional persistent and priority pollutants such as polychlorinated biphenyls and polycyclic aromatic hydrocarbons to the emerging micro-contaminants (Carraro, et al., 2016; Hu, et al., 2017). Among them, pharmaceutical residues, personal care products, and endocrine disrupting chemicals are the most important classes. Additionally, some hepatotoxic, cytotoxic, and/or neurotoxic cyanotoxins, released by cyanobacteria blooms, have also emerged as a significant concern to public health and the environment. These micropollutants are frequently detected in water and wastewater at concentrations ranging from ng/L to μg/L. These contaminants pose adverse ecological and human health effects (Jiang, et al., 2013; Luo, et al., 2014). Notably, some of them have been identified as persistent or pseudo-persistent contaminants of concern due to their continuous release into the environment and to their bioaccumulative potential in aquatic species (Li, 2014; Ruhi, et al., 2016). Therefore, searching for effective treatments to remove these contaminants has attracted increasing attention worldwide. In this thesis, mitigation of the most well-known cyanotoxin, named microcystin-LR (MC-LR), and two representative antibiotics, i.e., sulfadiazine (SDZ) and flumequine (FLU), in water was sought.

Chlorination, chloramination, and ozonation methods have been widely utilized to eliminate emerging pollutants during conventional water and wastewater treatments (Luo, et al., 2014; Postigo and Richardson, 2014). However, these processes can produce

disinfection byproducts, which can pose adverse effects on the public health. More recently, iron-based oxidants, namely ferrates, have garnered considerable attention owing to their high redox potential and subsequent coagulation/precipitation property as ferric hydroxide (Sharma, et al., 2015, 2016a). Ferrates are also superior to the aforementioned traditional technologies in that they have powerful disinfection properties to inactivate a wide range of bacteria and viruses. Additionally, the removal of natural organic matter or disinfection byproduct precursors and heavy metals using ferrates can also be achieved (Sharma et al., 2015, 2016a). The basic properties of ferrates and their effectiveness to treat a wide range of pollutants are given in the next section.

1.2. Chemistry and application of ferrates

Iron, which is one of the most common elements in the earth's crust, performs very important roles in many fields ranging from biological oxidation processes to industrial production. Iron has a wide range of oxidation states, ranging from −2 to +6. In low oxidation states, such as +2 and +3, iron as a catalyst can catalyze iron-centered reactions including hydroxylation, hydrogenation, additions to carboxylic substrates, and nucleophilic substitutions (Sharma, et al., 2015, 2016a). High oxidation states of iron are believed to participate in the biological oxidation process in living organisms. In recently years, several studies have been performed to study the mechanisms of a couple of different nonheme and heme enzymes, including cytochrome P450 and chloroperoxidase (Prat et al., 2011). The results indicated that high-valent iron species, Fe(V) and Fe(IV), were involved in the catalytic process by facilitating the oxidation reaction of

hydrocarbons. Based on this research, it is believed that the oxidation reactivity of high-valent iron compounds is determined by the structures of the ligands and the oxidation states of the iron centers. These high oxidation states of irons can also be involved in others reactions, such as cyclization, decarboxylation, and epoxidation reactions. (Sharma et al., 2015).

In the last few years, research on high-valent tetraoxy iron species, which are commonly called ferrates ($Fe^{VI}O_4^{2-}$, Fe^{VI}; $Fe^{V}O_4^{3-}$, Fe^{V}; and $Fe^{IV}O_4^{4-}$, Fe^{IV}) in an aqueous environment, has been explored for a wide range of applications in waste remediation, energy materials, and green organic synthesis. For example, Fe^{VI} is suggested as a greener oxidant agent in the synthetic organic chemistry due to its capability of hydrocarbon bond activation and selectivity. Thus, hydrocarbons can be hydroxylated and alcohols can be transformed to ketone by means of a high-valent state of iron species (Sharma, 2002b). $Fe^{VI}O_4^{2-}$ has been used in the decomposing of pharmaceuticals and personal care products (PPCPs) and endocrine disrupting chemicals (EDCs) in surface water (Karlesa, et al., 2014; Lee, et al., 2005; Lee, et al., 2009; Yang, et al., 2012; Yang, et al., 2014; Yang, et al., 2016). Applications of Fe^{VI} in degrading organosulfur compounds, amines, phenols, carboxylic acids, alcohols, carbohydrates and sucralose, ascorbate, hydrocarbons, and DNA and its constituents, biological species has also been demonstrated (Carr, 2008; Lee, et al., 2004; Noorhasan, et al., 2008; Sharma, 2013; Sharma, et al., 2013, 2016a).

In the water and waste water treatment field, only $Fe^{VI}O_4^{2-}$ was widely studied, while for $Fe^{V}O_4^{3-}$, and $Fe^{IV}O_4^{4-}$, only a handful of studies are available due to their short

lives in aqueous solutions. $Fe^{VI}O_4^{2-}$ is a promising water and wastewater treatment reagent. Although it has not been applied in water treatment plants due to its lower stability in aqueous solution/form and higher cost when compared with permanganate and chlorine, its application prospects are also promising. In the following sections, basic characterization and properties of ferrates are summarized.

Mössbauer spectroscopy, which is known as nuclear gamma resonance spectroscopy, is a versatile technique based on the Mössbauer effect (Kopelev, 1997). The Mössbauer effect, which was first described by Mössbauer in 1958, involves the occurrence of recoilless nuclear resonance absorption, and the emission of gamma-radiation in a solid phase. This finding resulted in the development of the capability of Mössbauer spectroscopy to characterize a nucleus with chemical and environmental changes. This technique can be used in several different fields, such as chemistry and physics, to provide accurate information about material properties (Sharma, et al., 2015; Sharma and Zboril, 2015).

One of the very useful applications of Mössbauer spectroscopy is based on the fact that it can readily recognize different oxidation states of iron in compounds of ferrates species ($Fe^{VI}O_4^{2-}$, $Fe^{V}O_4^{3-}$, and $Fe^{IV}O_4^{4-}$) in their solid phases, based on the value of the isomer shift. Fig. 1.1 shows the Mössbauer spectroscopy measurements of ferrates. When oxidation states of iron increase, the values of the isomer shift decrease. The area of blue color represents a Mössbauer spectrum of Fe^{VI}, where the value of the isomer shift is -0.90 mm/s; the yellow color area is a Mössbauer spectrum of Fe^{V}, where the isomer shift of Fe (V) is -0.54 mm/s; the pink color area is a Mössbauer spectrum of

Fe^{IV}, and its isomer shift is -0.22 mm/s.

Ultraviolet-visible spectroscopy is a widely used method of identifying different analytes in chemical research. Aquatic analytes, such as transition metal ions in solution, can be identified based on the maximum absorption of ultraviolet-visible light spectroscopy. The quantity of analytes can also be determined based on the Beer-Lamber law. The concentration of the analyte in the solution is directly proportional to the absorbance of the solution. Fig. 1.2 shows the spectra of Fe^{VI}, Fe^{V}, and Fe^{IV} in visible regions. A red line represents the spectra of Fe^{VI}, which has a maximum absorbance at 510 nm; A green line represents the spectra of Fe^{V} with a maximum absorbance at 380 nm. A blue line represents the spectra of Fe^{IV}, which has a maximum absorbance at 430 nm.

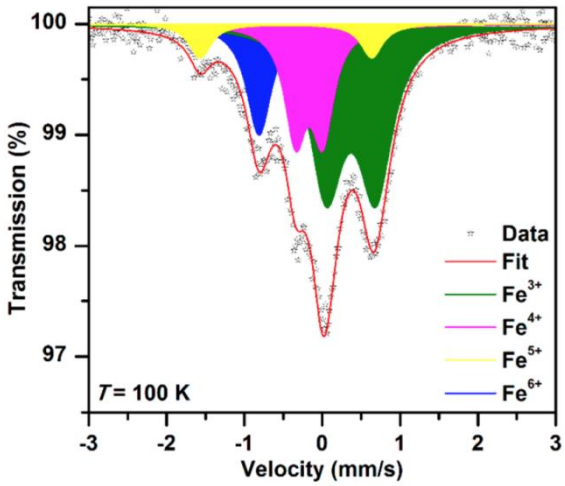

Fig. 1.1. Mossbauer spectroscopy measurement of iron in different oxidation states of iron. Reprinted from Sharma et al. (2015)

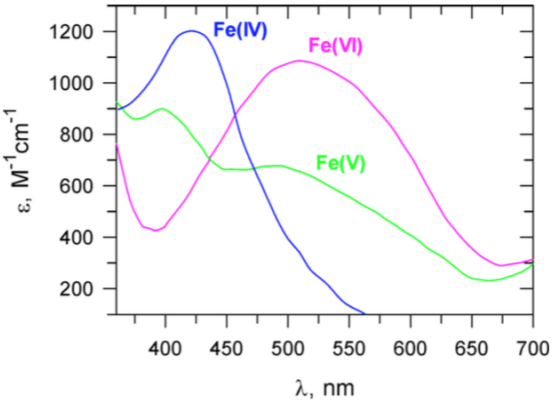

Fig. 1.2. Visible spectroscopy measurements of ferrate species in aqueous solution. Reprinted from Rush and Bielski (1986).

Acid-base equilibrium of Fe^{VI} and Fe^{V} species are represented by Eqs. 1.1-1.6.

$H_3Fe^{VI}O_4^+ \rightleftharpoons H^+ + H_2Fe^{VI}O_4$ $pK_{a1} = 1.6 \pm 0.2$ (Cavazza, et al., 2010) (1.1)

$H_2Fe^{VI}O_4 \rightleftharpoons H^+ + HFe^{VI}O_4^-$ $pK_{a2} = 3.5$ (Bernasconi, et al., 2007) (1.2)

$HFe^{VI}O_4^- \rightleftharpoons H^+ + Fe^{VI}O_4^{2-}$ $pK_{a3} = 7.3 \pm 0.1$ (Chanda, et al., 2006) (1.3)

$H_3Fe^{V}O_4 \rightleftharpoons H^+ + H_2Fe^{V}O_4^-$ $5.5 \leq pK_{a1} \geq 6.5$ (Cataldo, et al., 2011) (1.4)

$H_2Fe^{V}O_4^- \rightleftharpoons H^+ + HFe^{V}O_4^{2-}$ $pKa_2 \approx 7.2$ (Cataldo, et al., 2011) (1.5)

$HFe^{V}O_4^{2-} \rightleftharpoons H^+ + Fe^{V}O_4^{3-}$ $pKa_3 = 10.1$ (Rush and Bielski, 1989) (1.6)

In the pH range from alkaline to acidic conditions, Fe^{VI} has four different species, including deprotonated, monoprotonated, diprotonated, and triprotonated species, as well as Fe^{V}. The values of pK_a have been applied to evaluate the speciation of the ferrate species (Fig. 1.3). Fig. 1.3 suggests a right shift of ~ 3 - 4 pH units in the speciation of ferrate species when the oxidation state of iron changes from +6 to +5. The fraction of speciation of the ferrate species in different pH conditions can be determined based on the p*K*a values. In a basic condition, Fe^{VI} has two major species (and), and

Fe^{V} has three major species. The p*K*a values of each Fe^{VI} species are lower than the counterpart p*K*a values of each Fe(V) species, which means that the proton releases of protonated Fe^{V} species are more difficult than the proton releases of protonated Fe^{VI} species.

The redox potentials of $Fe^{VI}O_4^{2-}$, $Fe^{V}O_4^{3-}$, and $Fe^{IV}O_4^{4-}$ have been suggested to be pH dependent (Sharma, 2013). Fe^{VI} shows a high oxidation potential in acidic conditions compared to its oxidation potential in basic conditions. The redox potential of Fe(VI) in an acidic condition and in a basic condition are 2.20 and 0.70, respectively (Wood, 1958). At an acidic pH, the redox potential of $Fe^{VI}O_4^{2-}$ is the highest one among hypochlorite, chlorine dioxide, ozone, and permanganate. Under basic conditions, the redox potential order is as follows: ozone > chlorine dioxide > hypochlorite > Fe(VI) > permanganate. The Fe^{III} end product of $Fe^{VI}O_4^{2-}$ can also been used as a coagulant for further removal of organics, metals, and bacteria in water. $Fe^{VI}O_4^{2-}$ has been reported as an effective oxidant for persistent compounds, micropollutants, bacteria, viruses, heavy metals, and arsenic in water (Sharma, et al., 2015, 2016a). The focus of the present research is on the oxidation of microcystin-LR (MC-LR), sulfadiazine (SDZ), and flumequine (FLU). The sections below discuss human and health aspects of these micropolutants.

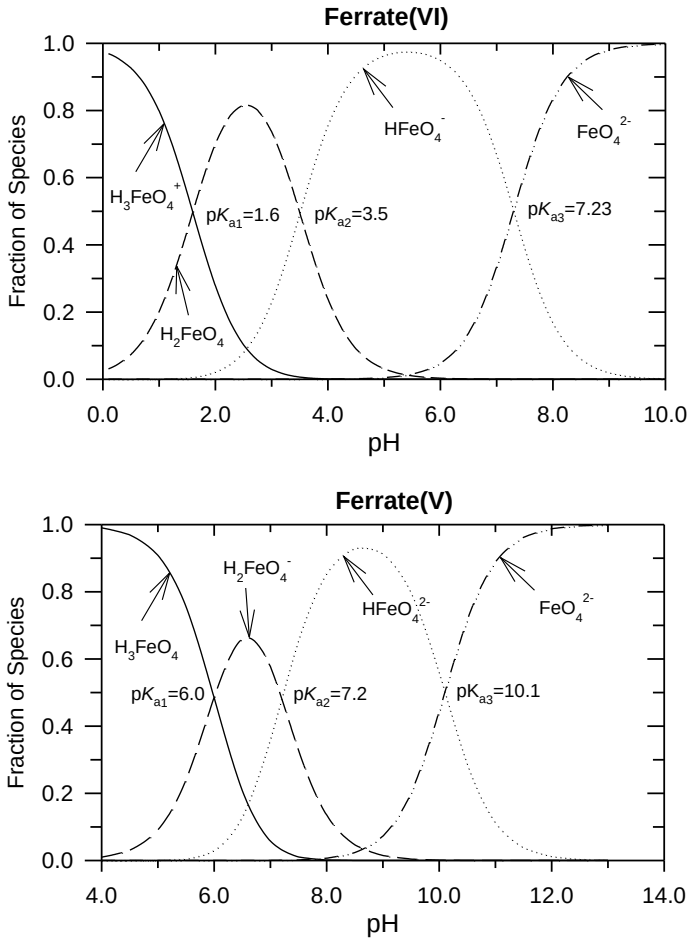

Fig. 1.3. Speciation of Fe^{VI} and Fe^{V}. Reprinted from Sharma (2013).

1.3. Microcystin-LR

The molecular structure of MC-LR contains three D-amino acids, alanine (Ala), methyl aspartic acid (MeAsp), and glutamic acid (Glu); two unusual amino acids (3-amino-9-methoxy-2,6,8-trimethyl-10-phenyldeca-4,6-dienoicacid (Adda), and N-methyldehydroalanine (Mdha); and two L-amino acids (leucine, Leu and arginine, Arg) (Fig. 1.4). Below is a description of the potential effects of MC-LR on public and ecological health.

1.3.1. Metabolism of microcystin-LR in humans

Microcystin-LR is one of the most frequently detected cyanotoxins in the world. It is a tumor promoter and is hepatotoxic. Pathways of the metabolism of MC-LR in humans are shown in Fig. 1.5. Microcystin-LR may be metabolized via a glutathione conjugation pathway (Šetlíková and Wiegand, 2009). This conjugation of glutathione with microcystin-LR can be performed by catalysis of glutathione-S-transferases in rats (Takenaka, 2001). It has been confirmed that human glutathione-S-transferases, such as T1-1, P1-1, and M1-1, can also catalyze this conjugation reaction to form a glutathione adduct and is called a microcystin-LR-glutathione conjugation (Buratti, et al., 2011). The conjugation reaction of glutathione with microcystin-LR starts with the nucleophilic reaction of the sulfur of the glutathione to the carbon double bond of the Mdha moiety of microcystin-LR; a glutathione and cysteine adduct has been reported in mice (Kondo, et al., 1992).

Initially, microcystin-LR is metabolized by a conjugation reaction of the double bond on the Mdha moiety of microcystin-LR to glutathione, and which results in a glutathione conjugate of microcystin-LR. Glutathione-S-transferase is involved in this reaction. Then, the microcystin-LR-cysteine-glycine conjugate is formed when the glutamic acid group of the microcystin-LR-cysteine-glycine conjugate is eliminated by glutamyltransferase. The microcystin-LR-cysteine conjugate is then formed after the removal of the glycine group of the microcystin-LR-cysteine-glucine conjugate. Finally, the microcystin-LR-mercapturic acid conjugate is produced by the oxidation of the microcystin-LR-cysteine conjugate by acetyl tranferase (Schmidt, et al., 2014).

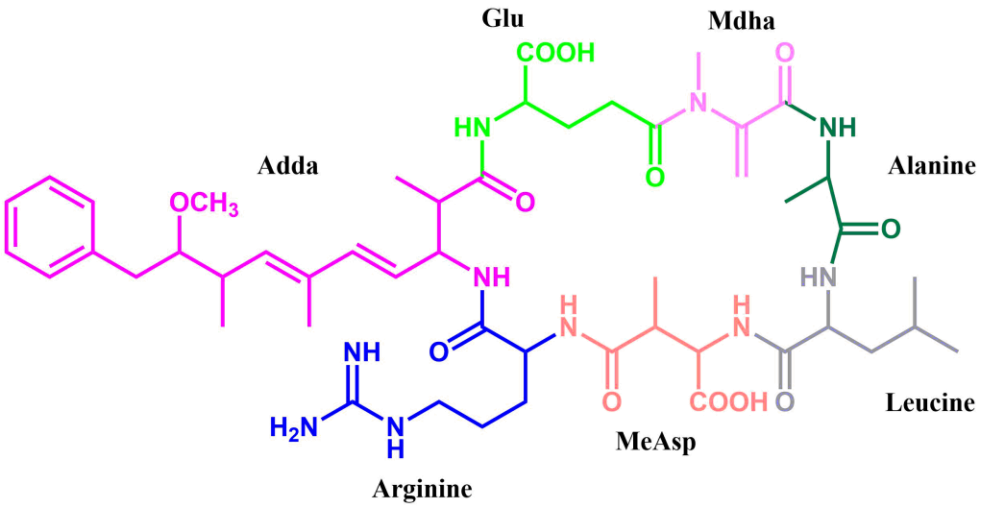

Fig. 1.4. Molecular structure of microcystin-LR.

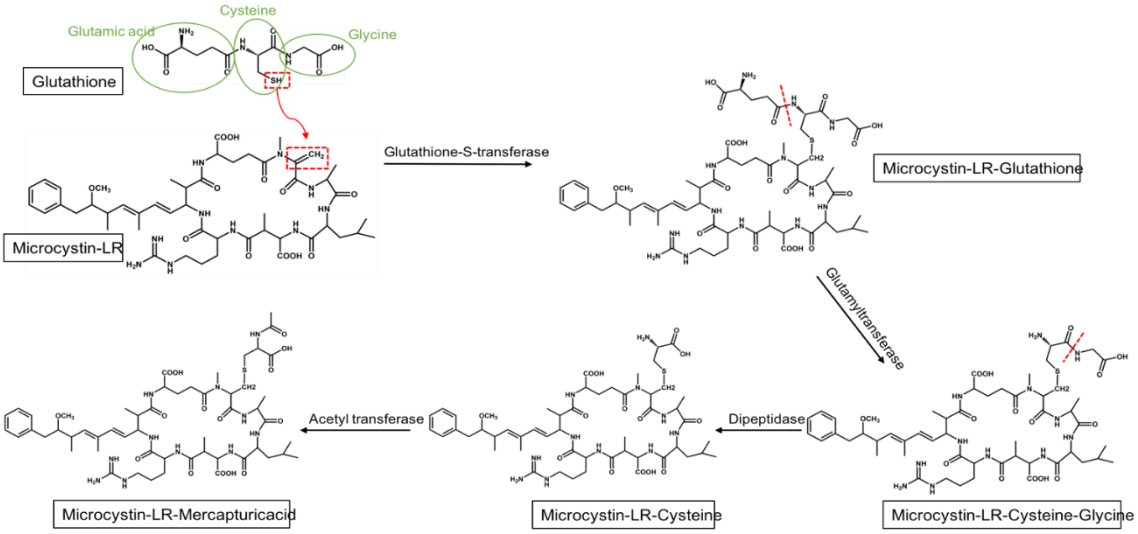

Fig. 1.5. The figure above shows the metabolism of microcystin-LR via the glutathione pathway in humans. Reprinted from Schmidt et al. (2014).

1.3.2. Mechanism of microcystin-LR toxicity

Microcystins can cause inhibition of a class of enzymes called protein phosphatases (PP1 and PP2A) (Craig, et al., 1996). This type of inhibition, which leads to the build-up of phosphorylated proteins, is regarded as a mechanism by which

microcystins devastate livers. Fig. 1.6 shows a surface structure of PP1 (Goldberg, et al., 1995). MC-LR binds to protein phosphatases such as PP-1c by way of interactions at three locations of the enzyme, including the C-terminal groove, the hydrophobic groove, and the catalytic location (Goldberg, et al., 1995).

Interactions at the catalytic site: MC-LR combines indirectly with the two catalytic metal atoms by means of two water molecules across the carboxyl group of the glutamic acid and the adjacent carbonyl oxygen of the toxin (Goldberg, et al., 1995). The carboxyl group of the glutamic acid of microcystin is imperatively compulsory for toxicity by the peptide inhibitor in cycles. Moreover, since the carboxyl group of the Masp of MC-LR has interplay with Arg-96 and Tyr-134 of PP- 1 (Fig. 1.7), in consequence, MC-LR totally obstructs entry into the active center of the enzyme PP-1 (Dawson and Holmes, 1999).

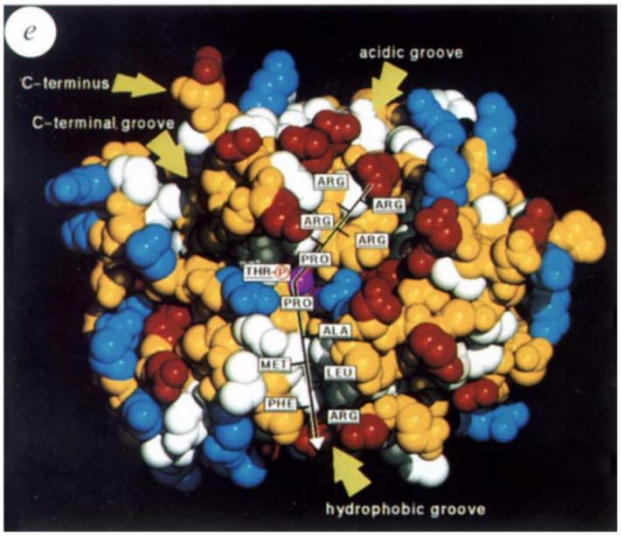

Fig. 1.6. The surface of enzyme PP-1. Reprinted from Goldberg et al. (1995).

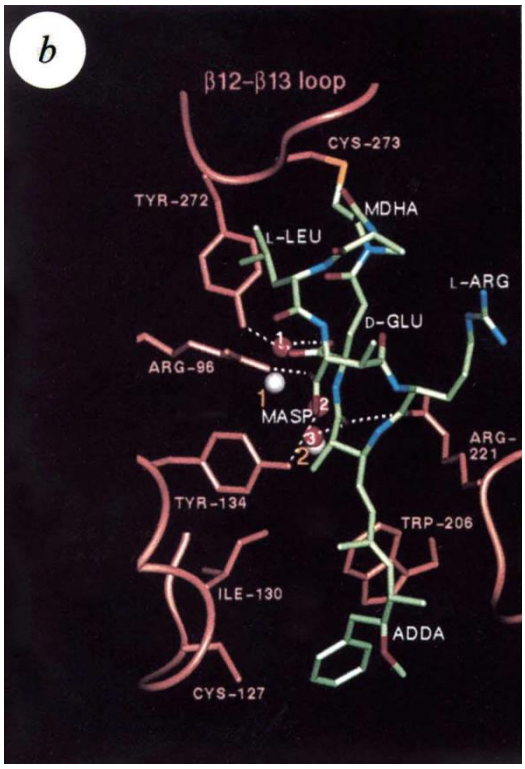

Fig. 1.7. Stereo view of microcystin-LR at the active site of PP-1. Reprinted from Goldberg et al. (1995).

Interactions at the C-terminal groove: It is demonstrated that MC-LR interactions with the C- terminal groove of the PP-1 enzyme occur when this toxin inhibits PP-1. The crystal structure illustrates that Tyr-272 remains close to the leucine of MC-LR. That accounts for biochemical evidence that PP-1c sensitivity to MC-LR is on the decrease during the mutation of Tyr-272, particularly during the replacement of the aromatic moiety of Tyr-272 (Goldberg, et al., 1995). The covalent connection between the Mdha side chain of the toxin and Cys-273 of PP-1 was also noticed in the structure of the crystal. The terminal carbon atom of the Mdha connected with the S atom of Cys 273 and then produced a covalent linkage (Dawson and Holmes, 1999).

Interactions at the hydrophobic groove: The Adda chain of MC-LR packs into the hydrophobic groove. The package of the Adda group to the PP-1 hydrophobic groove remains fairly close, implying that a considerable part of the binding potential for the toxin is obtained from hydrophobic interactions in the area (Dawson and Holmes, 1999). The result of adjustments in the Adda side chain has indicated that the whole form of the Adda chain is critical to the microcystin interaction. Geometrical isomers of microcystins, in which the diene double-bond on the Adda chain is altered from an expanded *trans* E configuration to the *cis* Z configuration, had reduced toxicity to a large extent. The toxicity might have been reduced when the diene double-bond on the Adda chain of the MC-LR was altered from a *trans* E configuration to the *cis* Z configuration. The toxicity test confirmed that the toxicity in IC50 of the toxins reduced 100-fold (Nishiwaki-Matsushima, et al., 1991).

Other microcystin species, such as microcystins-LA, microcystin-RR and microcystin-YR, have the same toxicity mechanism in that they can inhibit the same phosphatases and result in histological changes in rodent livers (Dawson and Holmes, 1999), with a mechanism similar to that of microcystin-LR. This mechanism proves that microcystin serves as an inhibitor of the activity of PP1 by obstructing substrate binding to the active center of the enzyme in a direct manner.

1.3.3. Microcystin at the level of the cell

Microcystin attaches exclusively to the protein phosphatases such as PP1 and PP2A, blocking them and resulting in a cluster of events triggering cell death (Fig. 1.8) (Valério, et al., 2010). By the blockage of PP1 and PP2A, microcystin seemingly keeps

some cellular processes under control. Microcystin can activate CaMKII, the calcium-calmodulin-dependent multifunctional protein kinase II, which may lead to ROS formation; Nek2 kinase, which takes part in the constraint of mitotic progression and chromosome segregation, can be activated by microcystin. This type of interplay can lead to cellular viability and tumorous growth; microcystin may regulate the expression of mitogen-activated protein kinases' (MAPKs) via the inhibition of PP-2A. MAPKs regulate several cellular activities, including proliferation and cell apoptosis (Valério, et al., 2010).

Moreover, the nuclear phosphoprotein P53 increases after microcystin exposure. P53 regulates the expression of the pro- and anti-apoptotic genes inclusive of Bax and Bid that are members of the Bcl-2 family. Bax and Bid play a pivotal role in the process of apoptosis, particularly in the mitochondria-dependent pathway. Research reveal that microcystin-LR makes P53 active by the blockage of PP2A, leading to a disequilibrium in the ratio of pro/anti-apoptotic members of the Bcl-2 family, giving rise to a pore opening through mitochondrial permeability and the discharge of apoptotic proteins into the cytosol, provoking caspase cascade activation and, in the end, apoptosis. The mitochondrial pathway is viewed as an essential pathway in MC-LR-induced apoptosis.

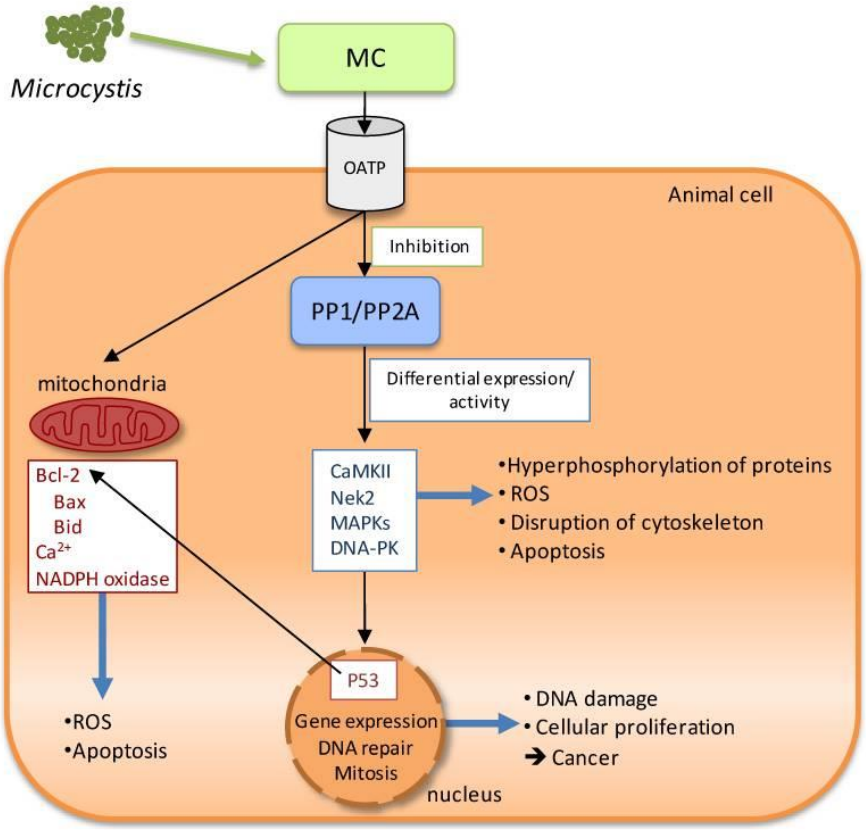

Fig. 1.8. The mechanisms of microcystins toxicity in cell. Reprinted from Valério et al. (2010).

1.3.4. Microcystin in the body at the organ level

Most oral and injection studies in laboratory animals have shown that the liver is a primary target organ for microcystin toxicity. Based on the results of these studies, death might occur as soon as a few hours after the injection of microcystins (Woolbright, et al., 2017). A large proportion of the understanding regarding the toxicity of microcystins is founded upon research with mice and rats which were given intra-peritoneal (IP) injections of MC-LR; that is to say, injections were administered into the abdominal cavity in a direct manner (Meneely and Elliott, 2013).

Manifestations of liver damage at early stages consist of an increase of liver enzymes in the serum, a sign that is symbolic of liver cell death, as well as extra liver weight due to intrahepatic hemodynamic shock (Chen, et al., 2016; Hu, et al., 2016). Then it leads to heart failure and death. Liver damage and cell death are likely to be watched microscopically 20 minutes after giving an injection containing a lethal dose of MC-LR. In sixty minutes, hepatocytes come to an end, their linkage to one another falls apart, and the normal architecture of the liver is shattered.

The main toxicity mechanism of microcystins is to block a type of enzyme referred to as a protein phosphatase. The function of these enzymes is to regulate the phosphorylation process, which results in the removal of phosphate from a protein (Máthé, et al., 2016). This inhibition of protein phosphatases by microcystins is believed to be the main mechanism of liver damage. Hepatocytes derived from animals which are treated with microcystins seem to draw to a close by cell suicide or a process of programmed cell death that is known as apoptosis. Cells which go through apoptosis vanish in a characteristic fashion, consuming their own cellular organelles. Other microcystin species, such as microcystins-LA, microcystin-RR and microcystin-YR, have the same toxicity mechanism in that they can block the same phosphatases and result in alterations related to histology in rodent liver, which is similar to the mechanism of microcystin-LR.

1.3.5 Public health impact of microcystin on humans

The cyanotoxins known as microcystins have brought about human intoxication events across the globe. The reported issues regarding health are most possibly

associated with microcystin exposure in long-term and low level concentrations due to the use of polluted food (agricultural products, and freshwater fish) and water (river, ponds and lakes), exposure through the skin, and breathing. In human beings, the most affected organ is the liver; other tissues and organs, such as kidneys and colon, can also be affected by exposure to the toxin (Fig. 1.9) (Rastogi, et al., 2014). In consequence, the health effects resulting from microcystin intoxication are liver and gastroenteritis illness (Zanchett and Oliveira-Filho, 2013).

Exposure to cyanobacterial toxins by using polluted drinking water has led to significant cases of poisoning in human beings, even causing deaths. As a result, in 1997 the World Health Organization set a temporary reference value of 1 μg/L for MC-LR in drinking water (Hudder, et al., 2007; Sharma, et al., 2012). Apart from the mouth, there also exists the likelihood of the parenteral route of exposure, when surface water full of cyanobacteria, utilized for the purpose of hemodialysis, enters the blood and consequently threatens patients' lives. The first authenticated occurrence of human poisoning related to cyanotoxins came to pass in Caruaru, Brazil in 1996, when patients who received renal dialysis treatment in a routine manner started to complain of vomiting, blurred vision, eye pain, headache, and other symptoms. Because of the use of water polluted by cyanotoxins (Freitas de Magalhães, et al., 2001), 76 patients succumbed to liver complications. An analysis was conducted, and it proved that in the clinic's water purification system, microcystins existed in activated carbon. In patients' liver and blood, microcystins were discovered. There are many other cases which have been publicized about human intoxication because of the dissolution of cyanotoxins in

water. An additional episode took place in Brazil, in which intoxication was ascribed to blooms from Microcystis and Anabaena species, and there were identified 88 deaths and 2000 confirmed cases of gastroenteritis within just 42 days (Ferrão-Filho and Kozlowsky-Suzuki, 2011; Rastogi, et al., 2014).

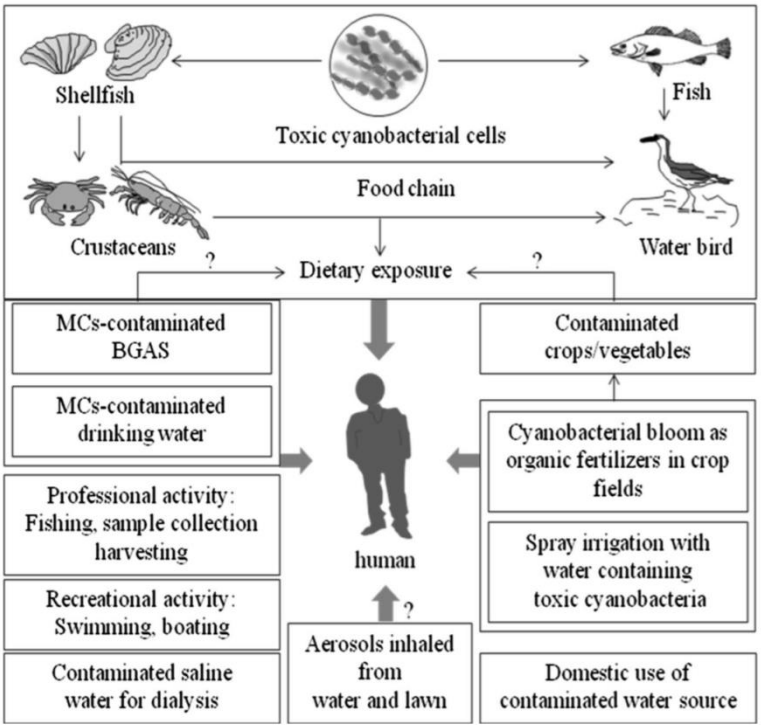

Fig. 1.9. Health concerns of microcystin and ecology. Reprinted from Rastogi et al. (2014).

However, in addition to possible human contamination by way of the water supply, it is also possible for contamination to occur through the food chain. In quite a few studies the bioaccumulation of cyanotoxins and their transfer via the food web has been authenticated. It is likely that these toxins affect human beings following their

consumption of aquatic food, such as fish. Some fish, such as carp and tilapia, are likely to consume cyanobacterial cells containing toxins in water, thereby gathering them in the muscles, liver, kidney, and viscera.

Besides the acute health impact brought about by cyanotoxins, long-time exposure to low doses of cyanotoxins is likely to result in the development of cancer and in human beings. Cancer is viewed as a predominant public health issue all over the world and is deemed the chief cause~~s~~ of mortality globally. The death rate is increasing with alterations in lifestyle and nutrition and with the worsening of global warming. It was estimated by the American Cancer Society that there were 7.6 million people who lost their lives to cancer the world over in 2007. The announcement that hepatotoxins produced by cyanobacteria lead to the inhibition of protein phosphatase has intimated alarmingly that human exposure to non-lethal doses of these toxins is likely to function as a contributor to the development of cancer. In the past few months, the International Agency for Research on Cancer (IARC) has registered microcystin-LR as a possible carcinogen for human beings (Group 2B).

In epidemiological investigations, an association has been established between the increased incidence of cancer and drinking water sources that are possibly polluted with microcystins in parts of China, where the rate of human hepatocellular carcinoma is one of the highest across the globe and differs from region to region. It has been observed that the highest cancer mortality rates are in areas where drinking water comes from ponds and ditches, in comparison with lower incidence in areas where drinking water issues from deep wells.

1.3.6. Public health impact of microcystin on ecological systems

Cyanobacteria and their poison can affect various species ranging from plants, algae and bacteria to more complex life forms, and their influence on aquatic invertebrates, especially zooplankton, have drawn particular attention. The zooplankton society structure can be affected by cyanotoxins, in particular when their food phytoplankton is dominated by cyanobacteria.

In the meantime, scientists also observed the untoward influences of the intake of microcystins by hydrobios. Experts have studied the intestinal absorption and influence of ingestion of microcystins of *Daphnia galeata. Daphnia* was placed in microcystins and its movements, intestine structure, microcystin density in blood, and external form were observed periodically (Herrera, et al., 2015). This observation has shown that the intake of microcystins led to fatal poisoning, so that a 1 mg weight of *Daphnia galeata,* which absorbed from 10.2 to 18.3 ng of microcystin, would die instantly.

Also, researchers investigated the influence of microcystins on *Daphnia magna*, which verified the fact that when injected into a high level of microcystins and exposed for, *Daphnia magna* would suffer fatal consequences, since microcystins started to accrue and restrain the enzyme phosphatase in the course of lasting exposure; on the contrary, it was noted that only low doses of microcystins cannot induce any toxic consequence (Ger, et al., 2014).

In addition, some other species such as cyanobacteria, daphnids, algae, plants, and diatoms as well as can also be influenced by cyanotoxins (Backer, et al., 2015). When exposed to MC-LR, photosynthesis and growing can be restrained in the

Anabaena and cyanobacteria *Nostoc muscorum.* The sub-aquatic plant, *Ceratophyllum demersum,* is also influenced by microcystin-LR, performing so that when infected ~~into~~ with 1.0 μg L^{-1} of microcystin-LR for 6 weeks, its growth would slow down, and a density of 5 μg L^{-1} of MC-LR can lead to the same marked shrinkage in growth after only 3 weeks (Romero-Oliva, et al., 2015; Szigeti, et al., 2010). Mollusks can also be influenced by cyanotoxins. It has been reported that exposure to microcystin-LR might result in a modest accumulation within the tissues of the gastropod pulmonate *Lymnaea stagnalis* (Lance, et al., 2010).

In addition to the influence of cyanobacteria on aquatic invertebrates, fish will be also injured by cyanobacteria, which can be supported by a histopathological study of deceased fish in cyanobacterial flowers (Botana, 2016; Zanchett and Oliveira-Filho, 2013). This pointed to the injury by cyanobacteria to the liver, alimentary canal, and gills as possibly the chief reason for fish death. Another possibility is that injury of the gill can increase the microcystin intake and thereby cause liver necrosis. Other pathological features of poisonous cyanobacterial flowers included impairment to the heart, liver, kidneys, gills, spleen and skin.

It is likely that some fish, particularly phytoplanktivorous types, can absorb microcystins when being fed, or via some passive approaches by which poisons can go through the gills when respiring. For young fish, they are usually susceptible to poisonous substances. In case of the adult fishes, the thin epithelium and fairly large surface, together with a high metabolism rate, results in their damage by microcystins. This injury tends to cause death, especially during the major growth stage of the fish.

The toxicity of microcystins in the embryolarval development of carp, *Cyprinus carpio,* has been studied (Drobac, et al., 2016). The results affirmed that exposure to microcystins showed embryotoxic effects such as significant fish mortality.

Also, scientists have studied the influence of microcystin on yearling *rainbow trout* in which microcystin was placed intraperitoneally or which was soaked in water with algae (Svircev, et al., 2015). The rainbow trout absorbed microcystin chiefly by liver, and when the toxin arrived at the liver, it would lead to large-scale hepatic necrosis. Ibelings et al. (2005) have found that the amount of microcystin is particularly great inside the liver of planktivorous fish, which then places birds which took the fish as food at high danger. They also pointed out that 80 percent of zooplankton samples and 89 percent of samples of *Dreissena polymorpha* contained microcystins (Ibelings, et al., 2005). Hence, the conclusion was drawn that microcystin can indeed travel through the food link, in spite of the deficiency of bio-magnification.

1.4. Sulfadiazine

Sulfadiazine (SDZ) is 4-amino-N-(2-pyrimidinyl) benzenesulfonamide) (Fig. 1.10). SDZ is one of the most widely used sulfonamide antibiotics due to its extensive utilization for humans and livestock. It is commonly detected in aquatic environments because of its resistance to biodegradation and persistence in the natural environment (Gothwal and Shashidhar, 2015). Recently, the concerns regarding the occurrence of SDZ as well as other antibiotics in aquatic environments have attracted increasing attention. The biological activity of sulfonamide residues in the aquatic ecosystem may contribute to the growth of antibiotic resistance in microbial communities, which is

believed to be a worldwide issue of human health. SDZ has been detected in aquatic environments globally. The concentration range of sulfadiazine is from ng/L to µg/L. The maximum concentration of sulfadiazine was up to 4.13 µg/L, which was identified in surface water in the UK (Boxall, et al., 2012). Among the various antibiotics, sulfadiazine is one of the most commonly detected sulfonamides in China. More details on SDZ are in Section 4.

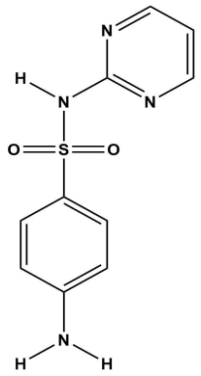

Fig. 1.10. Molecular structure of sulfadiazine (SDZ).

1.5. Flumequine

Currently, more than 5000 different pharmaceutical compounds have been on the market worldwide for intended use for human and veterinary applications (Dorival-García, et al., 2013). These pharmaceuticals continue to be released into the environment, resulting in great concerns due to their potential effects on human health and biota.(Barbosa, et al., 2016; Van Doorslaer, et al., 2014). There has been an increase in the consumption of antibiotics due to the increase in population worldwide and the aging of people in developed countries (Khetan and Collins, 2007). Among antibiotics,

luoroquinolones (FQs) are of tremendous significance because they are wide spectrum antibacterials with an increasing use in veterinary and household applications (Chierentin and Salgado, 2016; Rutgersson, et al., 2014). Fluoroquinolone antibiotics are applied as treatment for bacterial infections in animals and humans (Chierentin and Salgado, 2016; Rutgersson, et al., 2014). Interestingly, FQs account for a 17% share of the global market (Hamad, 2010). Significantly, FQs antibiotics are excreted unmetabolized (≤ 70%) (Tran, et al., 2016). Hence, their release into the environment promotes antibiotic resistant bacteria and antibiotic resistant genes (Cizmas, et al., 2015; Sharma, et al., 2016b). The research presented herein deals with flumequine (FLU), which is a class of fluroquinolone antibiotics (Fig. 1.11). More details on FLU are provided in Section 5.

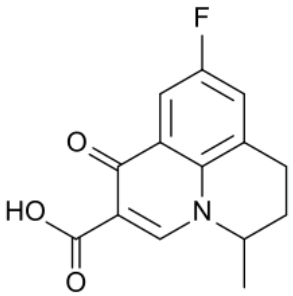

Fig. 1.11. Structure of flumequine.

1.6. Remediation methods

Conventional water treatment technologies include membrane separation, coagulation, sedimentation, and activated carbon adsorption (Campinas and Rosa, 2010; Lee and Walker, 2008; Pavagadhi, et al., 2013; Sun, et al., 2012; Teixeira and Rosa,

2005). These methods are not effective in removing MC-LR, particularly as it cannot be removed methodically from the environment. Other alternate treatments include oxidation by advanced oxidation processes (AOP) and chemical oxidants (He, et al., 2015; Sharma, et al., 2012). These processes are TiO_2/UV, modified-TiO_2/visible light, ultrasound irradiation, and Fenton and photo-Fenton systems (De Freitas, et al., 2013; Eskandarian, et al., 2016; Fotiou, et al., 2016; Rajasekhar, et al., 2012). AOPs generally generate hydroxide radicals ($^{\bullet}OH$) and sulfate radicals ($SO_4^{-\bullet}$), which can degrade MC-LR efficiently in water (Antoniou, et al., 2010; Song, et al., 2009). Chlorine, chloramine, ozone, and permanganate are examples of chemical oxidants (Acero, et al., 2008; Liu, et al., 2009; Miao, et al., 2010; Wert, et al., 2014). Chlorination can easily degrade MC-LR, but it produces potentially toxic chlorinated byproducts (Zhang, et al., 2016; Zong, et al., 2015). Chloramine is not able to oxidize MC-LR. Ozone and permanganate are capable of degrading MC-LR (Acero, et al., 2008; Miao, et al., 2010; Rodríguez, et al., 2007). This paper deals with tetra-oxy iron(VI) anion ($Fe^{VI}O_4^{2-}$), commonly called ferrate(VI) (Fe^{VI}), which can address concerns with byproducts (Sharma, et al., 2015, 2016a). For example, Fe(VI) does not react with the bromide ion and thus does not directly form the carcinogenic bromate (BrO_3^-) ion (Sharma, 2010). Fe^{VI} as a preoxidant also decreased the level of disinfection byproducts during chlorination (Gan, et al., 2015; Yang, et al., 2015). Added advantages are that Fe^{VI} is simultaneously carrying out disinfection and coagulation to inactivate microorganisms and is removing toxic metals, respectively (Prucek, et al., 2015; Sharma, 2007). Applications of Fe^{V} and Fe^{IV} to treat

pollutants have also been forthcoming in recent years (Kralchevska, et al., 2016; Machalová Šišková, et al., 2016; Sharma, et al., 2008, 2015, 2016a).

In this thesis research, transformations of MC-LR, SDZ, and FLU by Fe^{VI}, Fe^{V}, and Fe^{IV} were carried out. Aims of the research are presented in Chapters 2, 3, 4, and 5. Results of the research are described in these chapters. Section 6 concludes the objectives achieved in the research. The future outlook for research in this area is also presented in Section 6.

2. OXIDATION OF MICROCYSTIN-LR BY FERRATE(VI), FERRATE(V), AND FERRATE(IV): DEGRADATION PRODUCTS

2.1. Introduction

The occurrence of blue-green algal (cyanobacterial) blooms is a worldwide phenomenon. Environmental conditions that facilitate the formation of blooms include a water temperature range of 15 – 30^{o} C, a pH level between 6 and 9, and moderate to high levels of phosphorous and nitrate or ammonia (Sharma, et al., 2012, 2017). The toxic form of cyanobacterium *Microcystis aeruginosa* in the waters of China, Japan, Norway, South Africa, the United Kingdom, the United States, and Canada have been suggested (Sharma, et al., 2012, 2017). The generation of toxin-producing cyanobacteria in water resources is a growing global issue because these toxins affect human population through drinking water. Species of strains that produce cyanotoxins include microcystins (MCs), cylindropermopsin (CYN), saxitoxins, and anatoxins . These species can affect neurological systems (Craig, et al., 1996). Reports also suggested that the species can also be potential genotoxins, carcinogens, and inhibitors of protein synthase (Valério, et al., 2010). In certain cases, fatal intoxication of the human population from cyanobacterial species has occurred (Woolbright, et al., 2017). Moreover, cyanobacteria are capable of producing metabolites (e.g. 2-methylisoborneol and geosmin), which cause problems of unpalatability of water due to taste and odor problems-(Gurbuz, et al., 2016; Weirich and Miller, 2014). This chapter deals with the mitigation of one of the microcystins, microcystin-LR (MC-LR), in water.

Microcystins (MCs), comprising a large group of cyclic heptapeptide toxins, are produced by cyanobacterial species such as *Anabaenopsis Hapalosipon* and Microcystis (Harke, et al., 2016). Contamination of water with MCs has become a serious public health and environmental safety concern due to frequent occurrence of blue-green algae (cyanobacteria) blooms in water (Gurbuz, et al., 2016; Weirich and Miller, 2014). A number of MCs (> 90) have been identified, which have a general structure consisting of D-alanine, γ-linked-D-glutamic acid, D-*erythro*-*β*-methylaspartic acid (Adda), *N*-methyl dehydroalanine, and two variable L-amino acids (Flores and Caixach, 2015; Qi, et al., 2014). Microcystine-LR (MC-LR) contains leucine (L) and arginine (R) in positions 2 and 4, respectively. In the past decade, MC-LR has received more attention because it has acute toxicity (He, et al., 2016; Zhou, et al., 2015), and it has been detected in waters of Asian and European countries as well as in water of North America (Gkelis and Zaoutsos, 2014; Lin, et al., 2016; Pick, 2016; Schmidt, et al., 2013). A guideline value for MC-LR in drinking water, recommended by the World Health Organization (WHO), is 1 µg/L (World Health Organization, 1997). Many treatment methods have been investigated to remove extracellular MC-LR from water (Sharma, et al., 2012, 2017).

Conventional water treatment technologies include membrane separation, coagulation, sedimentation, and activated carbon adsorption (Campinas and Rosa, 2010; Lee and Walker, 2008; Pavagadhi, et al., 2013; Sun, et al., 2012; Teixeira and Rosa, 2005). These methods are not effective removing MC-LR; particularly, it cannot be removed methodically from the environment. Other alternate treatments include oxidation by advanced oxidation processes (AOP) and chemical oxidants (He, et al.,

2015; Sharma, et al., 2012). These processes are TiO_2/UV, modified-TiO_2/visible light, ultrasound irradiation, and Fenton and photo-Fenton systems (De Freitas, et al., 2013; Eskandarian, et al., 2016; Fotiou, et al., 2016; Rajasekhar, et al., 2012). AOPs generally generate hydroxide radicals ($^{\bullet}OH$) and sulfate radicals ($SO_4^{-\bullet}$), which can degrade MC-LR efficiently in water (Antoniou, et al., 2010; Song, et al., 2009). Chlorine, chloramine, ozone, and permanganate are examples of chemical oxidants (Acero, et al., 2008; Liu, et al., 2009; Miao, et al., 2010; Wert, et al., 2014). Chlorination can easily degrade MC-LR, but it produces potential toxic chlorinated byproducts (Zhang, et al., 2016; Zong, et al., 2015). Chloramine is not able to oxidize MC-LR. Ozone and permanganate are capable of degrading MC-LR (Acero, et al., 2008; Miao, et al., 2010; Rodríguez, et al., 2007). This paper deals with a tetra-oxy iron(VI) anion ($Fe^{VI}O_4^{2-}$), commonly called ferrate(VI) (Fe^{VI}), which can address concerns of byproducts (Sharma, et al., 2015, 2016a). For example, Fe(VI) does not react with the bromide ion and thus does not directly form the carcinogenic bromate (BrO_3^-) ion (Sharma, 2010). Fe^{VI} as a preoxidant also decreased the level of disinfection byproducts during chlorination (Gan, et al., 2015; Yang, et al., 2015). Added advantages of Fe^{VI} are simultaneous disinfection and coagulation to inactivate microorganisms and to remove toxic metals, respectively (Prucek, et al., 2015; Sharma, 2007).

The research in the present chapter was stimulated by our previous finding of aromatic hydroxylation during the oxidation of MC-LR by Fe^{VI} (Jiang, et al., 2014). This was surprising because hydroxylation was observed in the oxidation of MC-LR by $^{\bullet}OH$ radicals (Fotiou, et al., 2016). We invoked intermediate high-valent iron species, Fe^{V} and

Fe^{IV} during the oxidation of MC-LR by Fe^{VI} to induce the formation of hydroxylated derivatives of MC-LR. Recently, we were able to synthesize solid compounds of Fe^{V} (K_3FeO_4) and Fe^{IV} (Na_4FeO_4) (Kralchevska, et al., 2016; Machalová Šišková, et al., 2016), which allowed us to demonstrate for the first time that Fe^{V} and Fe^{IV} could attack the benzene moiety to yield aromatic hydroxylation of MC-LR. The objectives of the current study were to (i) identify the transformation products of the oxidation of MC-LR by Fe^{VI}, Fe^{V}, and Fe^{IV} to learn the moieties of the parent molecule involved in oxidation, (ii) to learn the similarities and differences of the three high-valent iron species in reaction pathways to oxidize MC-LR by varying the concentrations of Fe^{VI}, Fe^{V}, and Fe^{IV}, and (iii) to evaluate the effectiveness of ferrates, based on the general trend of observed oxidized products from the oxidation by Fe^{VI}, Fe^{V}, and Fe^{IV}.

2.2. Experimental methods

2.2.1 Chemicals

Sodium hydrogen phosphate (Na_2HPO_4), sodium hydroxide, and hydrochloric acid were purchased from Sigma-Aldrich (St. Louis, MO, USA) and Fisher Scientific (Austin, TX, USA). A solid powder of potassium ferrate (K_2FeO_4) with purity of > 98% was prepared by a wet chemical technique (Luo, et al., 2011). Potassium ferrate(V) (K_3FeO_4) and sodium ferrate(IV) (Na_4FeO_4) were the salts of Fe^{V} and Fe^{IV} species used in the study. Both of these salts were synthesized by thermal techniques, and details are given elsewhere (Machalová Šišková, et al., 2016). The purities were tested by ^{57}Fe Mössbauer spectroscopy (Machalová Šišková, et al., 2016; Yates, et al., 2014). The purity of solid K_3FeO_4 was 75 % and the remaining 25 % was Fe(VI). A solid powder of

Na_4FeO_4 was of high purity (>90 %). Salts of all the ferrate species were kept in a glove box, purged with nitrogen. A laboratory culture of *Microcystis aeruginosa* (CCMP299) was purified to obtain MC-LR (Song, et al., 2005). De-ionized water, before use in preparing solutions, was passed through an 18 MΩ cm Millipore water purification system (Waters Alliance, Milford, MA, USA). Solutions of MC-LR were prepared in a 0.01 M phosphate buffer solution. The pH of the buffer solution was adjusted to pH 7.0 using phosphoric acid. An Orion 720A pH meter and an Accumet pH probe were utilized to fix the pH of the solution to 7.0.

2.2.2 Product studies

In this study, a 10 mL solutions containing 5.0 µM MC-LR was prepared and placed in a glove box. Salts of Fe^{VI}, Fe^{V}, and Fe^{IV} species of different amounts were weighed in the anaerobic chamber of the glove box and immediately added into vials containing 10 mL of 5.0 µM MC-LR. The final concentrations of the three ferrate species in the mixtures were 200 µM, 400 µM, and 850 µM. The reaction of Fe^{VI} was allowed to occur until no pink violet color of the Fe^{VI} could be seen. The spectra of mixed Fe^{VI} and MC-LR solutions were run to make sure no Fe(VI) was present after the completion of the reaction. This mixed solution was filtered using a 0.45 µm filter before identifying the oxidized products. In studying the reactions between Fe^{V} and Fe^{IV} species with MC-LR, the mixed solutions were immediately subjected to the addition of hydroxylamine, a quenching reagent. The addition of a quenching reagent to Fe^{V}/Fe^{IV} and MC-LR mixed solutions was done in less than 10 s. The quenching reagent reacted rapidly with Fe^{VI}, so no significant reaction of Fe^{VI} with MC-LR could happen (Johnson

and Hornstein, 2003). A salt of Fe^{V} had an impurity of Fe^{VI}, which could interfere with the reaction of Fe^{V} with MC-LR. Furthermore, both Fe^{V} and Fe^{IV} species also simultaneously reacted rapidly (Menton and Bielski, 1990; Rush and Bielski, 1989; Rush and Bielski, 1994)with the solvent of MC-LR solution (i.e., water) to give an Fe^{VI} ion (Yates, et al., 2014). Basically, a rapid addition of quenching reagent to the Fe^{V}/Fe^{IV} and MC-LR mixed solutions avoided any possible interference from the reaction of Fe^{VI} with MC-LR. This approach allowed us to study the products obtained only from the aimed-at reactions (Fe^{V} and MC-LR or Fe^{IV}-MC-LR).

The concentration of MC-LR in the final mixed solutions were tested using a ThermoFisher HPLC system (Ultimate 3000) equipped with an autosampler and a photodiode array detector. A mobile phase used a mixture of 0.05 % (v/v) trifluoroacetic acid (TFA) in acetonitrile (40 %) and 0.1 % (v/v) TFA aqueous solutions (60 %). The stationary phase applied was a Luna RP C18 column (250×4.6 mm I.D., 5 μm).

2.2.3 Analysis of oxidized products

A high-resolution LC-MS/MS system was used to characterize the Fe^{VI}, Fe^{V}, and Fe^{IV} mediated oxidation products (OPs) of MC-LR. A QExactive mass spectrometer equipped with a Hypersil Gold column (100 mm × 2.1 mm, 3 μm) (Thermo Scientific, San Jose, CA, USA) and a Heated Electrospray Ionization source was used in the positive ionization mode to analyze OPs. The parameters of the analysis were: sheath gas flow: 30 arbitrary units; auxiliary gas flow: 20 arbitrary units; spray voltage: 4.4 kV; capillary temperature: 300 °C; heater temperature: 250 °C. Identification of the OPs was based on accurate mass measurements using a mass tolerance of 2 ppm. MS experiments

were performed at 17,500 resolutions using the following parameters: normalized collision energy (% NCE): 20-50; automatic gain control (AGC) target: 2×10^4, maximum injection time (IT): 40 ms; and isolation width: 2.0 m/z. The mobile phase in analyzing OPs was (A) acetonitrile and (B) 0.1 % formic acid in water. The gradient solution was 15-25 % A for 6 min followed by a linear increase to 40 % for 15 min and 80 % for 20 min followed by a decrease to 15 % for 22 min, and held constant for an additional 3 min.

2.3. Results and discussion

Transformation products of the oxidation of MC-LR by Fe^{VI}, Fe^{V} and Fe^{IV} were analyzed using their three different concentrations, namely high (H), medium (M), and low (L) concentrations of Fe^{VI}, Fe^{V} and Fe^{IV}. More details of their levels are given in the experimental section. For simplicity, different species are written as Fe^{VI}(L), Fe^{VI}(M), and Fe^{VI}(H) for Fe^{VI} species, Fe^{V}(L), Fe^{V}(M), and Fe^{V}(H) for Fe^{V}, and Fe^{IV}(L), Fe^{IV}(M), and Fe^{IV}(H) for Fe^{IV} species, for low, medium, and high concentrations of these ferrate species, respectively.

An approach used in identifying the oxidized products (OPs) of MC-LR by Fe^{VI}, Fe^{V}, and Fe^{IV} species was similar to that used by other researchers to characterize the products obtained by other oxidation technologies such as ultrasonic, UV/H_2O_2, radiolysis, photocatalytic, sulfate radicals permanganate, and electrochemical (Huang, et al., 2008; Liao, et al., 2014; Liu, et al., 2003; Song, et al., 2006; Song, et al., 2007; Su, et al., 2013; Zhang, et al., 2013). The molecular formulas for the observed products were obtained by identifying the best match of the high-resolution mass spectral data

(observed) to the calculated exact masses (theoretical) of different molecular formulas (Table 2.1). The differences between the *m/z* of the experimental and the theoretical results for most of the OPs were ≤2.0 ppm (Table 2.1). Specific MS spectra and structures associated with each of the products are provided in Fig. 2.1-2.17. Quantitative determinations of OPs on the MS were not carried out because of the lack of products standards.

Three different hydroxylated derivatives of MC-LR, with molecular weights (MWs) of 1028.5542, 1044.5492, and 1030.5699 were observed in the experiments with low concentrations of all three high-valent iron species (i.e., Fe^{VI}(L), Fe^{V}(L) and Fe^{IV}(L)) and medium concentrations of Fe^{V}, and Fe^{IV} (Fe^{V}(M) and Fe^{IV}(M)). The hydroxylated product with a MW of 1026.5386 was observed only in the experiment with Fe^{VI}(L). Three clearly resolved peaks with a MW of 1028.5542 correspond to the addition of two HO groups without the loss of H atoms (M+34). Dihydroxy-MC-LR could have two different structures, one that corresponds to the dihydroxylation at the conjugated pi system of the Adda moiety and its isomers, and another that relates to the dihydroxylation at the carbon−carbon double bond in the Mdha moiety. These proposed products have been reported in our previous study of the oxidation of MC-LR by Fe^{VI} species (Jiang, et al., 2014) and in other oxidation studies (Huang, et al., 2008; Liao, et al., 2014; Liu, et al., 2003; Song, et al., 2006; Song, et al., 2007; Su, et al., 2013; Zhang, et al., 2013).

Simultaneous hydroxylation through the addition of two HO groups (M+34) and the substitution of hydrogen for an OH group at the aromatic ring in the Adda moiety

(M+16) results in a MW of 1044.5492 (M+50). In this study, the full scan chromatogram has three different peaks that could correspond to two main structures with different isomer variations. These product structures have also been proposed in other investigations, UV/H_2O_2 (Zong, et al., 2013), sulfate radicals (Antoniou, et al., 2010), permanganate (Huang, et al., 2008), and ultrasonic (Song, et al., 2006). One structure was assigned to 1,2 and 1,4 di-hydroxylation at the Adda moiety plus the *ortho*, *metha* and *para* monohydroxylation in the benzene ring. Another structure was assigned to dihydroxylation at the carbon−carbon double bond in the Mdha moiety plus the *ortho*, *metha* and *para* monohydroxylation in the benzene ring.

The structure corresponding to the MW of 1030.5699 was also reported in the oxidation of MC-LR carried out by ClO_2 and TiO_2-photocatalytic processes (Fotiou, et al., 2013; Kull, et al., 2004). This product could be formed by hydration at two different vulnerable sites in MC-LR. One possibility is the double hydration of the double bonds in the Adda moiety. Another possibility is one hydration in the Adda chain plus one hydration in the Mdha chain.

Double hydroxylation of the aromatic ring by the substitution of two hydrogens with two hydroxyl groups at the benzene ring is suggested for the structures corresponding to a MW of 1026.6386 (M+32). This product was observed in our previous findings of aromatic hydroxylation during the oxidation of MC-LR by Fe^{VI} (Jiang, et al., 2014). The OPs were further differentiated based on the degradation pathways described in the following three reaction schemes.

Table 2.1. Mass and molecular formulas for the observed products, *m/z* experimental and theoretical, and mass error between theoretical and experimental *m/z*.

	Mass	Proposed formula	Theoretical m/z[a]	Experimental m/z[b]	Mass error (ppm)
MC-LR	994.5488	C49H74N10O12	995.5560	995.5558	-0.20
P_1044	1044.5492	C49H76N10O15	1045.5564	1045.5560	-0.38
P_1030	1030.5699	C49H78N10O14	1031.5772	1031.5763	-1.16
P_1028	1028.5542	C49H76N10O14	1029.5615	1029.5608	-0.68
P_1026	1026.5386	C49H74N10O14	1027.5459	1027.5457	-0.19
P_1014	1014.5386	C48H74N10O14	1015.5459	1015.5452	-0.69
P_1008	1008.5280	C49H72N10O13	1009.5353	1009.5347	-0.59
P_964	964.5382	C48H72N10O11	965.5455	965.5450	-0.52
P_810	810.3872	C34H54N10O13	811.3945	811.3941	-0.49
P_794	794.3923	C34H54N10O12	795.3985	795.3994	1.13
P_782	782.3923	C33H54N10O12	783.3995	783.3992	-0.38
P_758	758.3923	C31H54N10O12	759.3995	759.3993	0.26
P_744	744.3766	C30H52N10O12	745.3839	745.3836	-0.40
P_742	742.3974	C31H54N10O11	743.4046	743.4046	0
P_704	704.2977	C27H44N8O14	705.3050	705.3051	0.14
P_674	674.3235	C27H46N8O12	675.3308	675.3305	-0.44
P_361	361.1889	C20H27NO5	362.1962	362.1964	0.55
P_345	345.1940	C20H27NO4	346.2013	346.2015	0.58

[a]Calculated using ChemDraw 2010. [b]Observed in Orbitrap mass spectrometer

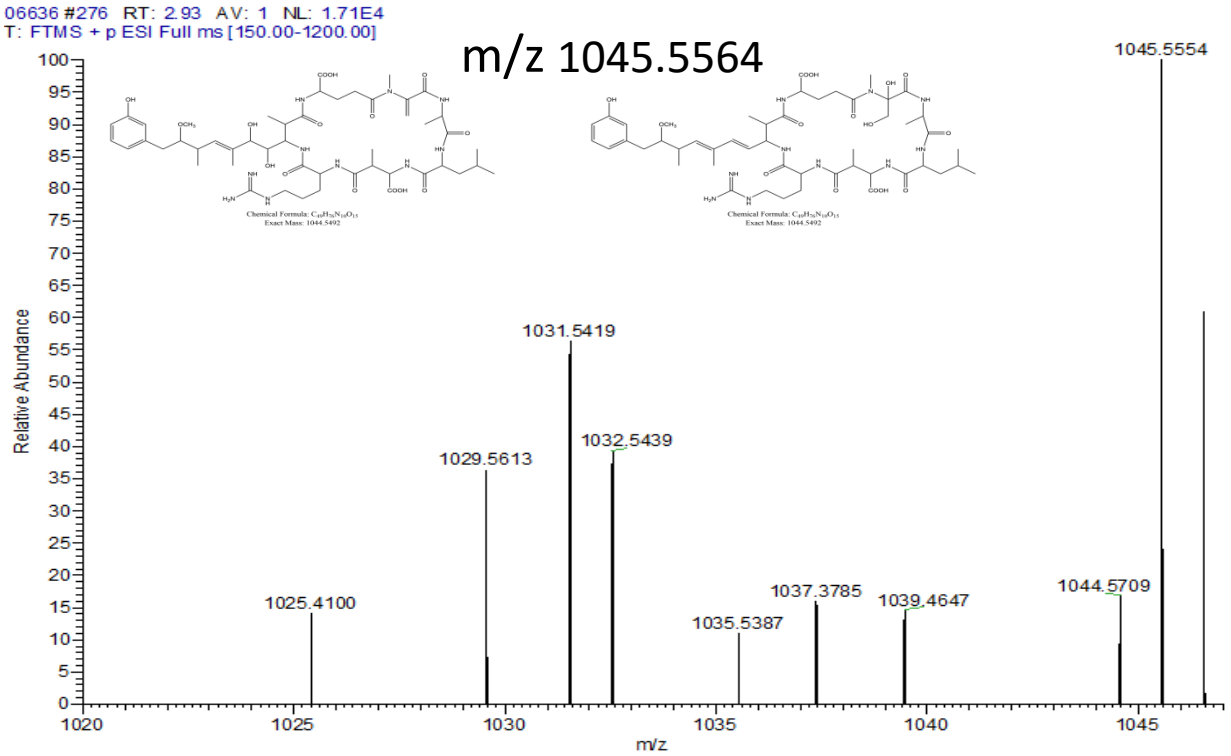

Fig. 2.1. Mass spectra of P_1044.

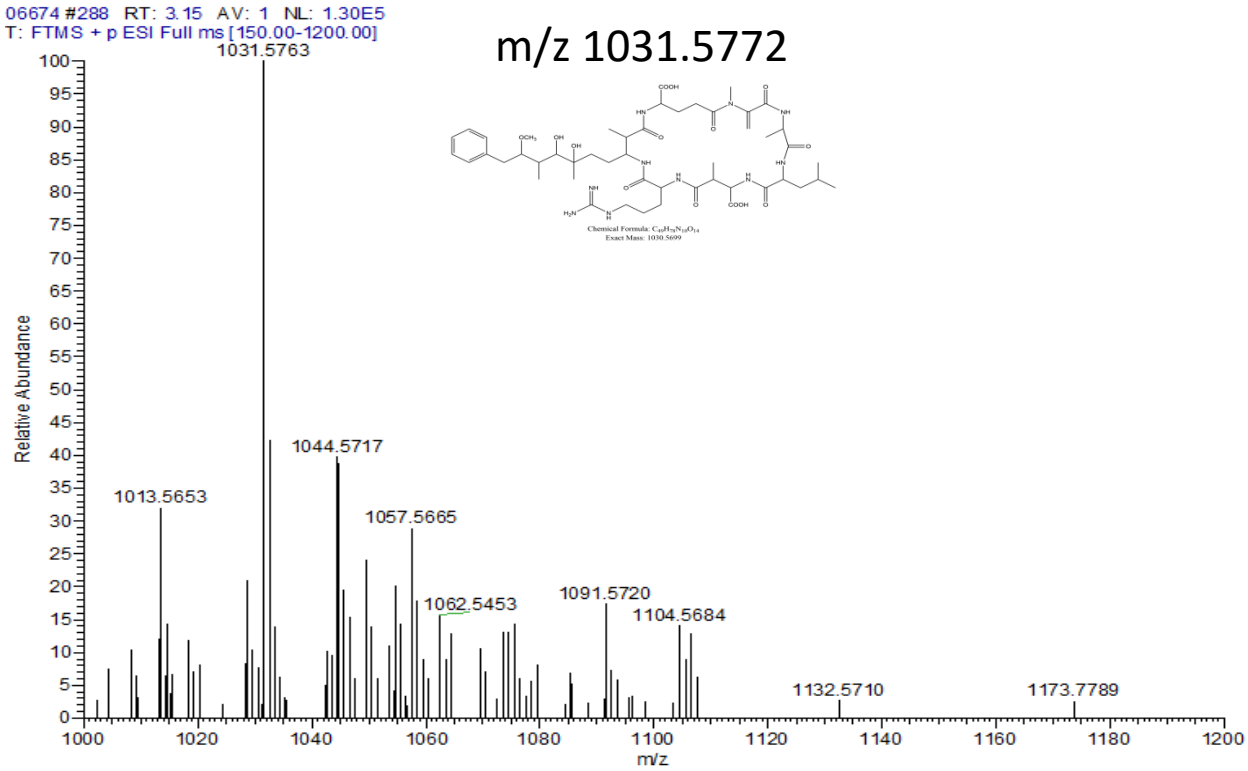

Fig. 2.2. Mass spectra of P_1030.

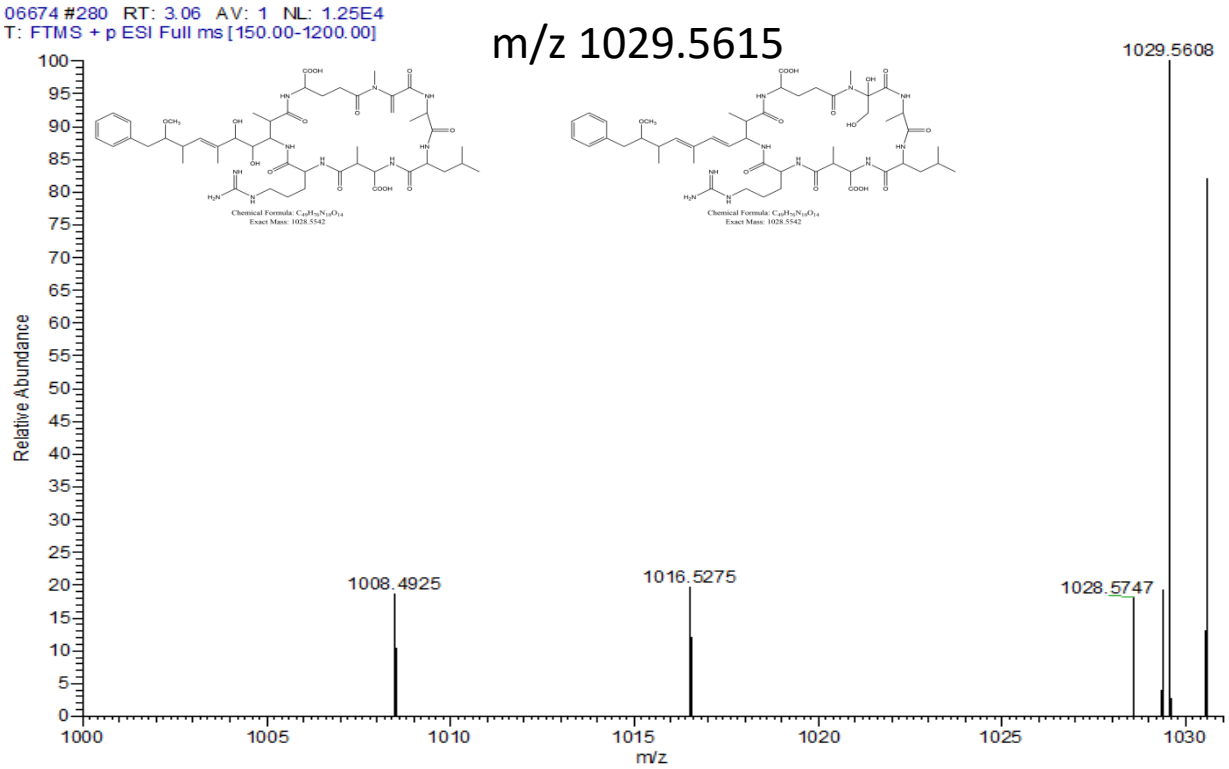

Fig. 2.3. Mass spectra of P_1028.

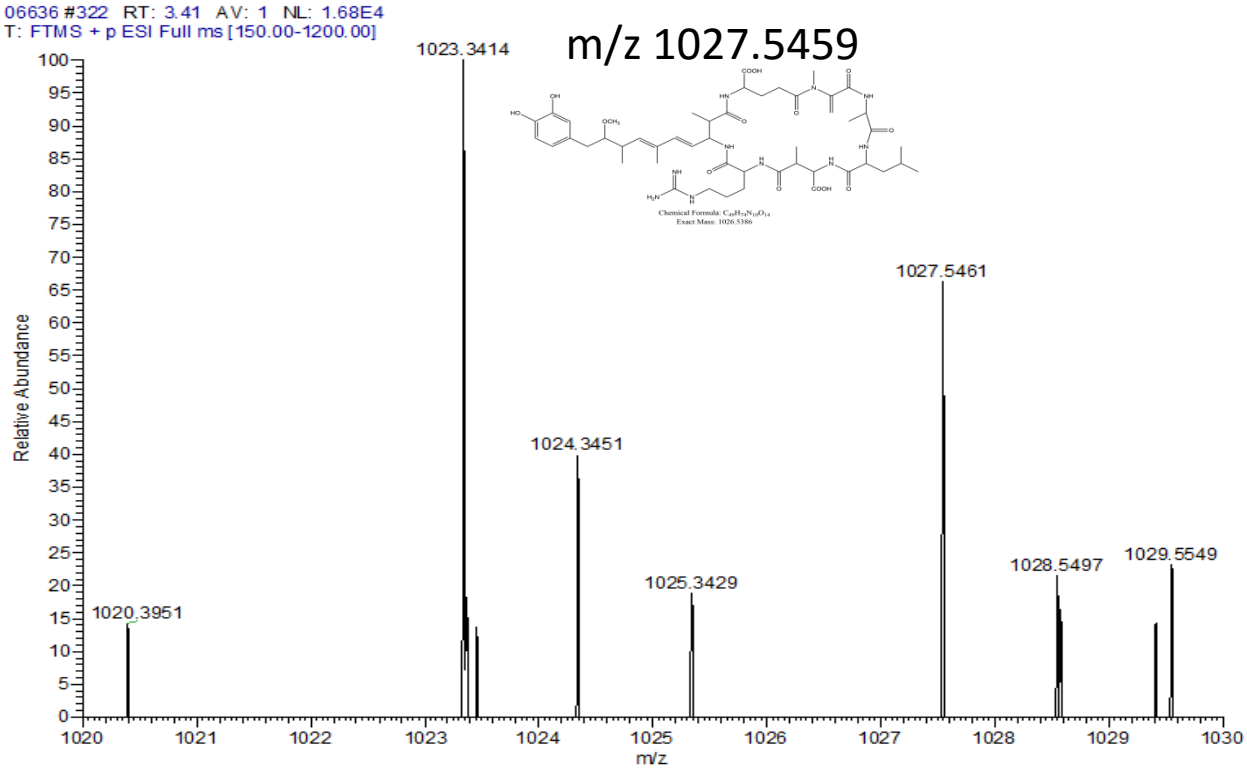

Fig. 2.4. Mass spectra of P_1026.

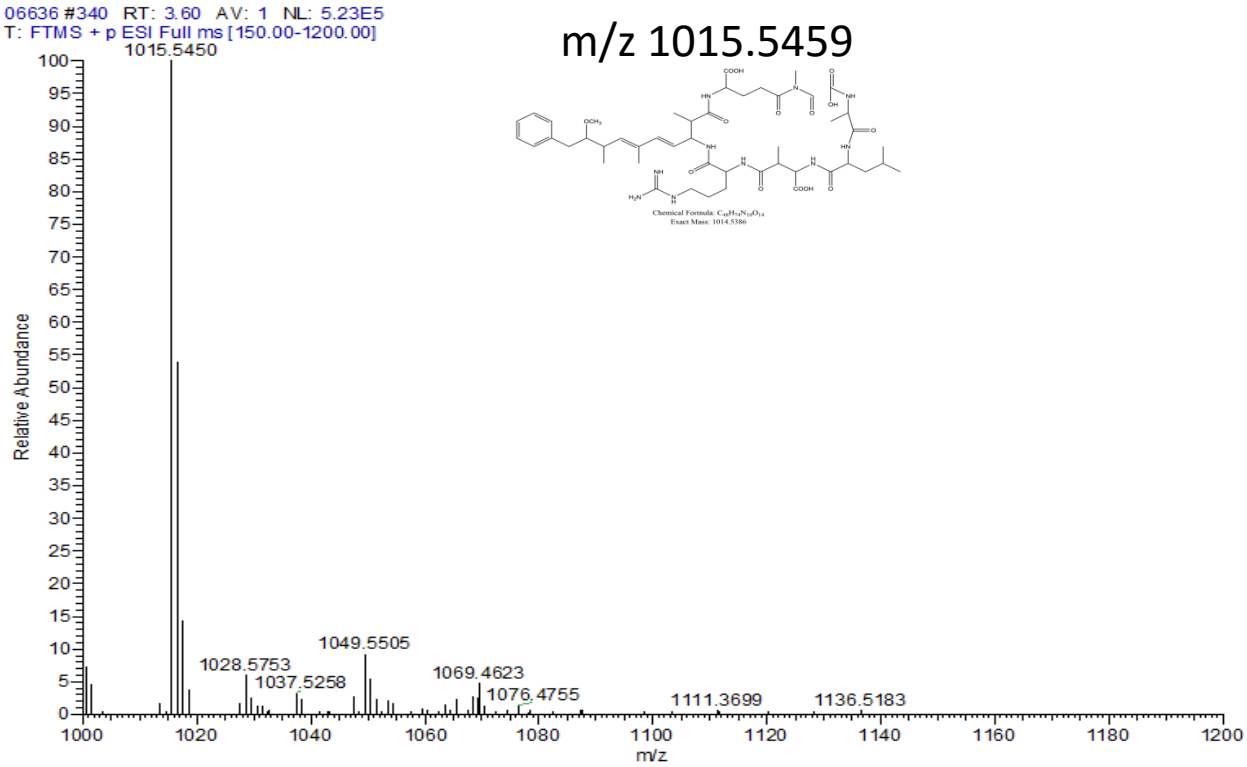

Fig. 2.5. Mass spectra of P_1014.

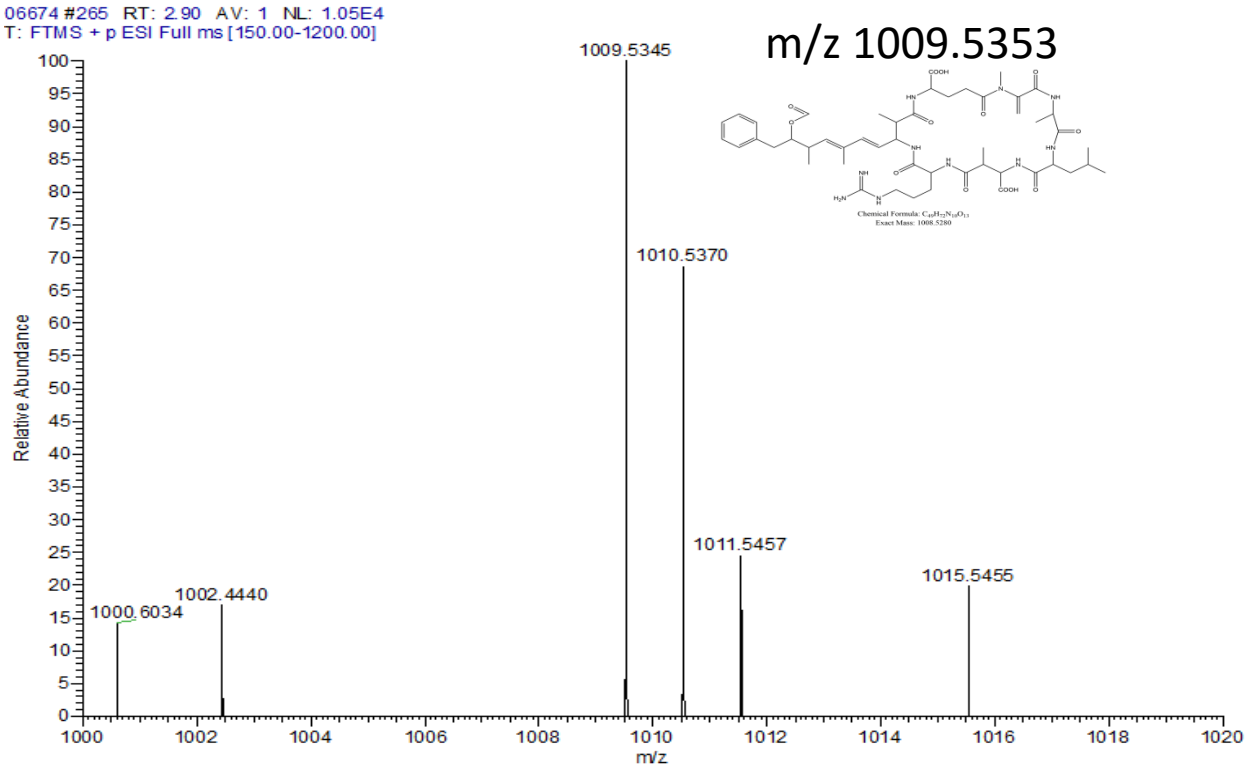

Fig. 2.6. Mass spectra of P_1008.

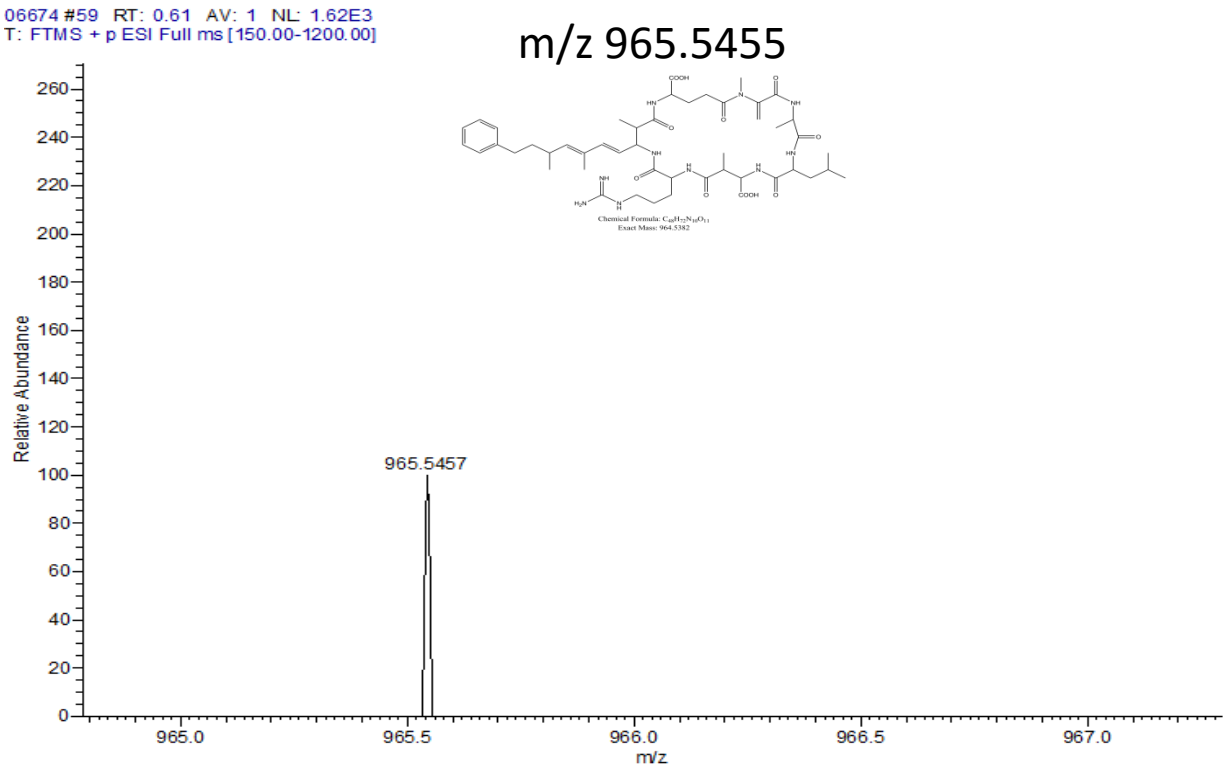

Fig. 2.7. Mass spectra of P_964.

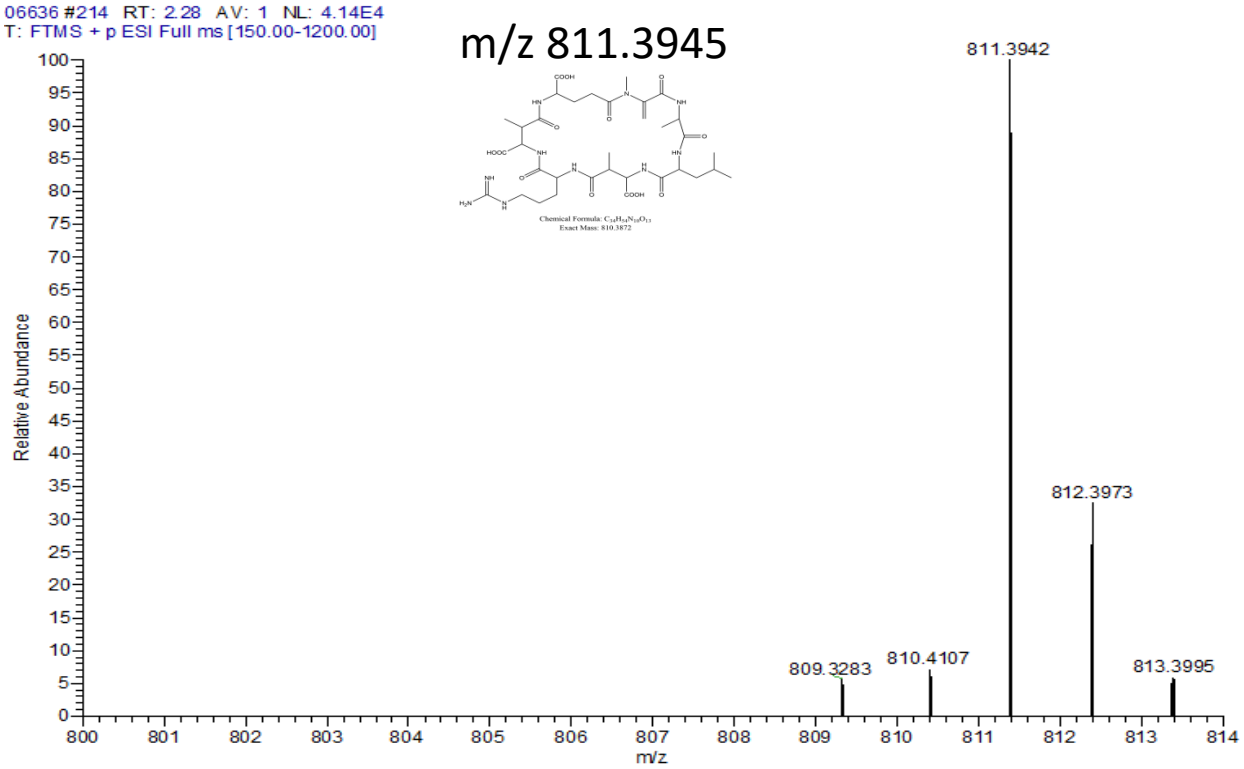

Fig. 2.8. Mass spectra of P_810.

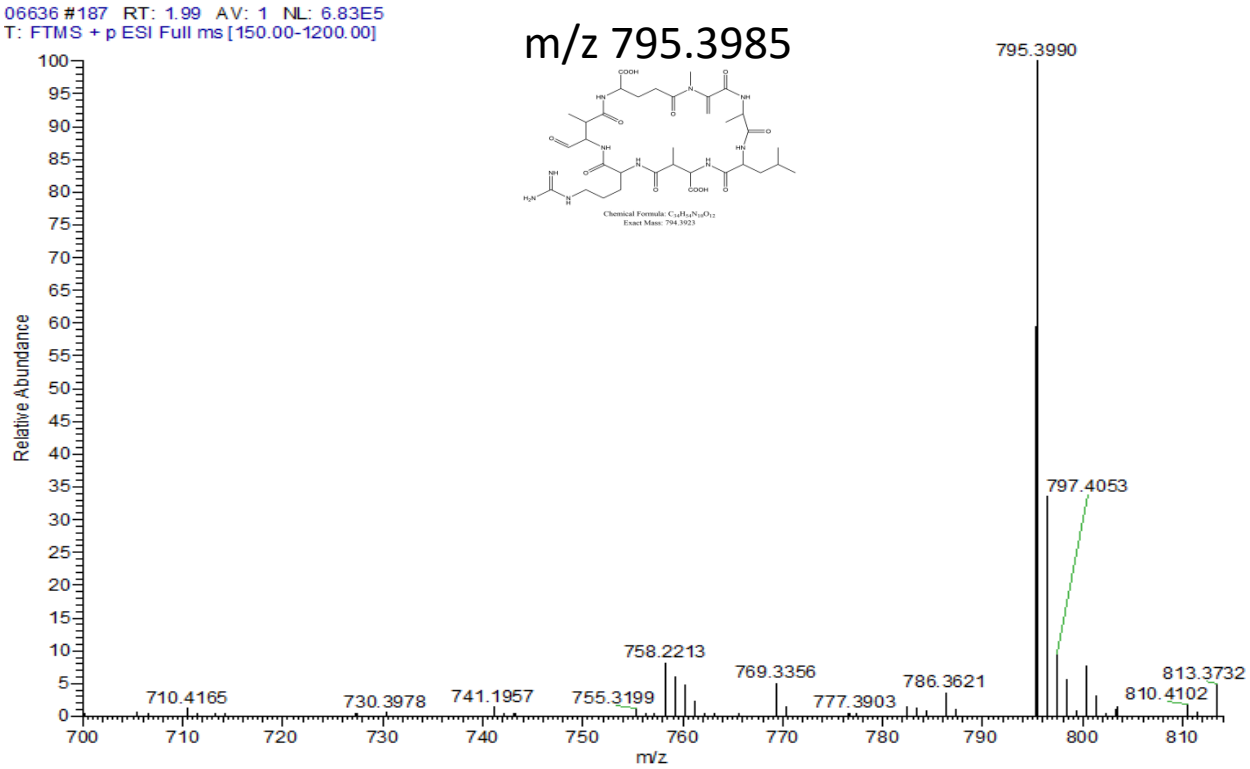

Fig. 2.9. Mass spectra of P_794.

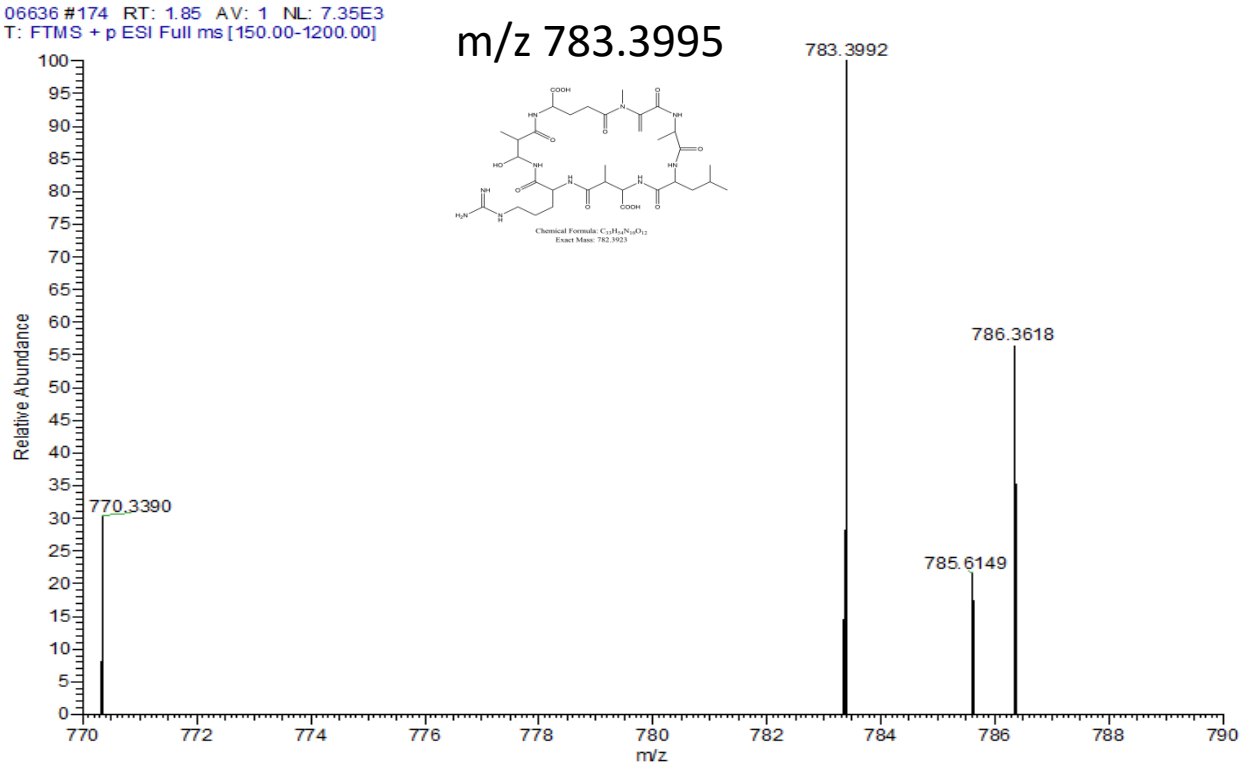

Fig. 2.10. Mass spectra of P_782.

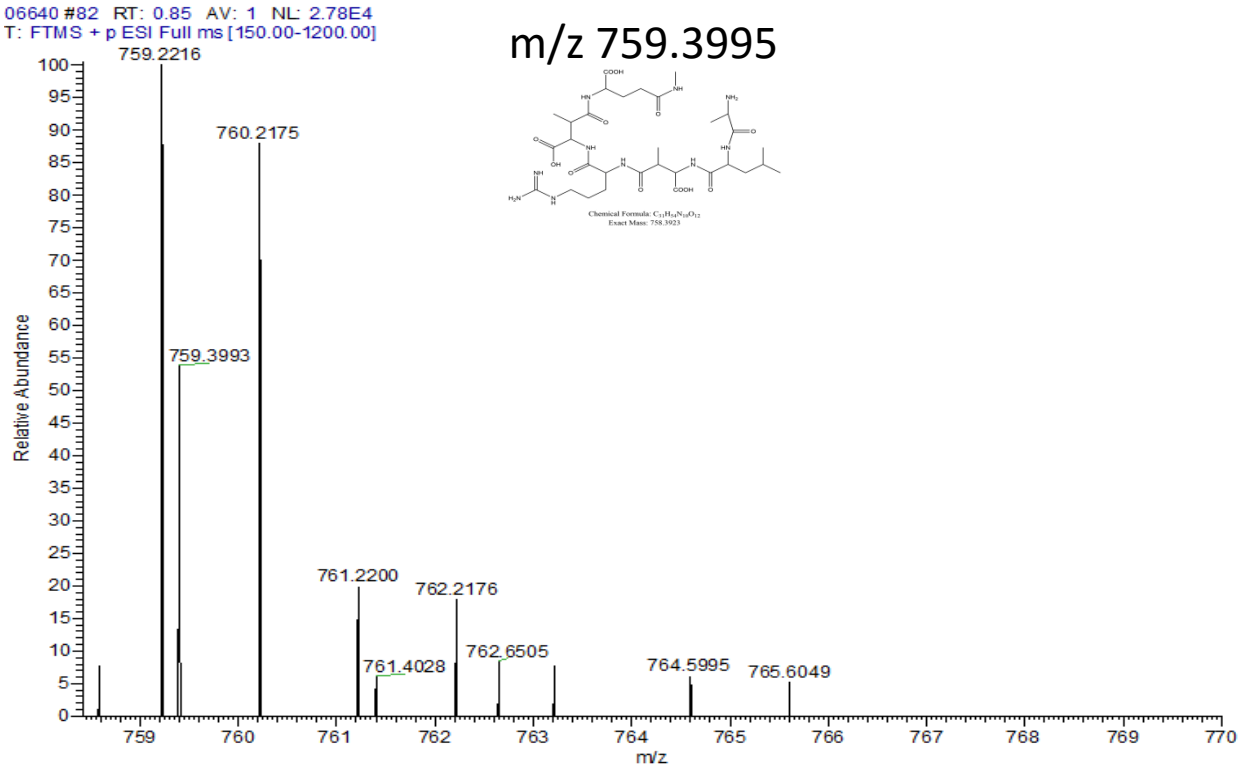

Fig. 2.11. Mass spectra of P_758.

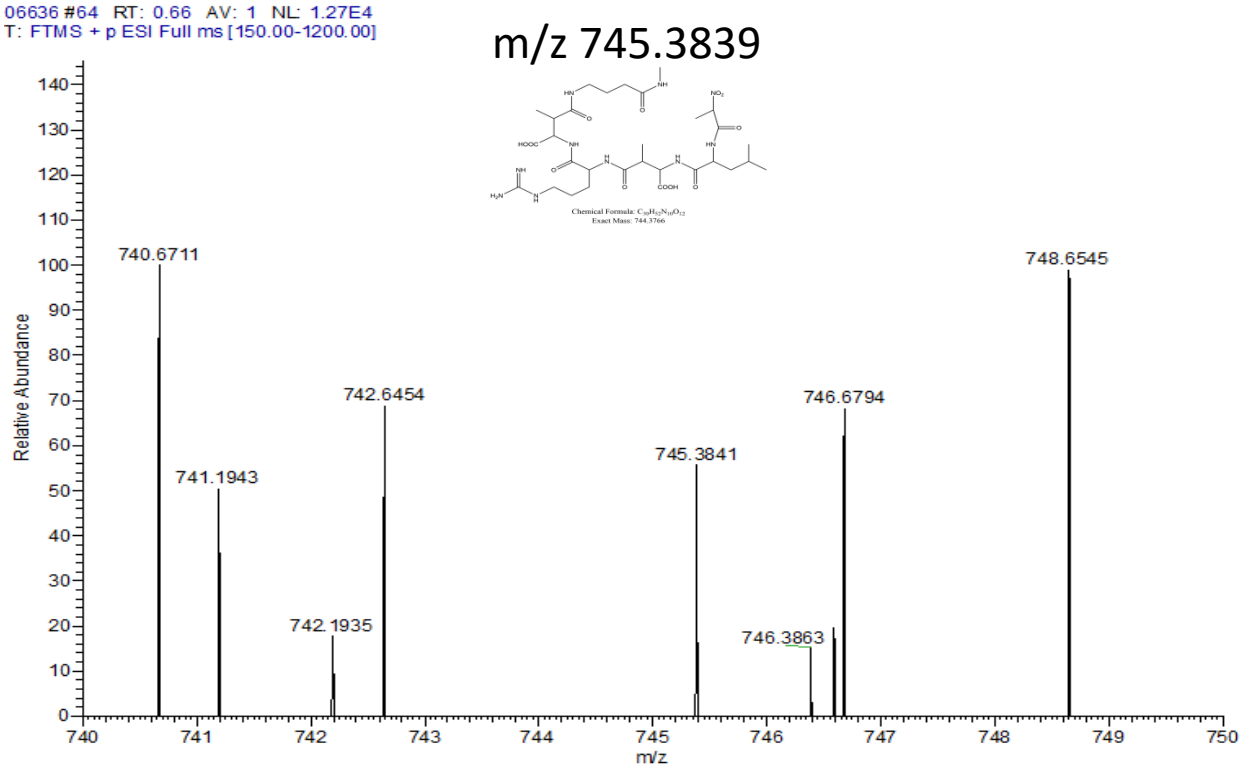

Fig. 2.12. Mass spectra of P_754.

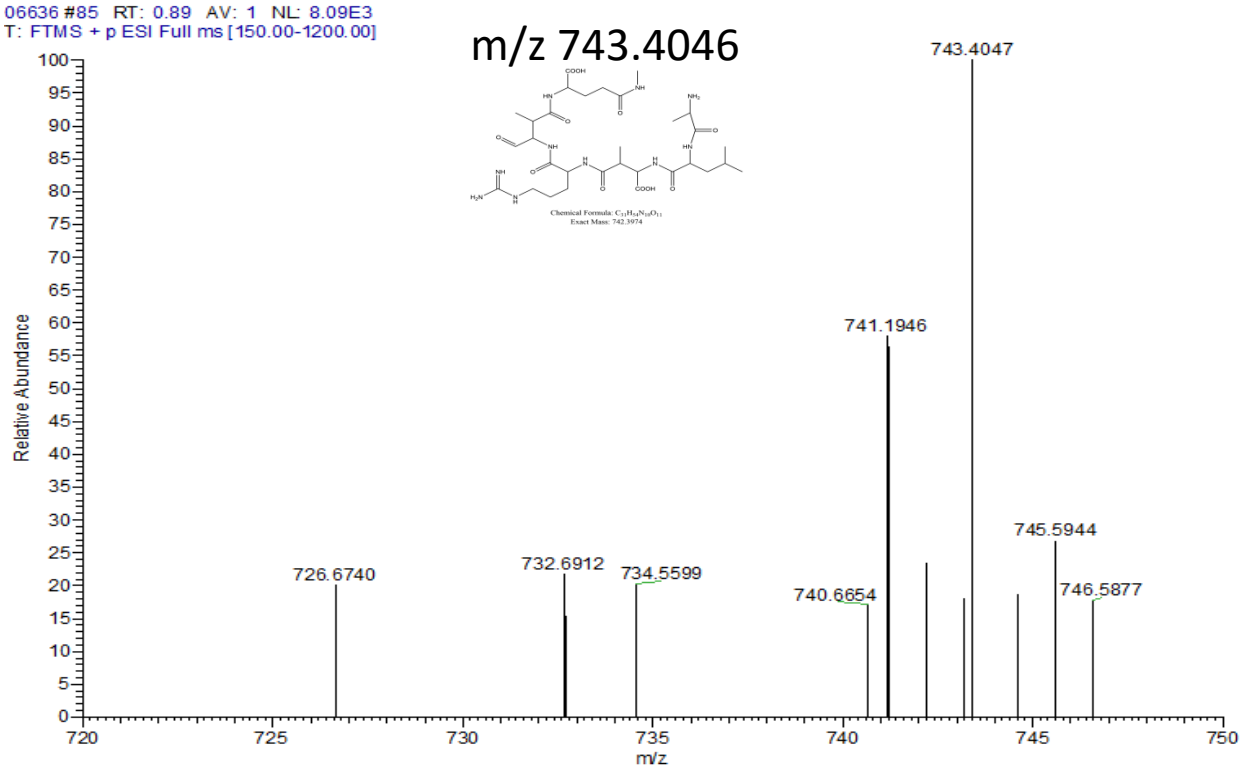

Fig. 2.13. Mass spectra of P_742.

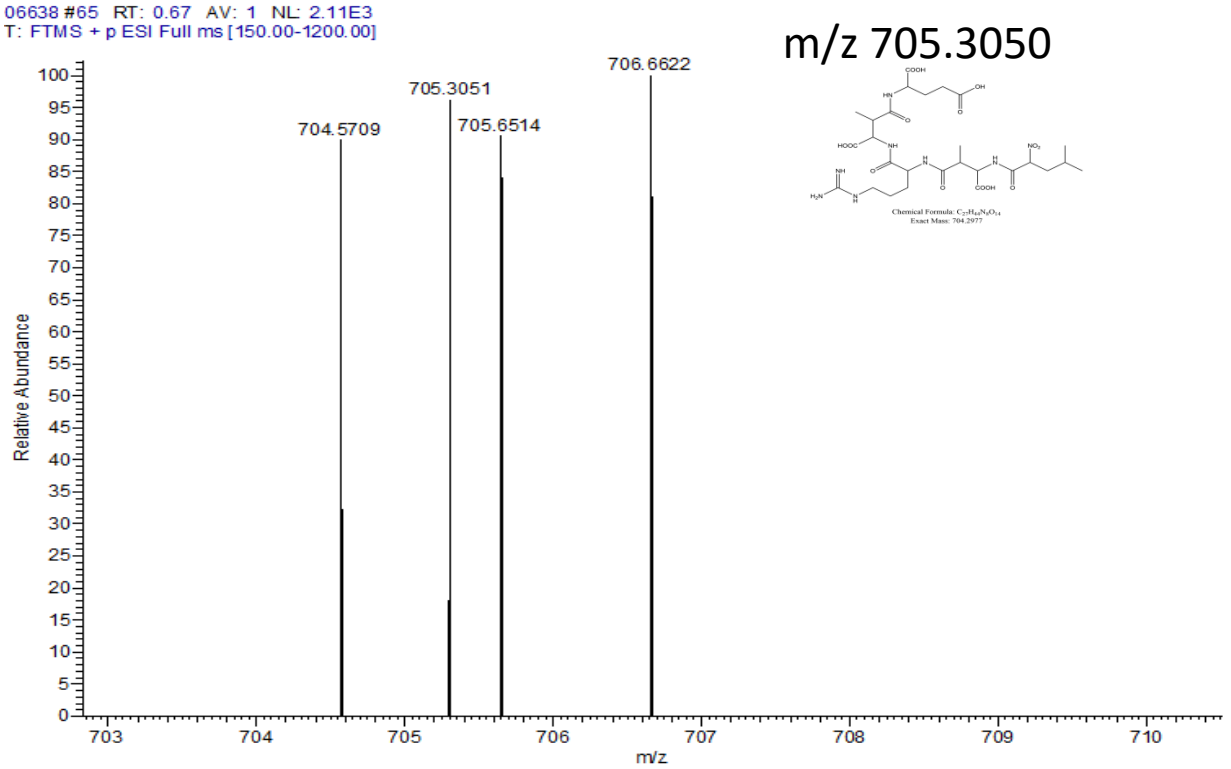

Fig. 2.14. Mass spectra of P_705.

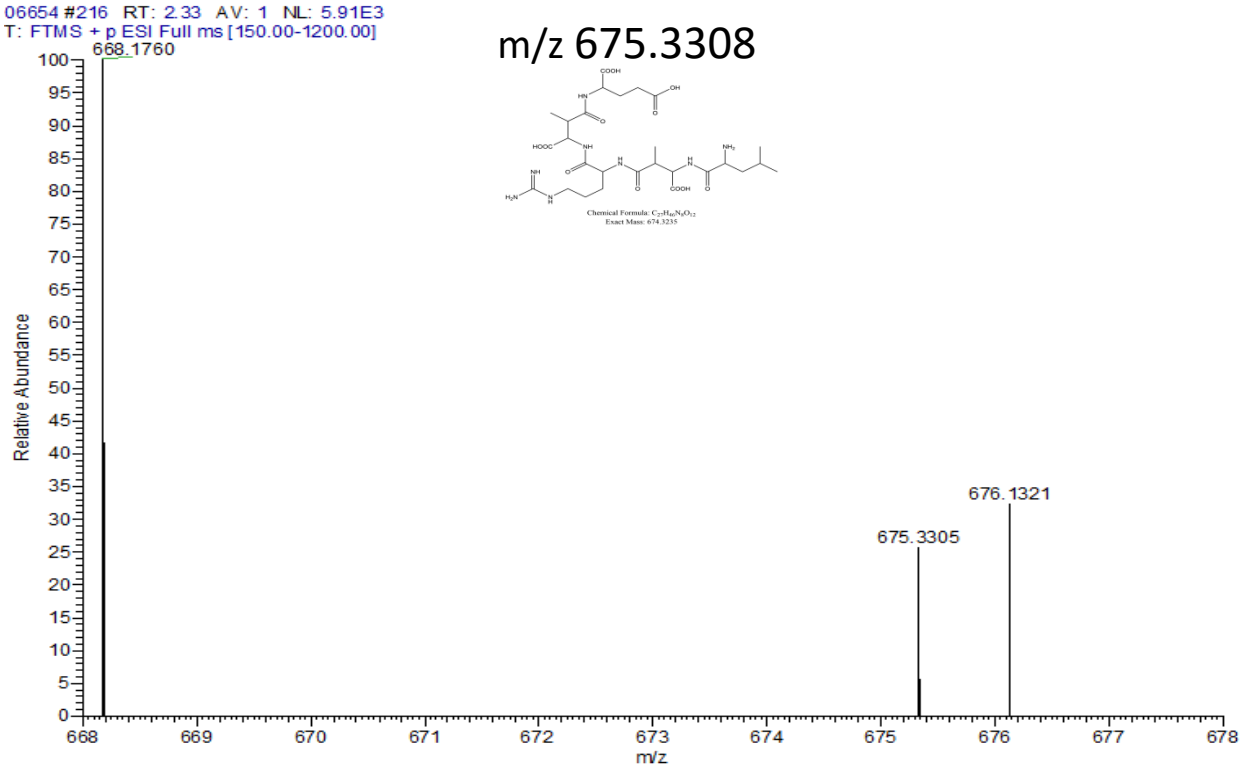

Fig. 2.15. Mass spectra of P_674.

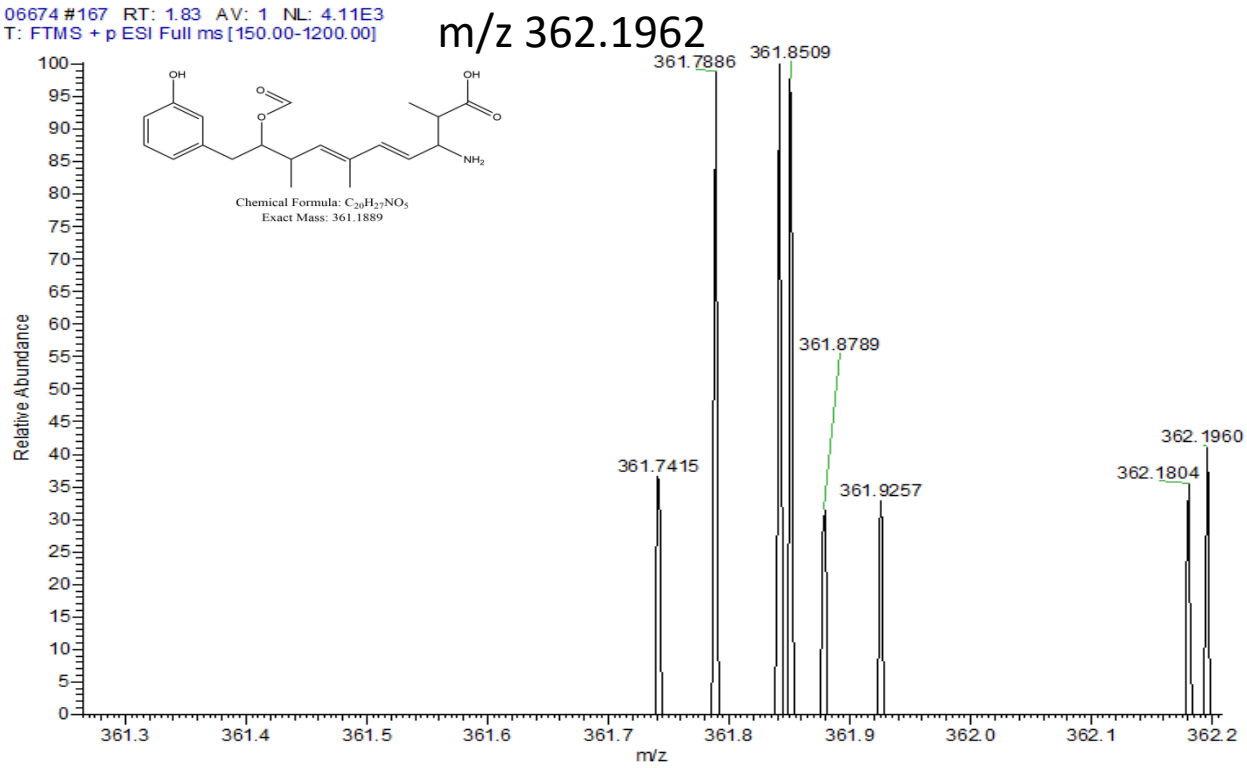

Fig. 2.16. Mass spectra of P_361.

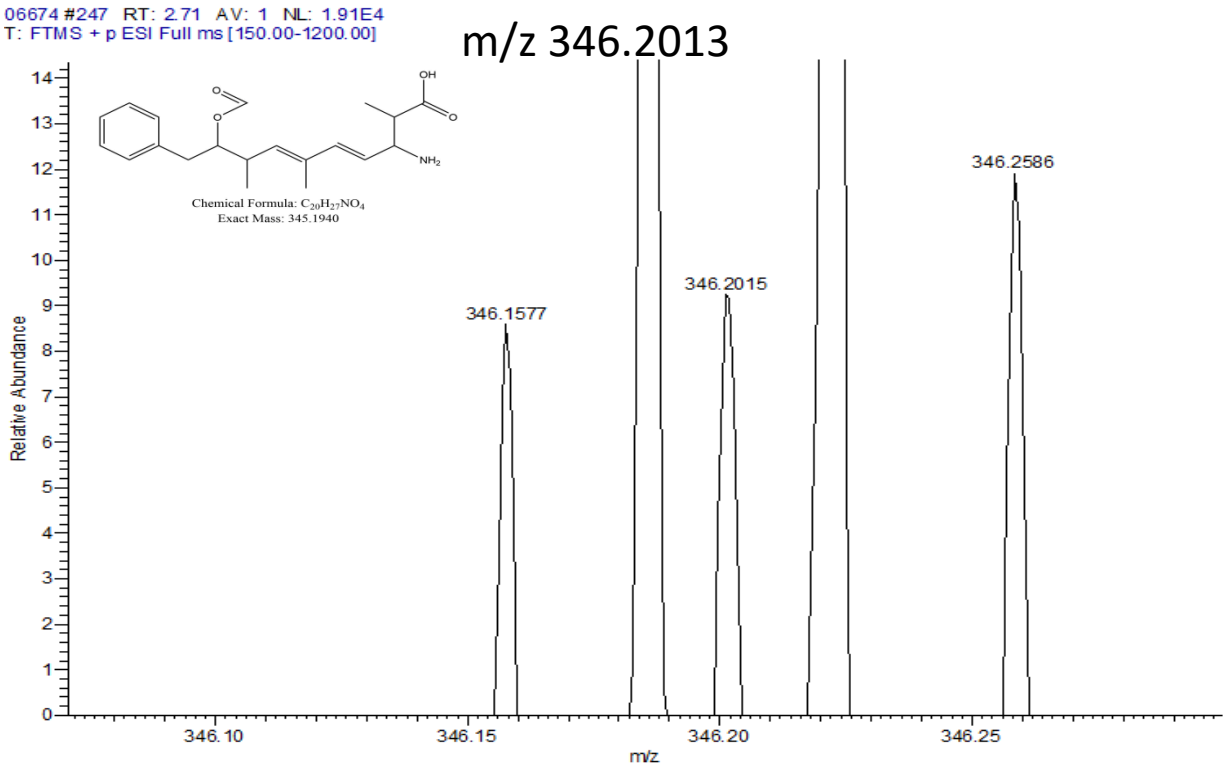

Fig. 2.17. Mass spectra of P_361.

2.3.1 Hydroxylation at the Adda diene

Fig. 2.18 gives *Scheme 1*, which involves the hydroxylation of MC-LR, followed by the removal of the Adda amino acid, and finally the breakage of the heptapeptide ring. In this proposed pathway, the Adda chain or the benzene ring is the most vulnerable attack site. The products with a MW of 1044.5492 correspond to the simultaneous mono-hydroxylation of MC-LR at the benzene ring and dihydroxylation at the Adda moiety. A MW of 1028.5542 relates to isomers of a 1,2 or 2,4 hydroxyl addition to the Adda diene, and the product with a MW of 1026.6386 is obtained from the di-hydroxylation of the benzene ring. In *Scheme 1*, the subsequent oxidation of hydroxylated intermediates led to the removal of the Adda chain. Products with a MW of 794.3923, 782.3923, and 810.3872 correspond to the intact heptapeptide ring with either an O, OH or COOH, respectively. The final products of this pathway yielded from the further cleavage of the heptapeptide cyclic structure have MWs of 674.3235 and 704.2977.

Both Fe^{V} and Fe^{IV} species showed the mono-hydroxylation of the benzene ring of the MC-LR (P_1044 in *Scheme 1*). This is the consistent with our previous finding that these intermediate reduced iron species are produced during the oxidation of MC-LR by Fe^{VI} species in order to hydroxylate the benzene ring of the MC-LR (Jiang, et al., 2014). In the biological systems, ferryl (Fe(IV) and perferryl (Fe(V)) species have also shown hydroxylation of the benzene ring (Cho, et al., 2016; Nam, et al., 2014; Ray, et al., 2015; Sharma and Zboril, 2015). The reactivities of Fe^{V} and Fe^{IV} species with compounds are orders of magnitude higher than the Fe^{VI} species (Sharma, 2002a;

Sharma, et al., 2008; Sharma, 2013); therefore, the observation of a mono-hydroxylation derivative of MC-LR by all the ferrate species is reasonable. Significantly, di-hydroxylation at the benzene ring was only observed in the Fe^{VI}(L) experiments, evidenced by the absence of a product with a MW of 1026.6386 in Fe^{V} and Fe^{IV} experiments regardless of concentration tested (*Scheme 1*). Fe^{V} and Fe^{IV} species, which are highly unstable, were also simultaneously self-decomposed (Bielski, et al., 1994; Menton and Bielski, 1990; Sharma, 2011) and were not available to result in further hydroxylation of the aromatic ring.

In the oxidation of MC-LR by Fe^{V} species, the heptapeptide ring with OH was not stable, demonstrated by the absence of a product with a MW of 782.3923 (*Scheme 1*). Nevertheless, a more oxidized product (MW 810.3872) was present at all concentrations of Fe^{V} species (*Scheme 1*). At all levels of Fe^{VI} species (L, M, and H), the oxidized product with a MW of 674.3235 was not observed. This indicates that this product was either not persistent or that Fe^{VI} oxidized the intermediate directly into a transformation product having a nitro group (P_704 in *Scheme 1*). This is in agreement with products observed in the oxidation of amines by ferrate species (Carr, 2008; Johnson and Hornstein, 2003; Johnson, et al., 2008). Experiments with Fe^{IV} species showed cleavage of the Adda diene, but no further breakage of the heptapeptide cyclic ring was seen. The simultaneous self-degradation of Fe^{IV} species may be occurring (Menton and Bielski, 1990; Sharma, 2011), and no significant amount of Fe^{IV} was available to carry out additional oxidation.

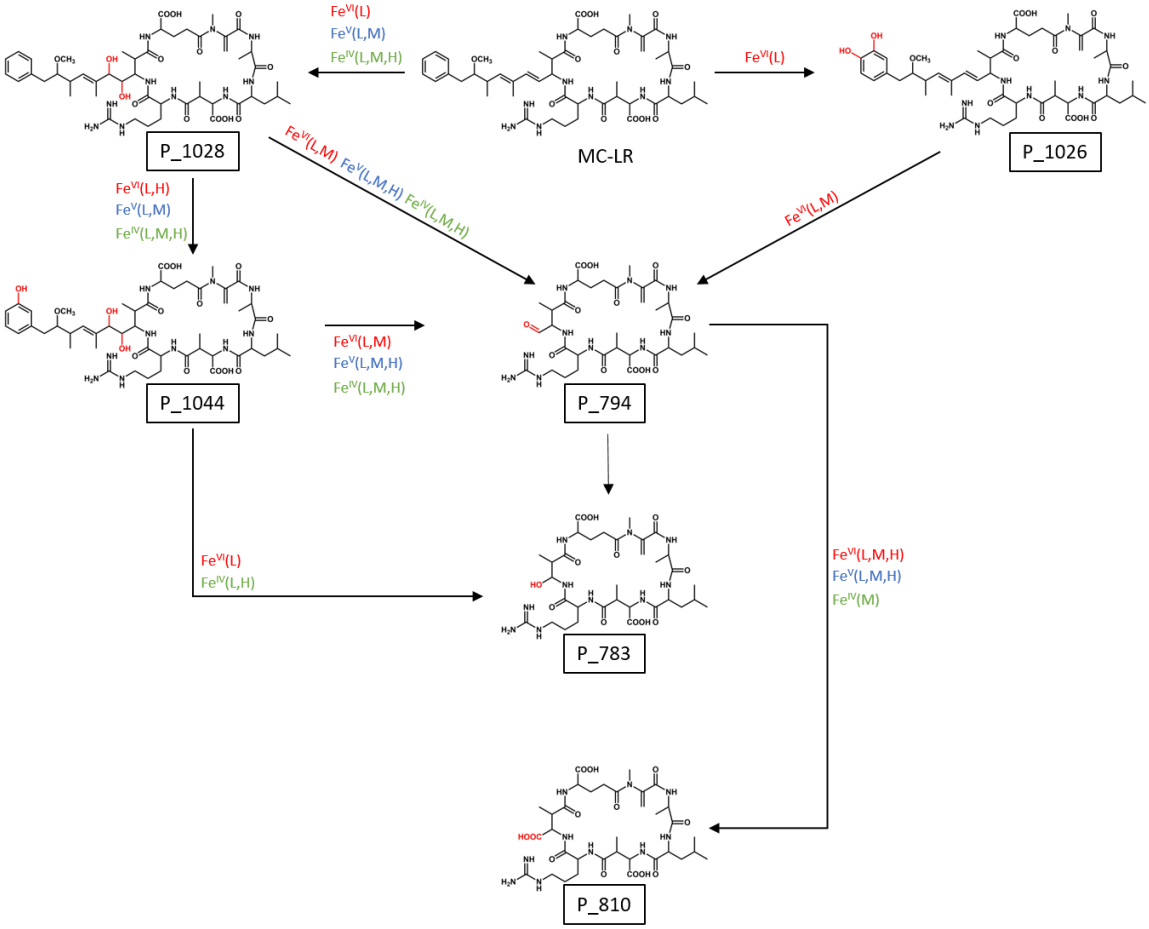

Fig. 2.18. *Scheme 1* - hydroxylation at the Adda diene, indicating products observed under high (H), medium (M), and low (L) concentrations of Fe^{VI}, Fe^{V} and Fe^{IV}.

2.3.2 Elimination of the methoxy group of the Adda diene

Fig. 2.19 shows the proposed *Scheme 2* that shows the attack of ferrate species at the methoxyl at the Adda moiety, followed by hydrolysis of the intermediate products. The structure assigned to a compound with a MW of 1008.5280 is of a formic acid ester MC-LR (Antoniou, et al., 2008; Su, et al., 2013). Further oxidations in this pathway of *Scheme 2* resulted in the complete removal of the methoxy group (MW of 964.5382). Breakage of the heptapeptide ring was also shown with the presence of a MW of 345.1940. Fe^{VI} species have the capability to oxidize peptide bonds (Noorhasan, et al., 2010), and the proposed product with a low MW is well justified. A combination of breakage of the heptapeptide ring and monohydroxylation of the benzene ring yield a product with a MW of 361.1889. This step is similar to the reported pathway in the photocatalytic transformation of MC-LR using TiO_2 (Antoniou, et al., 2008; Su, et al., 2013).

At the medium concentration of Fe^{IV}, a compound with MW 964.5382 was found, which was not seen at other levels of Fe^{IV} species (*Scheme 2*). It appears that this compound was further degraded by the addition of Fe^{IV} because it is only present at a medium concentration of Fe^{IV} (i.e., Fe^{IV}(M)). Another significant observation of *Scheme 2* was the absence of the intermediate of MC-LR without the methoxy group (i.e., P_1008.5280) at every concentration of Fe^{VI}. However, this compound was present during the oxidation of MC-LR by Fe^{IV} and Fe^{V} (*Scheme 2*). The formation of the MWs of 345.1940 and 361.1889 at even a low concentration of Fe^{VI} (Fe^{VI}(L)) implies that the

product compound with MW 1008.5280 could be oxidized by Fe^{VI} species step-wise to low MW OPs. Fe^{V} and Fe^{IV} species also yielded these low MW OPs (*Scheme 2*).

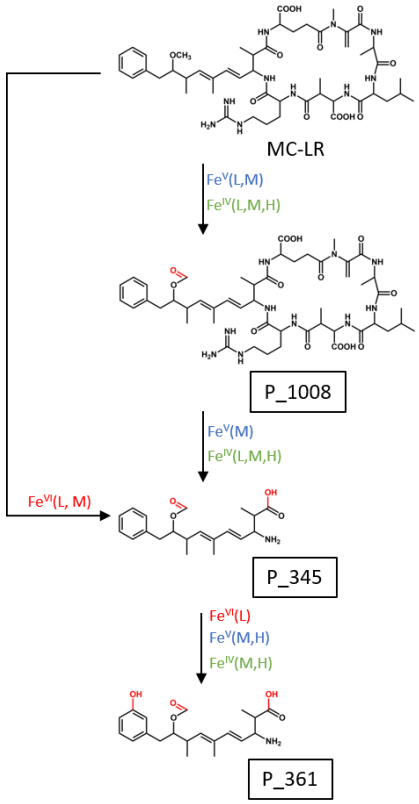

Fig. 2.19. *Scheme 2* - elimination of the methoxy group of the Adda diene, indicating products observed under high (H), medium (M), and low (L) concentrations of Fe^{VI}, Fe^{V} and Fe^{IV}.

2.3.3 Hydroxylation at the diene bond of the Mdha

Scheme 3 (Fig. 2.20) involved the hydroxylation of MCLR, followed by breakage of the cyclic structure, and finally the removal of the Adda amino acid. In this pathway, the peaks with a MW of 1028.5542 were related to hydroxylation at the Mdha. Multiple products of MW of 1044.5492 correspond to simultaneous mono-hydroxylation at the benzene ring and dihydroxylation at the Mdha. The double bond of the Mdha was an initiation site for the oxidation of the heptapeptide ring. In *Scheme 3*, we propose a cleavage at this site to form a MW of 1014.5386. Compounds with MWs of 1044.5492 and 1014.5386 undergo separation of the Adda chain and Mdha from the peptides to form a MW of 742.3974. Further oxidation resulted in the observed carboxylic acid with a MW of 758.3923. The amino group in the products of MW 758.3923 and 742.3974 could oxidize into a nitro group (see *Scheme 3*). The final oxidized product has a MW of 744.3766. Fe^{IV} species did not participate to give this transformation product.

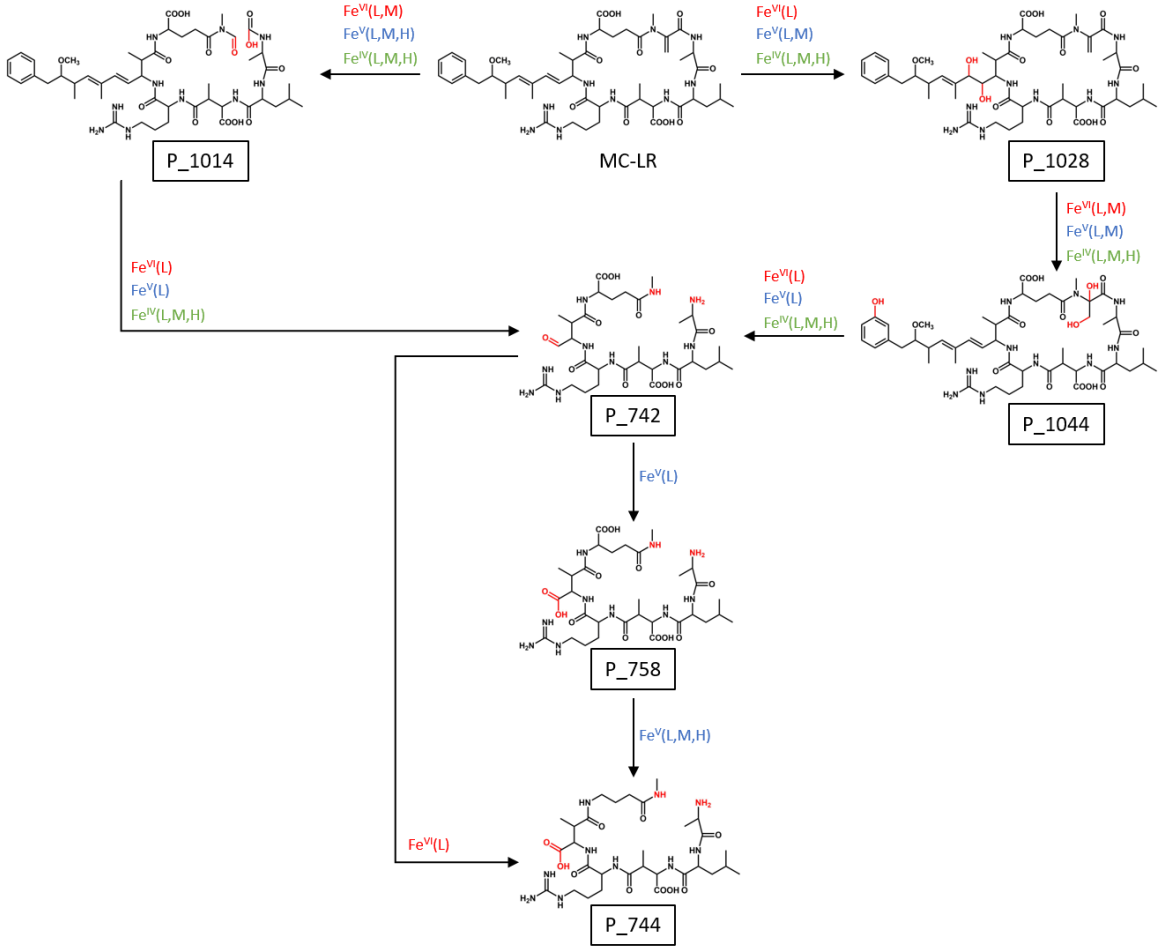

Fig. 2.20. *Scheme 3* - hydroxylation at the diene bond of the Mdha, indicating products observed under high (H), medium (M), and low (L) concentrations of Fe^{VI}, Fe^{V} and Fe^{IV}.

3. TRANSFORMATION PRODUCTS OF MICROCYSTIN-LR DEGRADATION BY FERRATE(VI), FERRATE(V), AND FERRATE((IV): INFLUENCE OF pH

3.1. Introduction

Increasing occurrence of cyanobacteria blooms (blue green algae) in eutrophied water is of pronounced concern worldwide (Pick, 2016; Sandrini, et al., 2016). Growth of cyanobacteria releases cyanotoxins of which microcystins (MCs) are among the priority hazards to animal and public health (Liyanage, et al., 2016). MCs are a group of cyclic heptapeptides, produced by *Microcystis aeruginosa* (Wood, 2016). MCs generate toxins which are damaging to the liver and the nervous system (Meneely and Elliott, 2013). Contamination by MCs has resulted in human poisoning (Weirich and Miller, 2014). Examples include the high prevalence of liver cancer in areas of the Chinese population which are dependent on surface drinking water (Hernández, et al., 2009; Tian, et al., 2013). Hepatic injury due to the use of MCs-contaminated water to treat more than 50 dialysis patients resulted in their deaths (Pouria, et al., 1998). Among the various identified MCs, microcystin-LR (MC-LR) is the common species detected in surface water (Hilborn, et al., 2007; Merel, et al., 2013). The structure of MC-LR consists of D-alanine, γ-linked-D-glutamic acid, D-*erythro*-*β*-methylaspartic acid (Adda), *N*-methyl dehydroalanine, and two variable amino acids, leucine (L) and arginine (R). MC-LR is highly stable for months or years in natural waters (Sharma, et al., 2012). Significantly, MC-LR can also persist in harsh environments, such as low pH and high temperature (Adamovsky, et al., 2015). The Adda group in MC-LR is one of the key constituents mainly responsible for its toxicity. The maximum level of 1.0 μg/L

of MC-LR in drinking water has been adopted as a guideline by the World Health Organization (WHO) (World Health Organization, 1997). Many investigations have been performed to seek efficient methods for detoxifying water contaminated with MC-LR (Merel, et al., 2013; Sharma, et al., 2012, 2017).

Physical adsorption/separation, chemical oxidation, and advanced oxidation processes (AOPs) have been studied to remove MC-LR in water (de la Cruz, et al., 2011; Fagan, et al., 2016; Lee and Walker, 2008; Sharma, et al., 2010; Sharma, et al., 2012; Svrcek and Smith, 2004; Teixeira and Rosa, 2005). These different treatment methods had mixed results. Physical methods potentially remove MC-LR in water, but it still remains in the environment. Chlorination contributes chlorinated derivatives of MC-LR and disinfection byproducts (DBPs) to the treated water (Zhang, et al., 2016). Applications of highly reactive hydroxyl ($^{\bullet}OH$) and sulfate ($SO_4^{\bullet-}$) radicals in AOPs (Antoniou, et al., 2010; He, et al., 2015; Sharma, et al., 2012) have shown efficient removal of MC-LR in water. In our recent studies, we have established the use of an iron oxide compound, ferrate(VI) ($Fe^{VI}O_4^{2-}$, Fe^{VI}), in detoxifying MC-LR in natural water (Jiang, et al., 2014). The half-life($t_{1/2}$) of the oxidation by Fe(VI) was 155 s for a dose of $Fe^{VI}O_4^{2-}$ as 2.2 mg L^{-1} at pH 7.0. Products from the oxidation of MC-LR were seen mainly from the hydroxylation of the double bond of the methyldehydroalanine (Mdha), the diene functionality, and the aromatic ring (Jiang, et al., 2014). The understanding of the hydroxylation of the aromatic moiety of the MC-LR by Fe^{VI} was explored by studying independently the formation of aromatic hydroxylated products obtained during oxidation carried out by the intermediate high-valent iron species, Fe^{V} (FeO_4^{3-}) and Fe^{IV}

(FeO_4^{4-}) (Chen, et al., 2017). In the literature, only a handful studies have been conducted on the oxidation of compounds by Fe^{VI}, Fe^{V}, and Fe^{IV} species (Kralchevska, et al., 2016; Machalová Šišková, et al., 2016; Sharma, et al., 2008, 2015, 2016a). Furthermore, almost no research has been carried out on determining the influence of pH on the mechanism of the reactions of these high-valent iron species with compounds.

In the present paper, we focus on studying the effect of pH on the formation of oxidized products (OPs) during the oxidation of MC-LR by Fe^{VI}, Fe^{V}, and Fe^{IV} species (Jiang, et al., 2014). The reasoning behind this investigation was two-fold: (i) the addition of solid Fe^{VI} species (e.g. potassium ferrate(VI), K_2FeO_4) to treat water with no buffer capacity may result in an increase of pH ($2Fe^{VI}O_4^{2-} + 5H_2O \rightarrow 2Fe^{3+} + 3/2O_2 + 10OH^-$), and it is imperative to learn what kind of OPs are formed under basic conditions. (ii) it is important to elucidate the effect of pH over the entire pH range from acidic to basic on the degradation pathways of the oxidation of MC-LR by Fe^{VI}, and subsequently by Fe^{V}, and Fe^{IV} species in water.

3.2. Experimental methods

3.2.1. Product studies

In this set of experiments, solids of salts of Fe^{VI} (K_2FeO_4), Fe^{V} (K_3FeO_4), and Fe^{IV} (Na_4FeO_4) were added into a buffered solution containing 5.00 µM MC-LR at pH 4.0, 7.0, and 9.0. Mixed solutions of Fe^{VI} and MC-LR were allowed to react until the characteristics color of Fe^{VI} disappeared. In the case of Fe^{V}/Fe^{IV} and MC-LR mixed solutions, the reactions were stopped immediately (<10 s) by adding excess hydroxylamine. Hydroxylamine as a quenching agent can stop any reactions that might

occur from the products of self-decomposition of Fe^{V} and Fe^{IV} with MC-LR (Machalová Šišková, et al., 2016). In addition, the salts of Fe^{V} have impurities of Fe^{VI}, which could interfere with the target reaction between Fe^{V} and MC-LR. Moreover, the self-decomposition of Fe^{IV} instantaneously forms Fe^{VI}, and hence an immediate addition of hydroxylamine could stop any possible reaction between Fe^{VI} and MC-LR. This approach allowed the study of only the reaction between Fe^{IV} and MC-LR. Products of reactions of Fe^{VI}, Fe^{V}, and Fe^{IV} with MC-LR were analyzed using liquid chromatography high resolution mass spectrometry. Details of the technique are provided in Chapter 2. Information on the products is available in Table 2.1.

3.3. Results and discussion

3.3.1. Influence of pH on Scheme 1: Hydroxylation of the Adda diene

In this *Scheme 1*, the products with MWs of 1028.5442 (P_1028), 1044.5492 (P_1044), 1026.6386 (P_1026), 794.3923 (P_794), 782.3923 (P_782), and 810.3872 (P_810) were formed during the oxidation of MC-LR by Fe^{VI}, Fe^{V}, and Fe^{IV} at different concentrations of oxidants and pH (Fig. 3.1). The di-hydroxylation of the benzene ring in MC-LR gave a product, P_1026. A product, P_1028 was formed by the 1,2 or 2,4 hydroxy addition to Adda diene of MC-LR. The subsequent aromatic hydroxylation of P_1028 yielded a product, P_1044. The elimination of the Adda chain from either P_1026 or P_1044 gave P_794 with an intact heptapeptide ring containing the C=O moiety. Further oxidation of P_794 by ferrates yielded a product, P_782. The product, P_810 was formed from the oxidation of –C=O in P_794 to a –COOH group (*Scheme 1*).

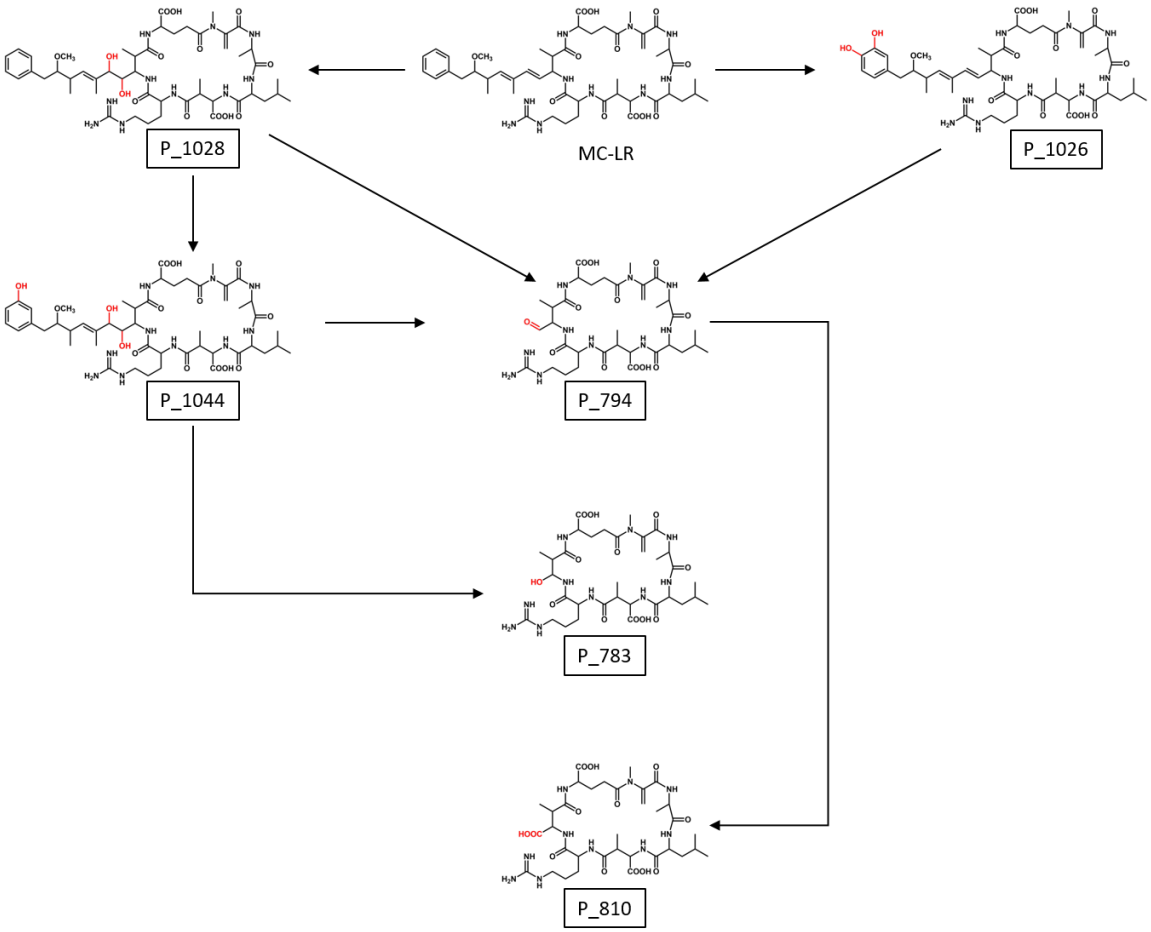

Fig. 3.1. *Scheme 1* - hydroxylation at the Adda diene by Fe^{VI}, Fe^{V} and Fe^{IV}.

The pH dependence of the products shown in *Scheme 1* is presented in Figs. 3.2-3.6. The formation of P_1026 by the oxidation of MC-LR by Fe^{VI}, Fe^{V}, and Fe^{IV} generally occurred predominately at an acidic pH (Fig. 3.2). In neutral media, this product was observed only in the Fe^{VI} oxidation of MC-LR. However, a basic pH was not favorable to the formation of P_1026 by Fe^{VI}. Both Fe^{V} and Fe^{IV} were able to oxidize MC-LR to P_1026 in a basic medium (Fig. 3.2). This suggests that aromatic hydroxylation of MC-LR by Fe^{V} and Fe^{IV} could occur in either acidic or basic pH media.

Hydroxylation of the Adda diene by Fe^{VI}, Fe^{V}, and Fe^{IV} was facilitated under acidic conditions (Figs. 3.3 and 3.4). All ferrate species could convert MC-LR to the product, P_1044, at pH 4.0 (Fig. 3.3). The intermediate product, P_1028, for the formation of P_1044 could also be seen at pH 4.0 (Fig. 3.4). Compared to pH 4.0, intensities of the P_1044 and P_1028 decreased significantly at pH 7.0 (Figs. 3.3 and 3.4). This indicates that the increase in pH from pH 4.0 to 7.0 produced a less favorable environment for the hydroxylation of the Adda diene of the MC-LR by ferrates. Interestingly, a further increase in pH showed the formation of P_1044 in basic pH 9.0. Almost no peak intensity or small intensity of the peak for product P_1028 was seen at pH 9.0. The product, P_1028, was the intermediate product of the hydroxylation of the diene of MC-LR before giving the product P_1044 (Fig. 3.3).

As shown in Fig. 3.5, the elimination of the Adda chain from the products, P_1026 and P_1044, to give a product, P_794, by Fe^{VI}, Fe^{V}, and Fe^{IV} could be seen over almost the entire pH range. However, intensities of the peak of this product suggest that an acidic environment was more favorable than neutral and basic conditions. The

oxidation of P_794 to P_810 by all ferrates usually had a similar trend with the pH as well (Fig. 3.6). A comparison of peak intensities between neutral pH and basic pH suggests that the formation of –COOH in the product, P_810, from the product, P_794, was facilitated by basic conditions (Fig. 3.6).

Fig. 3.7 presents the pH dependence of the formation of P_782 via the elimination of the Adda chain from P_1044. This step of elimination in *Scheme 1* was observed mostly at pH 4.0 (Fig. 3.7). This pH dependence for the formation of P_782 from P_1044 was seen for all oxidants (Fe^{VI}, Fe^{V}, and Fe^{IV}). At pH 7.0 and 9.0, Fe^{V} and Fe^{IV} did not yield the product, P_782. The formation of P_782 was shown in the oxidation of P_1044 by Fe^{VI}. No significant amount of P_794 at pH 9.0 was observed. Overall, the results of Fig. 3.7 indicate that the elimination of the Adda chain from the product, P_1044 was more pronounced in an acidic pH than in either a neutral or a basic pH.

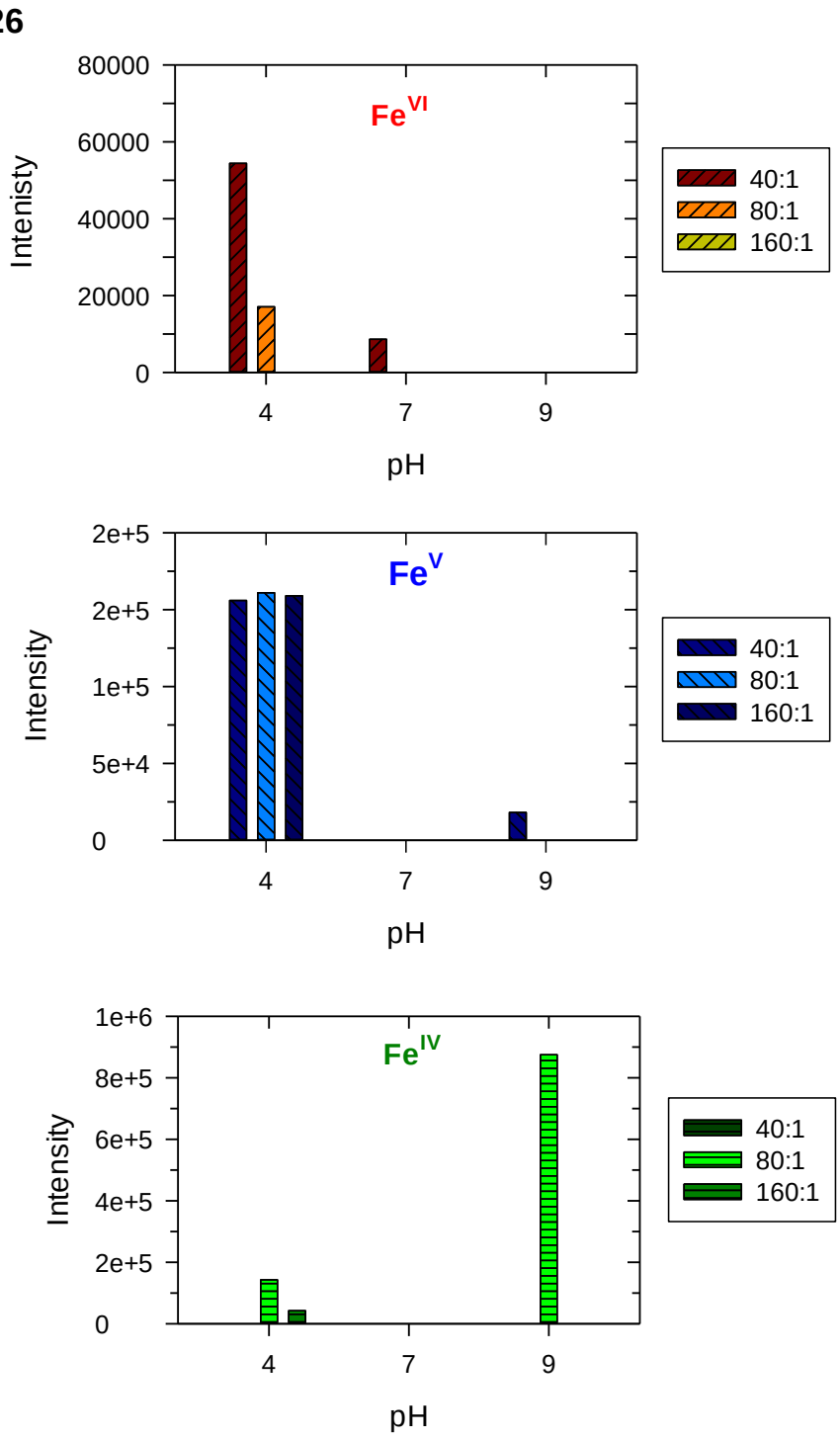

Fig. 3.2. Intensity of P_1026 during the oxidation of MC-LR by Fe^{VI}, Fe^{V}, and Fe^{IV} at different molar ratios of ferrates to MC-LR ([Ferrates] = 200-800 µM and [MC-LR] = 5 µM).

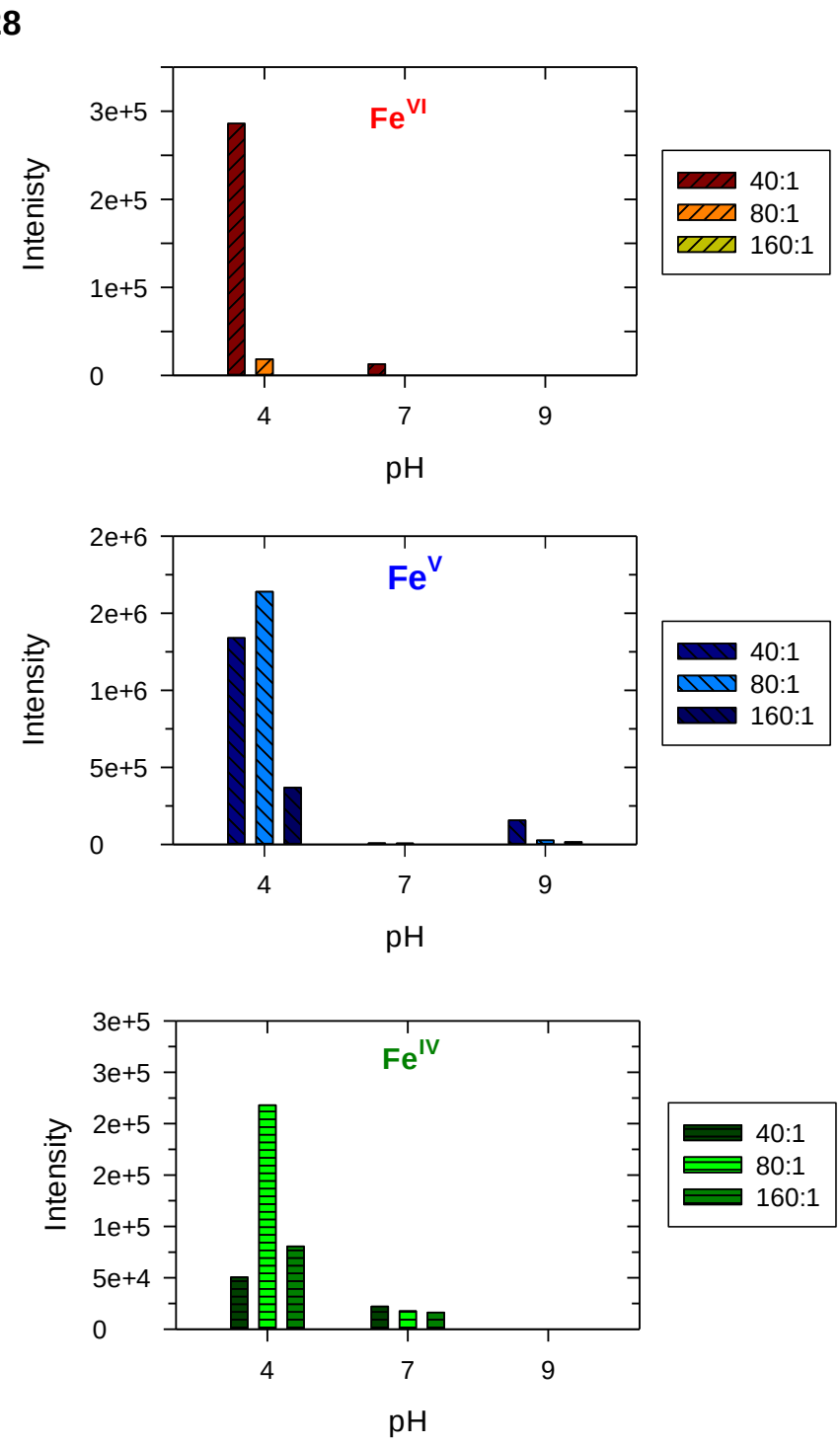

Fig. 3.3. Intensity of P_1028 during the oxidation of MC-LR by Fe^{VI}, Fe^{V}, and Fe^{IV} at different molar ratios of ferrates to MC-LR ([Ferrates] = 200-800 µM and [MC-LR] = 5 µM).

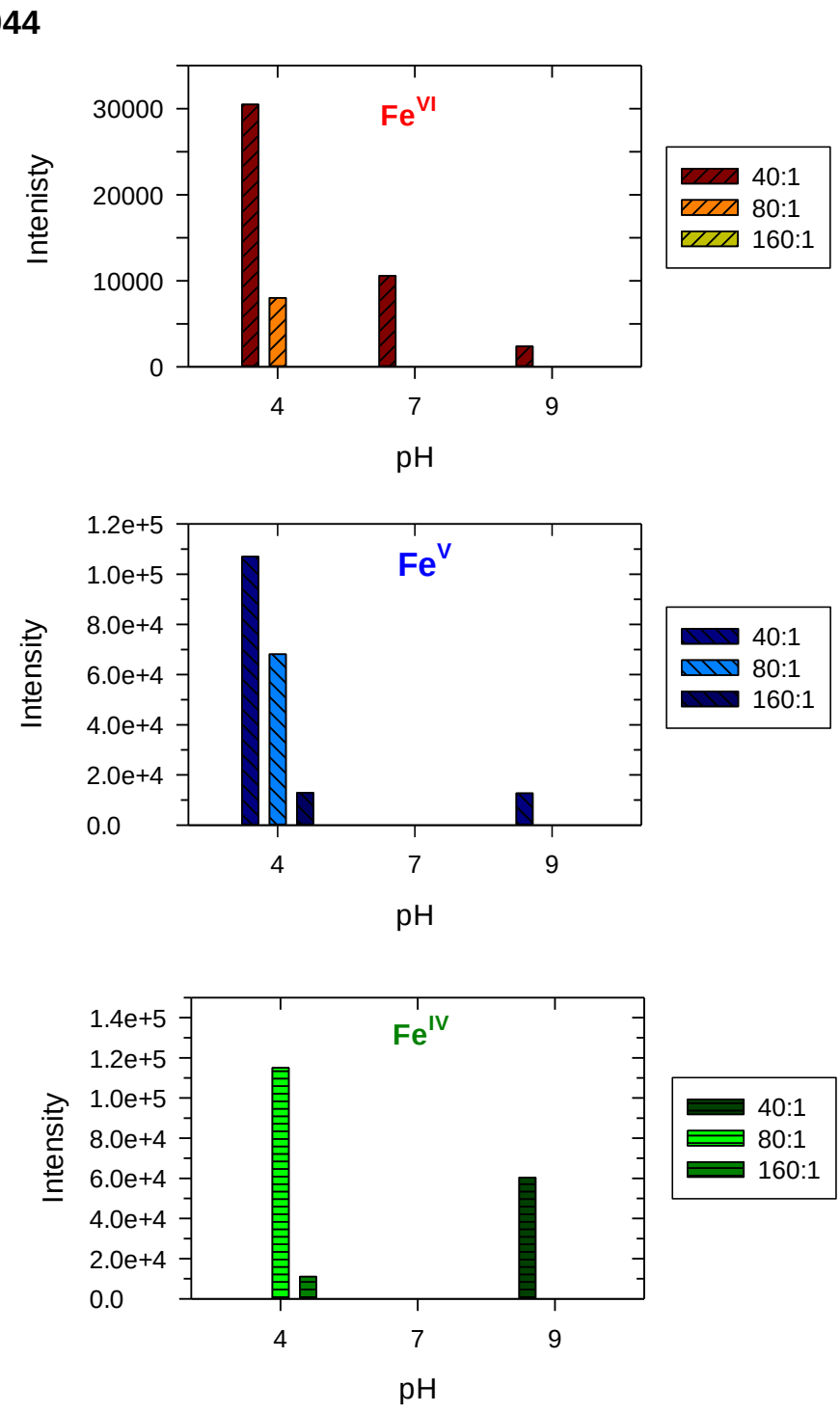

Fig. 3.4. Intensity of P_1044 during the oxidation of MC-LR by Fe^{VI}, Fe^{V}, and Fe^{IV} at different molar ratios of ferrates to MC-LR ([Ferrates] = 200-800 µM and [MC-LR] = 5 µM).

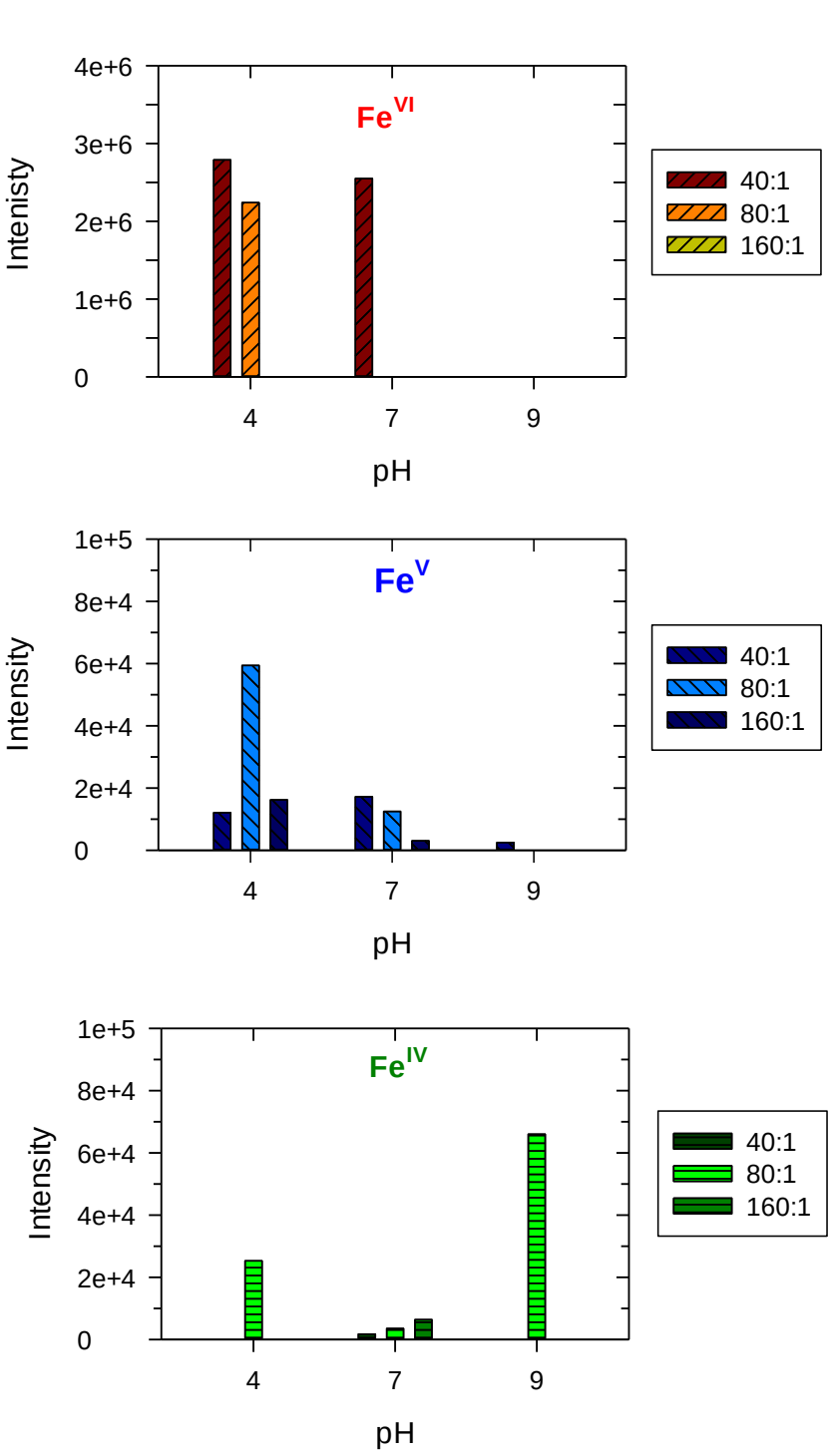

Fig. 3.5. Intensity of P_794 during the oxidation of MC-LR by Fe^{VI}, Fe^{V}, and Fe^{IV} at different molar ratios of ferrates to MC-LR ([Ferrates] = 200-800 µM and [MC-LR] = 5 µM).

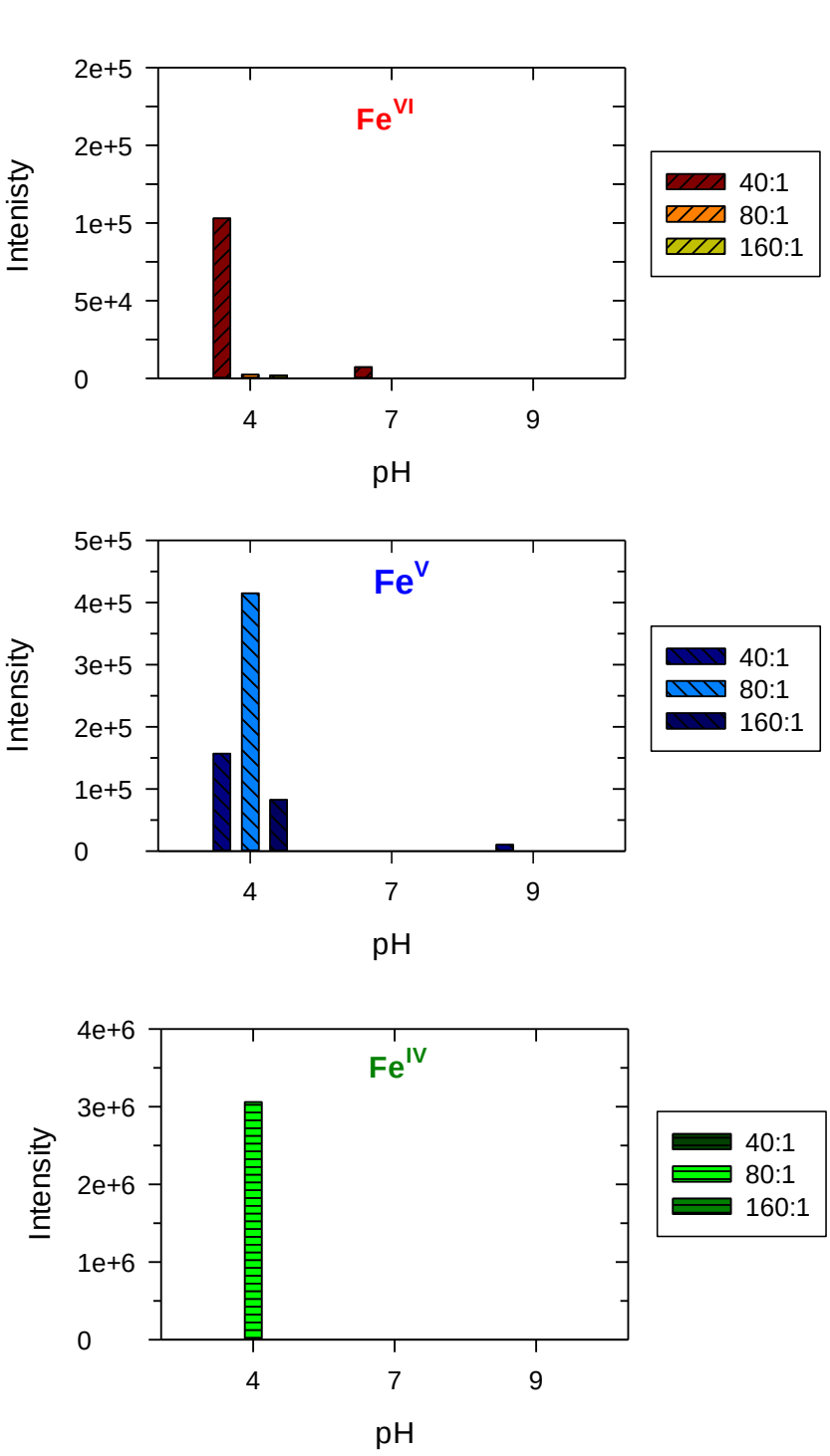

Fig. 3.6. Intensity of P_782 during the oxidation of MC-LR by Fe^{VI}, Fe^{V}, and Fe^{IV} at different molar ratios of ferrates to MC-LR ([Ferrates] = 200-800 µM and [MC-LR] = 5 µM).

3.3.2. Influence of pH on Scheme 2: Elimination of the methoxy group of the Adda diene

Scheme 2 involves three products from the oxidation of the methoxyl group of the Adda moiety (Fig. 3.8). Initially a compound with MW of 1008.5280 (P_1008) is formed, which is a formic ester of MC-LR (Antoniou, et al., 2008; Su, et al., 2013). Further oxidation of this compound resulted in two products with MWs of 345.1940 (P_345) and 361.1889 (P_361). Formation of a P_345 resulted from the breakage of the heptapeptide ring of P_1008. The aromatic hydroxylation of P_345 yielded P_361.

The influence of pH on the three products, P_1008, P_345, and P_361, from the oxidation of MC-LR by Fe^{VI}, Fe^{V}, and Fe^{IV} at three molar ratios of ferrates to MC-LR is presented in Figs. 3.9-3.11. The formation of P_1008 was not seen in the oxidation of MC-LR by Fe^{VI} at any of the studied pHs (Fig. 3.9). However, P_1008 was observed in the oxidation of MC-LR by Fe^{V} and Fe^{IV}. The formation of P_1008 was seen at all pHs. The oxidation of MC-LR by Fe^{V} had higher intensity under acidic pH than under either neutral or basic pH (Fig. 3.9). No such pH dependence was seen in the formation of P_1008 by the oxidation of MC-LR by Fe^{IV} (Fig. 3.9). Significantly, when Fe^{IV} was the oxidant, the formation of P_1008 was more prevalent under a basic condition at the lowest molar ratios of oxidant to MC-LR (Fig. 3.9).

P_345 and P_361 were seen in the oxidation of all three ferrate species (Figs. 3.10 and 3.11). This suggests that the formation of P_345 occurred without going through the P_1008 as was the case with oxidation of MC-LR by Fe^{V} and Fe^{IV} (see Fig. 3.10). Importantly, both P_345 and P_361 were observed over the entire pH range from

the acidic to basic pH range (Figs. 3.10 and 3.11). Also, similar intensities of these products were obtained at all concentrations of Fe^{VI} or Fe^{V} or Fe^{IV}. This indicates ferrates species not only reacted with MC-LR but were also consumed by self-decomposition reactions in water.

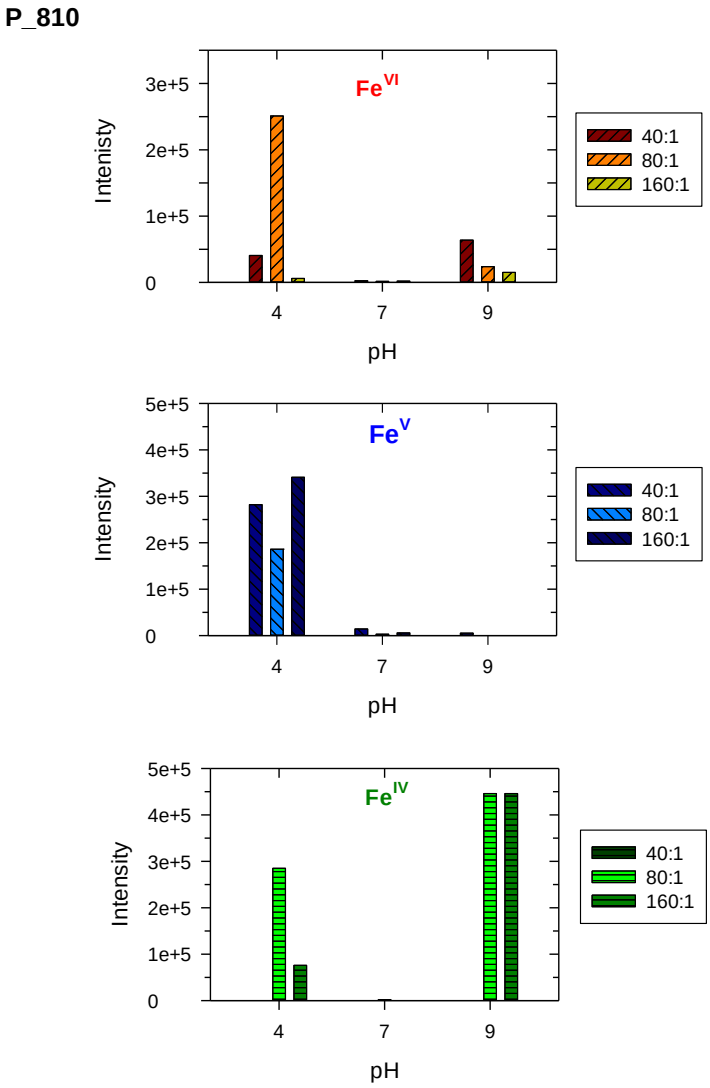

Fig. 3.7. Intensity of P_810 during the oxidation of MC-LR by Fe^{VI}, Fe^{V}, and Fe^{IV} at different molar ratios of ferrates to MC-LR ([Ferrates] = 200-800 µM and [MC-LR] = 5 µM).

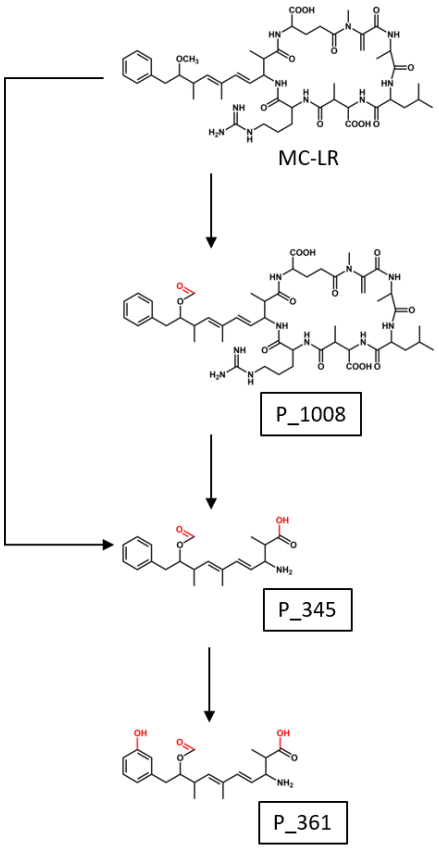

Fig. 3.8. *Scheme 2* - elimination of the methoxy group of the Adda diene by Fe^{VI}, Fe^{V} and Fe^{IV}.

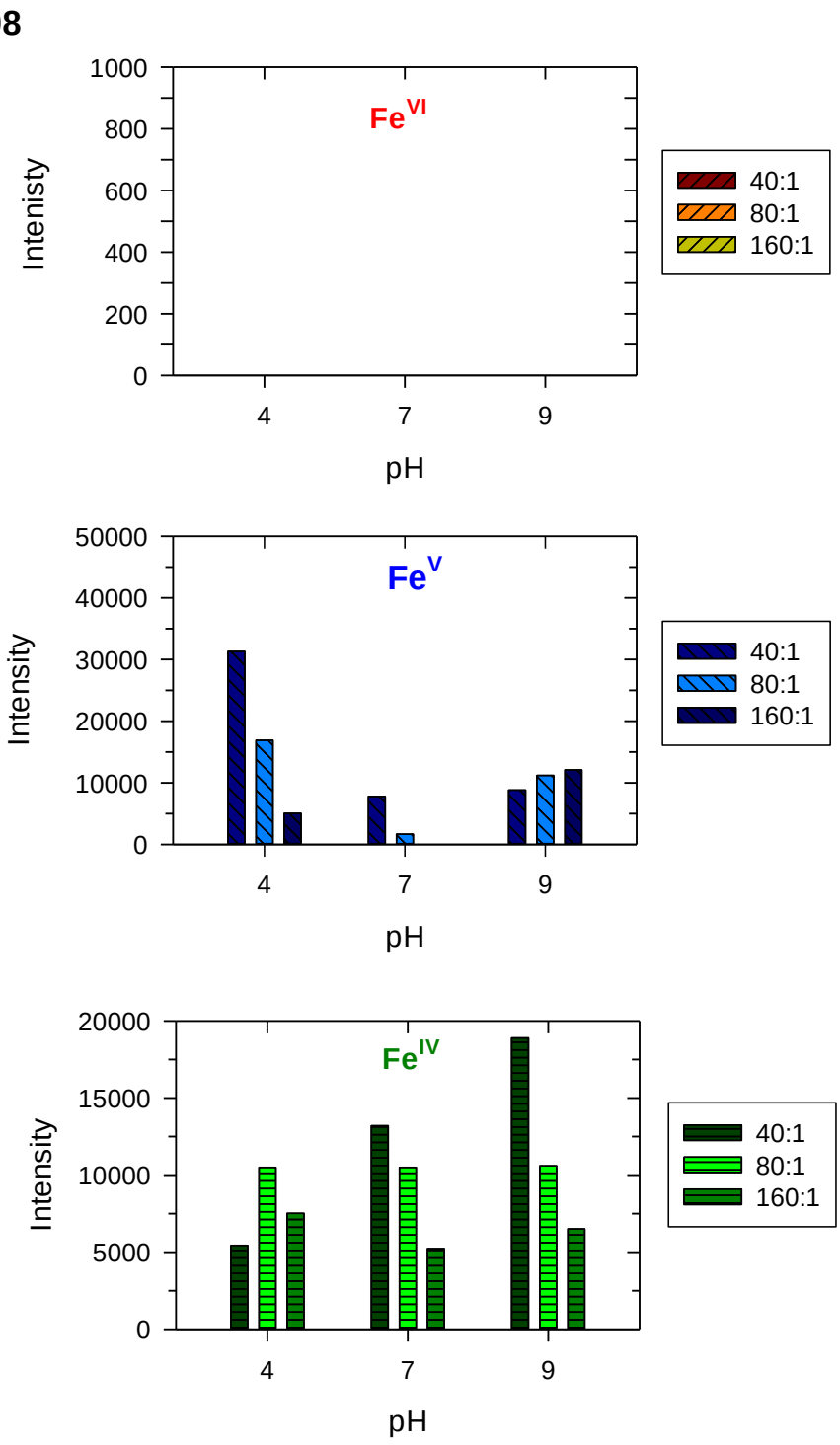

Fig. 3.9. Intensity of P_1008 during the oxidation of MC-LR by Fe^{VI}, Fe^{V}, and Fe^{IV} at different molar ratios of ferrates to MC-LR ([Ferrates] = 200-800 µM and [MC-LR] = 5 µM).

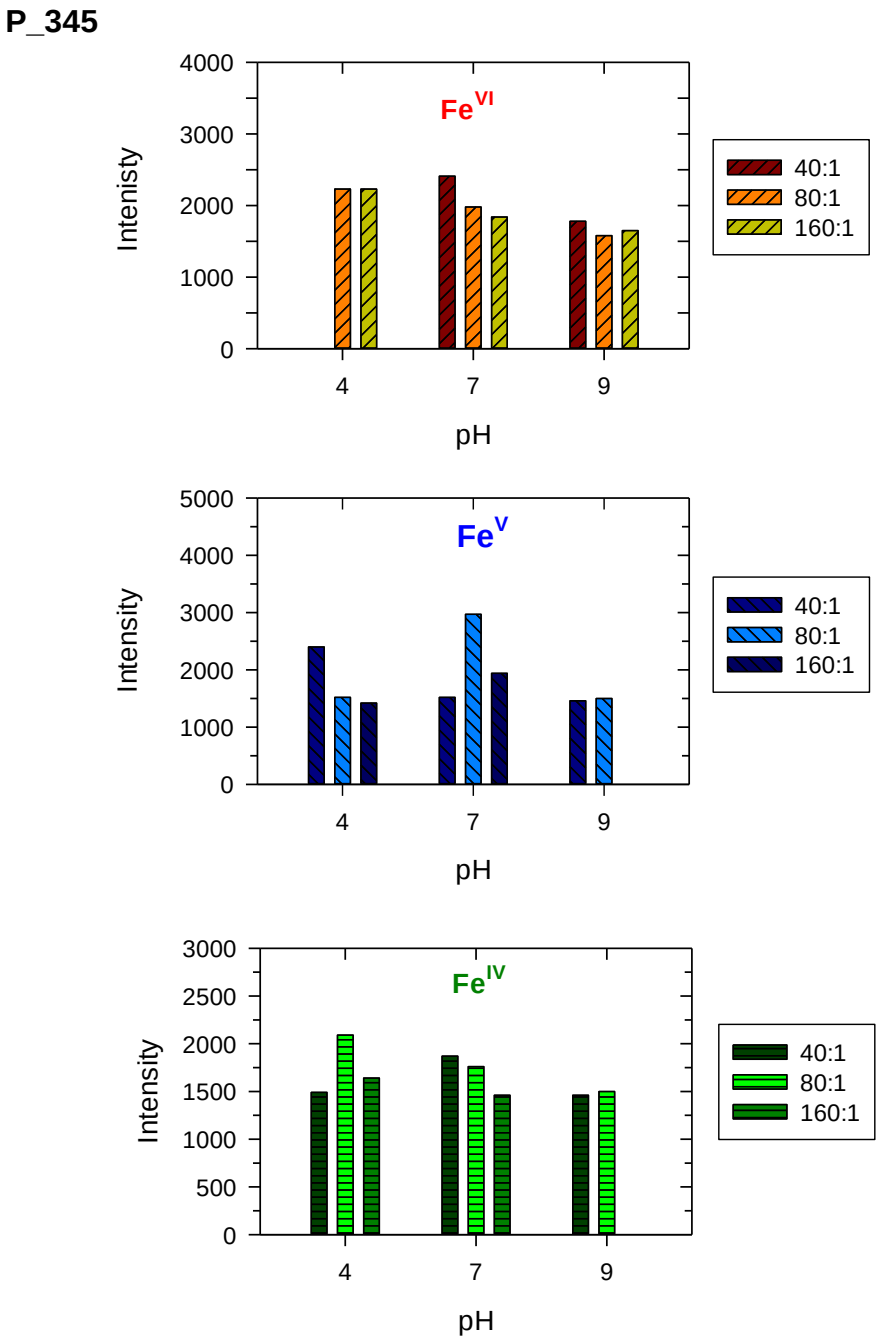

Fig. 3.10. Intensity of P_345 during the oxidation of MC-LR by Fe^{VI}, Fe^{V}, and Fe^{IV} at different molar ratios of ferrates to MC-LR ([Ferrates] = 200-800 µM and [MC-LR] = 5 µM).

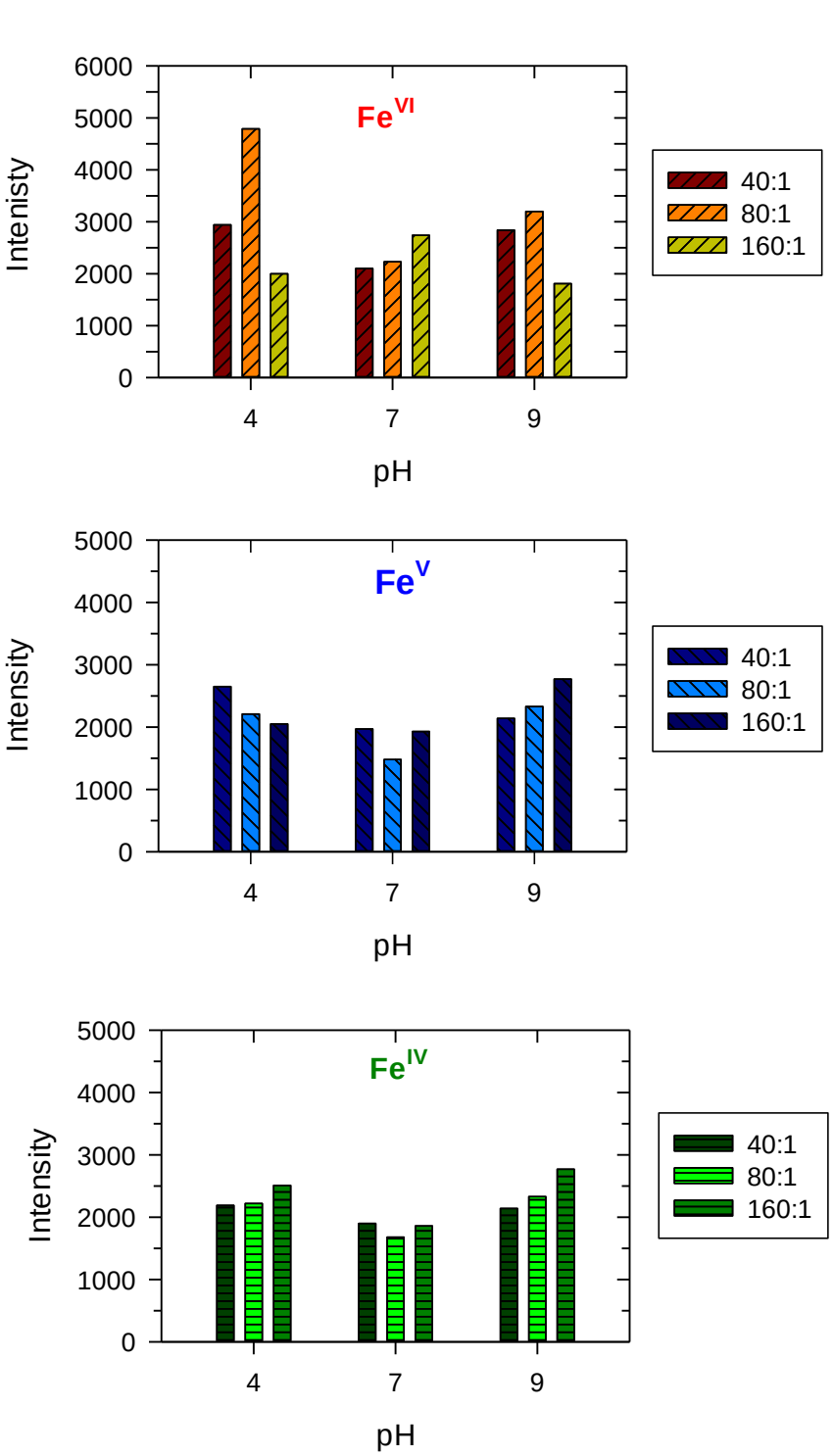

Fig. 3.11. Intensity of P_361 during the oxidation of MC-LR by Fe^{VI}, Fe^{V}, and Fe^{IV} at different molar ratios of ferrates to MC-LR ([Ferrates] = 200-800 µM and [MC-LR] = 5 µM).

3.3.3. Influence of pH on hydroxylation at the diene bond of the Mdha

Fig. 3.12 shows the hydroxylation at the Mdha of MC-LR, which resulted in a product with a MW of 1028.5542 (P_1028). The monohydroxylation of this product at the benzene ring gave a product with a MW of 1044.5492 (P_1044). The cleavage of the double bond of the Mdha by the oxidation of the heptapeptide ring yielded a product with a MW of 1014.536 (P_1014). As shown in *Scheme 3* of Fig. 3.12, the products, P_1044 and P_1014, formed a product with a MW of 742.3974 (P_742) via separation of the Adda chain and Mdha, respectively. Ferrate~~s~~ species further oxidized the P_742 and produced a compound with a carboxylic acid group with a MW of 758.3923 (P_758). The nitro group containing product was generated from P-758 that had a MW of 744.3766 (P_744) (Fig. 3.12).

The pH dependence of the products of the *Scheme 3* is given in Figs. 3.13-3.18. The formation of P_1044 through P_1028 by Fe^{VI}, Fe^{V}, and Fe^{IV} was preferable in an acidic medium compared to neutral and basic media (Fig. 3.14). In the case of the product P_1014, Fe^{VI} was able to form it only at a neutral pH (Fig. 3.14). In comparison, Fe^{V} and Fe^{IV} usually produced P_1014 at almost all concentrations over the entire pH range from 4.0 – 9.0 (Fig. 3.15). Both P_1044 and P_1014 resulted in P_742, which was mostly seen during the oxidation of MC-LR by Fe^{VI} at different pHs (Fig. 3.16). Since P_1014 resulting from oxidation by Fe^{VI} occurred mainly at a neutral pH, the formation of P_742 therefore predominantly resulted from P_1044 at acid and basic pH~~s~~. The product P_758 was formed mainly by Fe^{VI}. All species of ferrates (i.e. Fe^{VI}, Fe^{V}, and Fe^{IV}) gave the product, P_744, while the product P_758 appears to be an intermediate

during the oxidation of P_742 to P_744 by Fe^{V} and Fe^{IV} (see Figs. 3.16-3.18). All species of ferrates gave P_744 at pH 4.0. At pH 7.0, Fe^{VI} and Fe^{V} generated P_744, but Fe^{IV} was not able to produce this product (Fig. 3.18). In a basic medium, Fe^{VI} could not result in P_758 and P_744, and the final product of *Scheme 3* for the oxidation of MC-LR by Fe^{VI} was P_742. The final product of the oxidation of MC-LR by Fe^{V} and Fe^{IV} in *Scheme 3* (Fig. 3.12) under the basic medium was P_744.

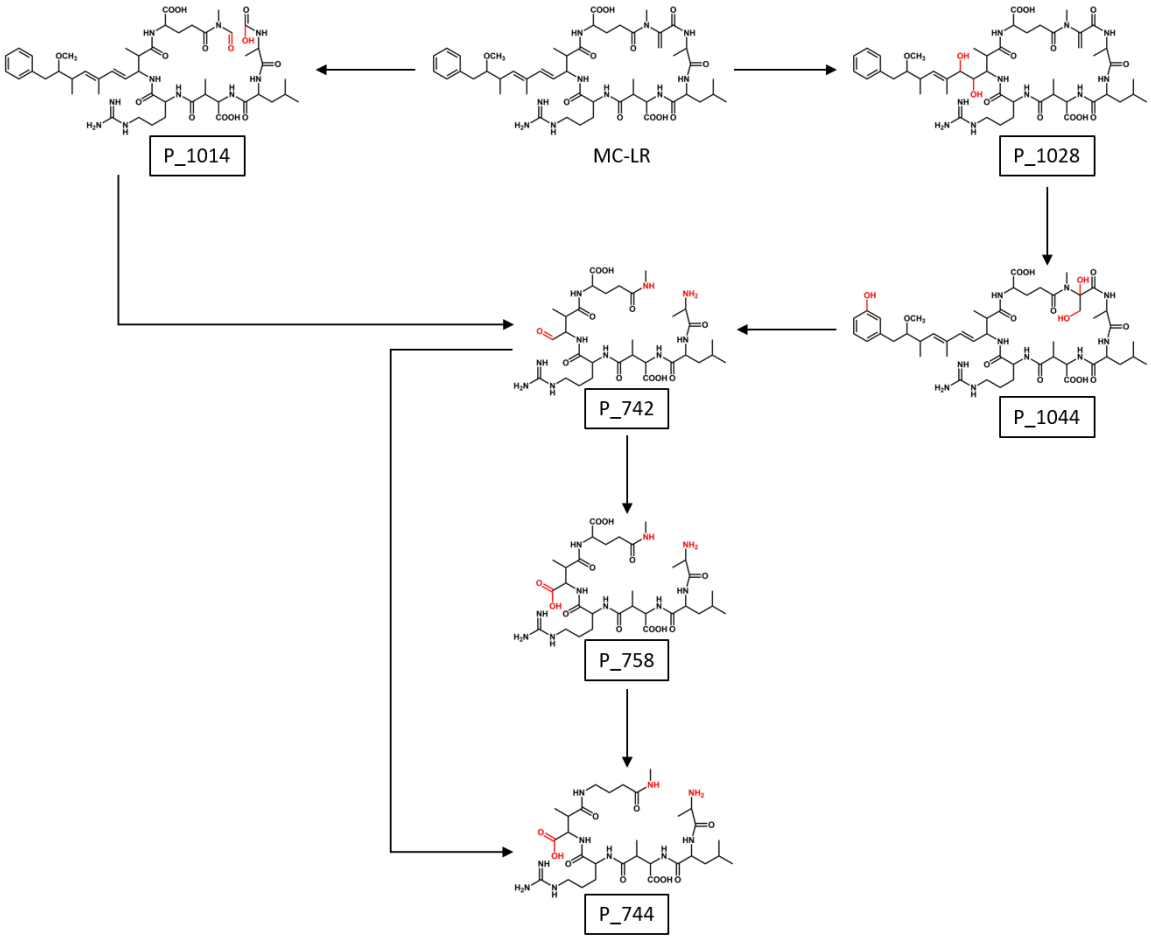

Fig. 3.12. *Scheme 3* - hydroxylation at the diene bond of the Mdha by Fe^{VI}, Fe^{V} and Fe^{IV}.

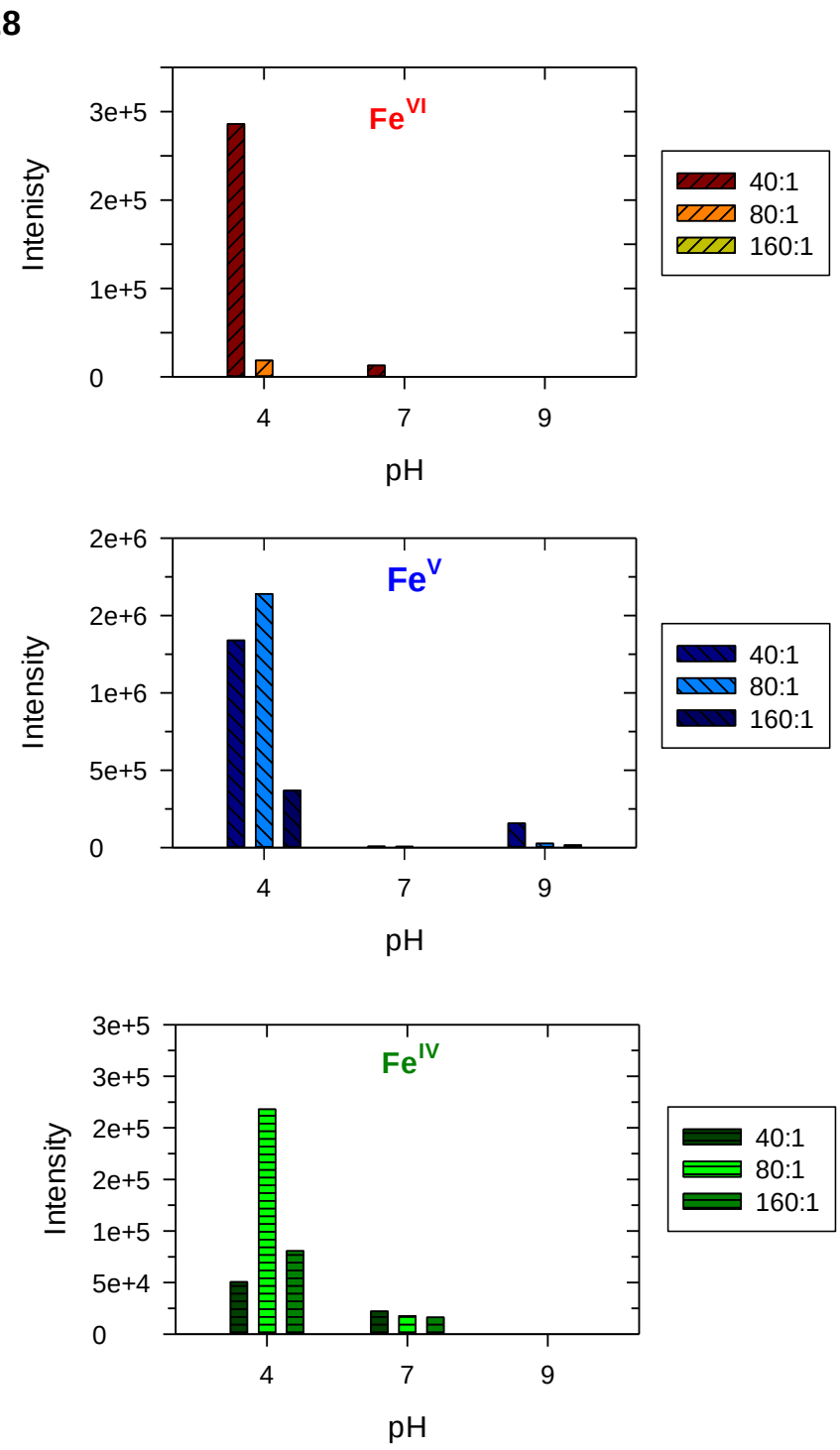

Fig. 3.13. Intensity of P_1028 during the oxidation of MC-LR by Fe^{VI}, Fe^{V}, and Fe^{IV} at different molar ratios of ferrates to MC-LR ([Ferrates] = 200-800 µM and [MC-LR] = 5 µM).

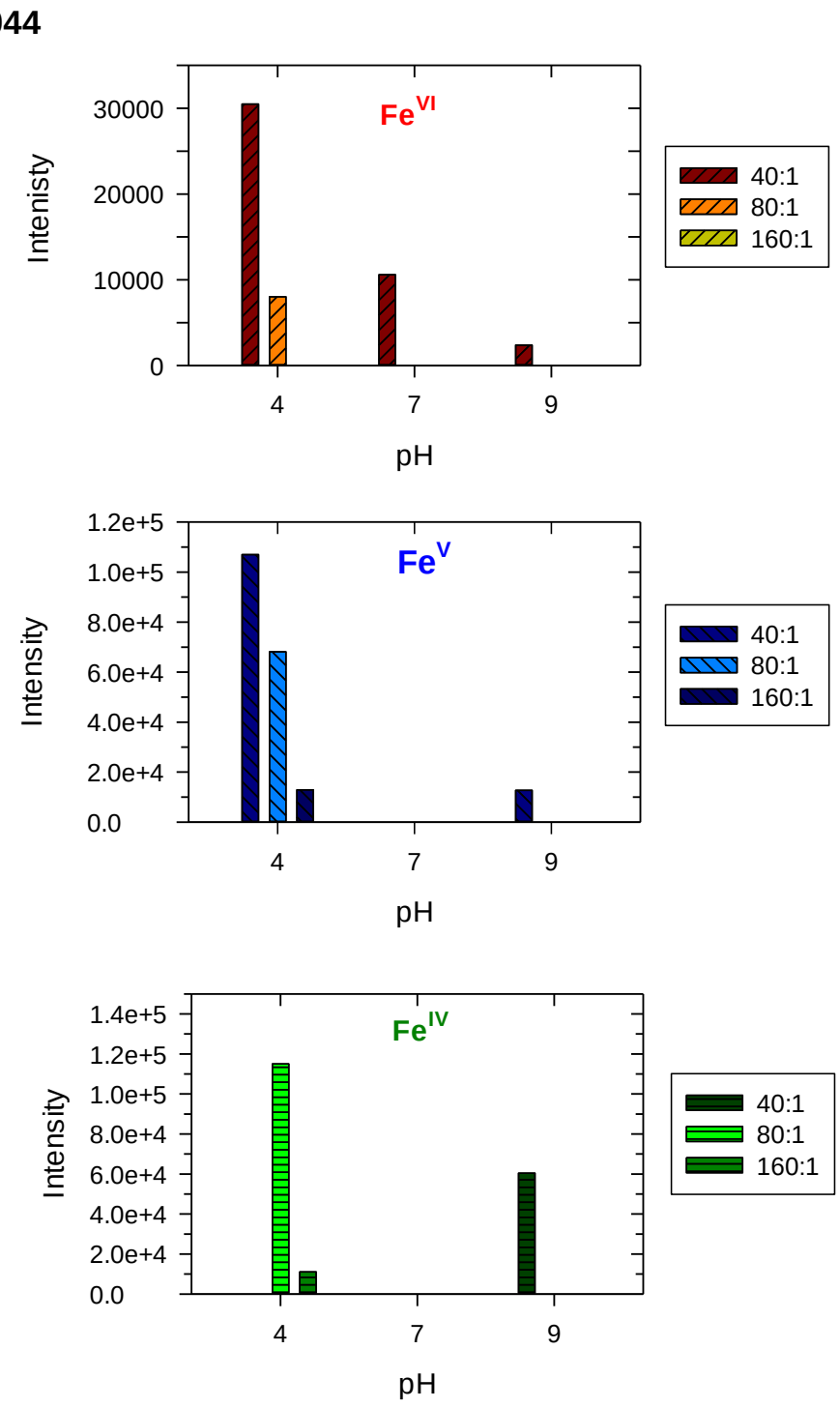

Fig. 3.14. Intensity of P_1044 during the oxidation of MC-LR by Fe^{VI}, Fe^{V}, and Fe^{IV} at different molar ratios of ferrates to MC-LR ([Ferrates] = 200-800 µM and [MC-LR] = 5 µM).

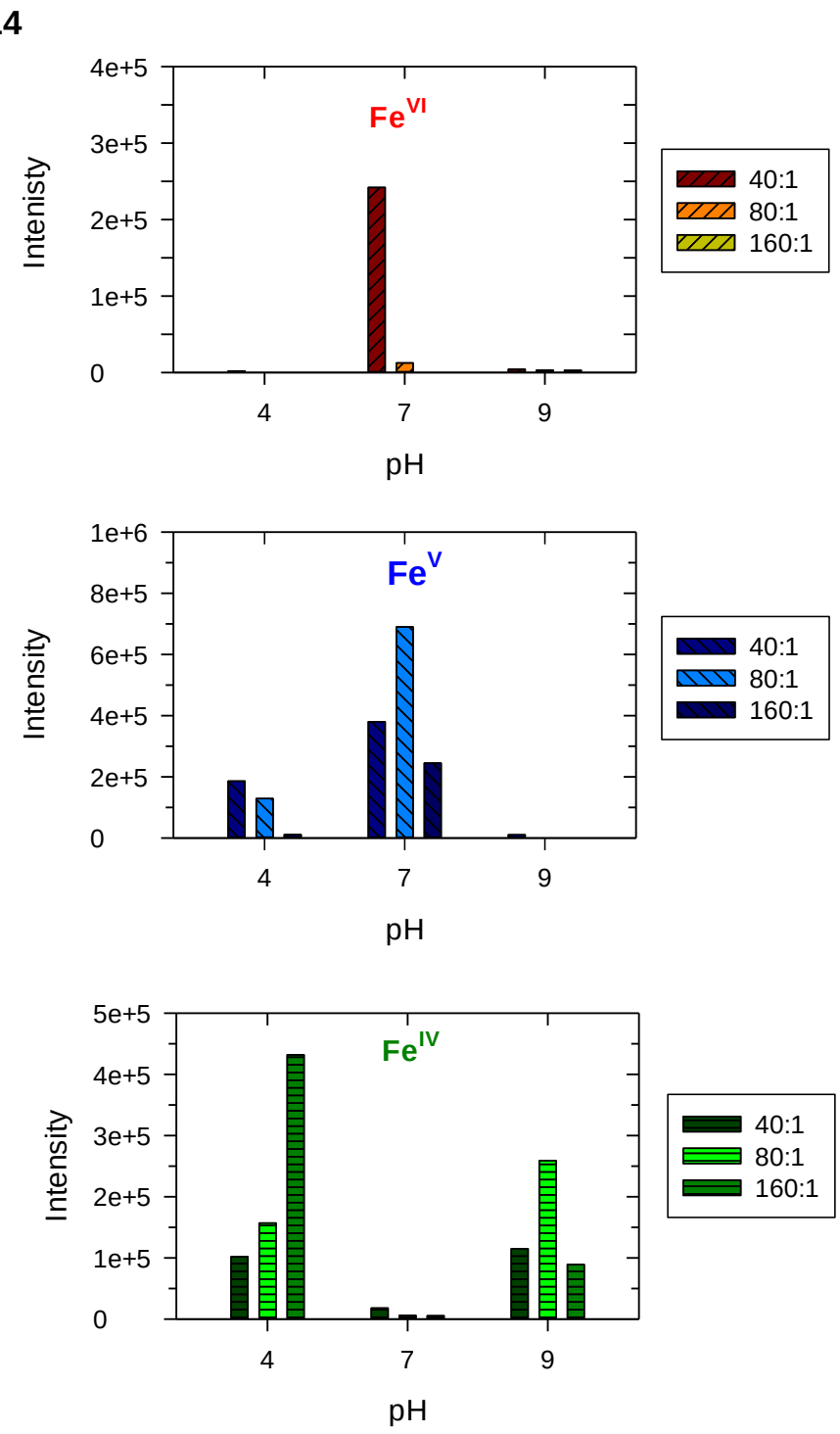

Fig. 3.15. Intensity of P_1014 during the oxidation of MC-LR by Fe^{VI}, Fe^{V}, and Fe^{IV} at different molar ratios of ferrates to MC-LR ([Ferrates] = 200-800 µM and [MC-LR] = 5 µM).

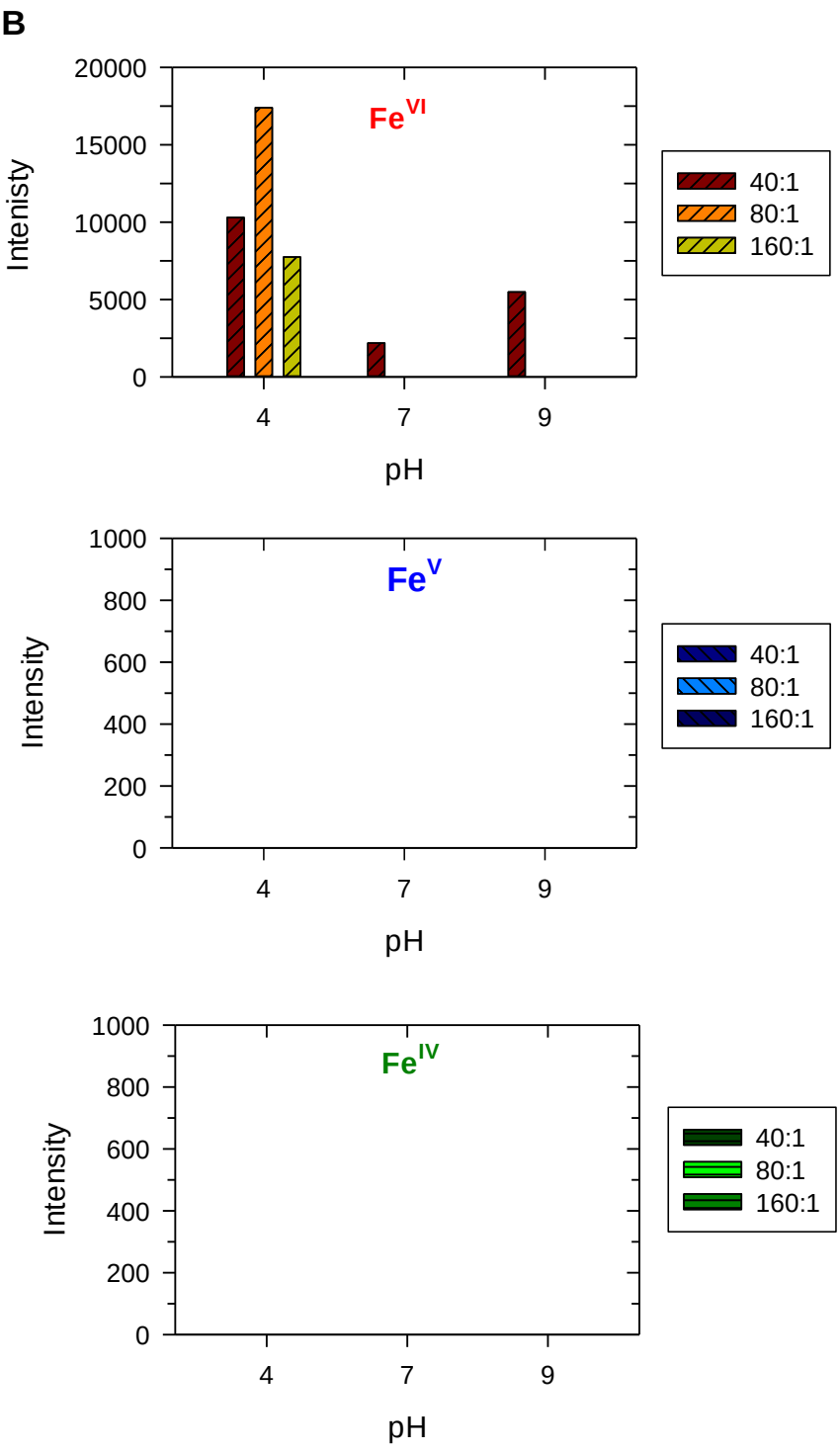

Fig. 3.16. Intensity of P_742 during the oxidation of MC-LR by Fe^{VI}, Fe^{V}, and Fe^{IV} at different molar ratios of ferrates to MC-LR ([Ferrates] = 200-800 µM and [MC-LR] = 5 µM).

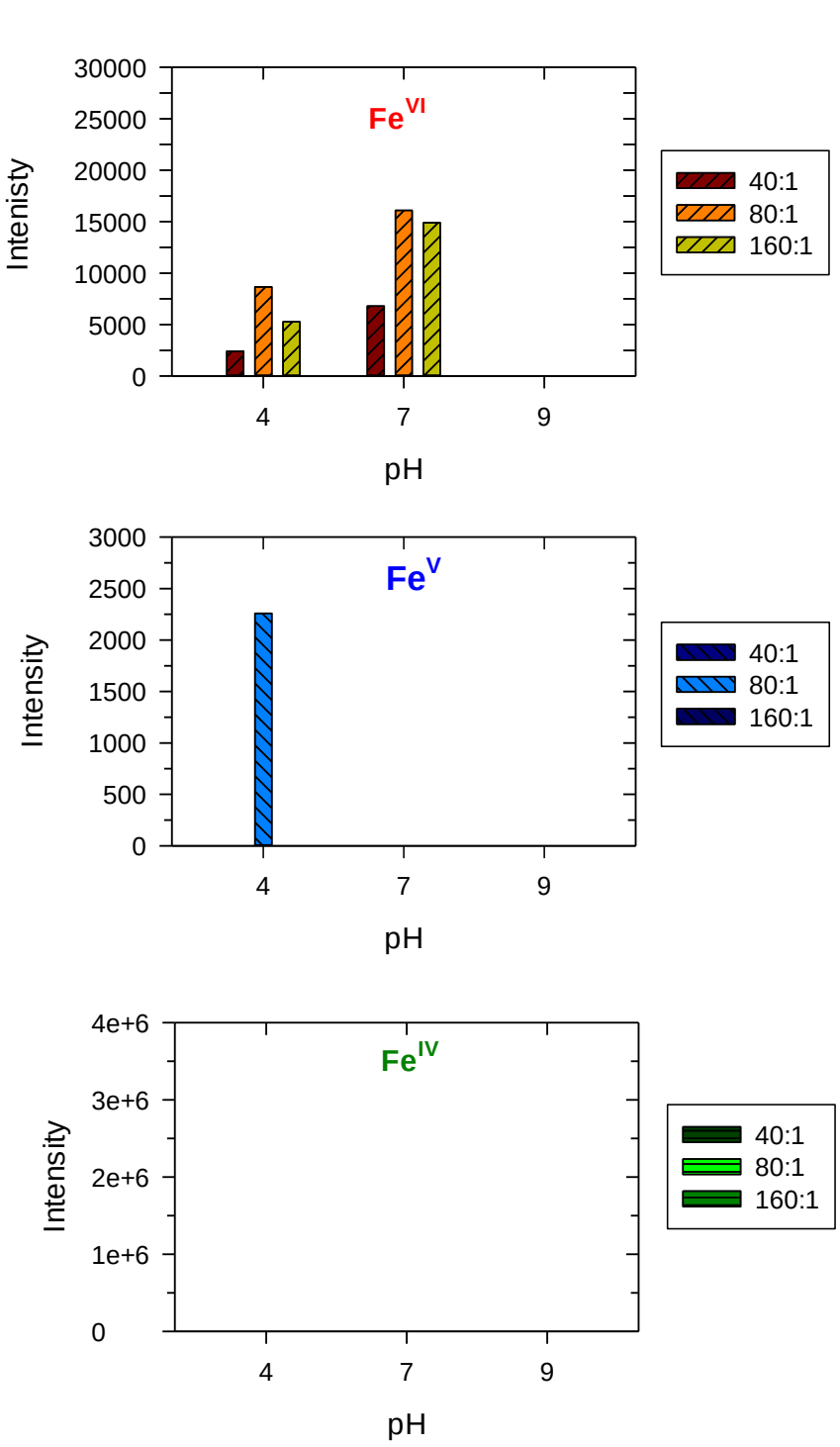

Fig. 3.17. Intensity of P_758 during the oxidation of MC-LR by Fe^{VI}, Fe^{V}, and Fe^{IV} at different molar ratios of ferrates to MC-LR ([Ferrates] = 200-800 µM and [MC-LR] = 5 µM).

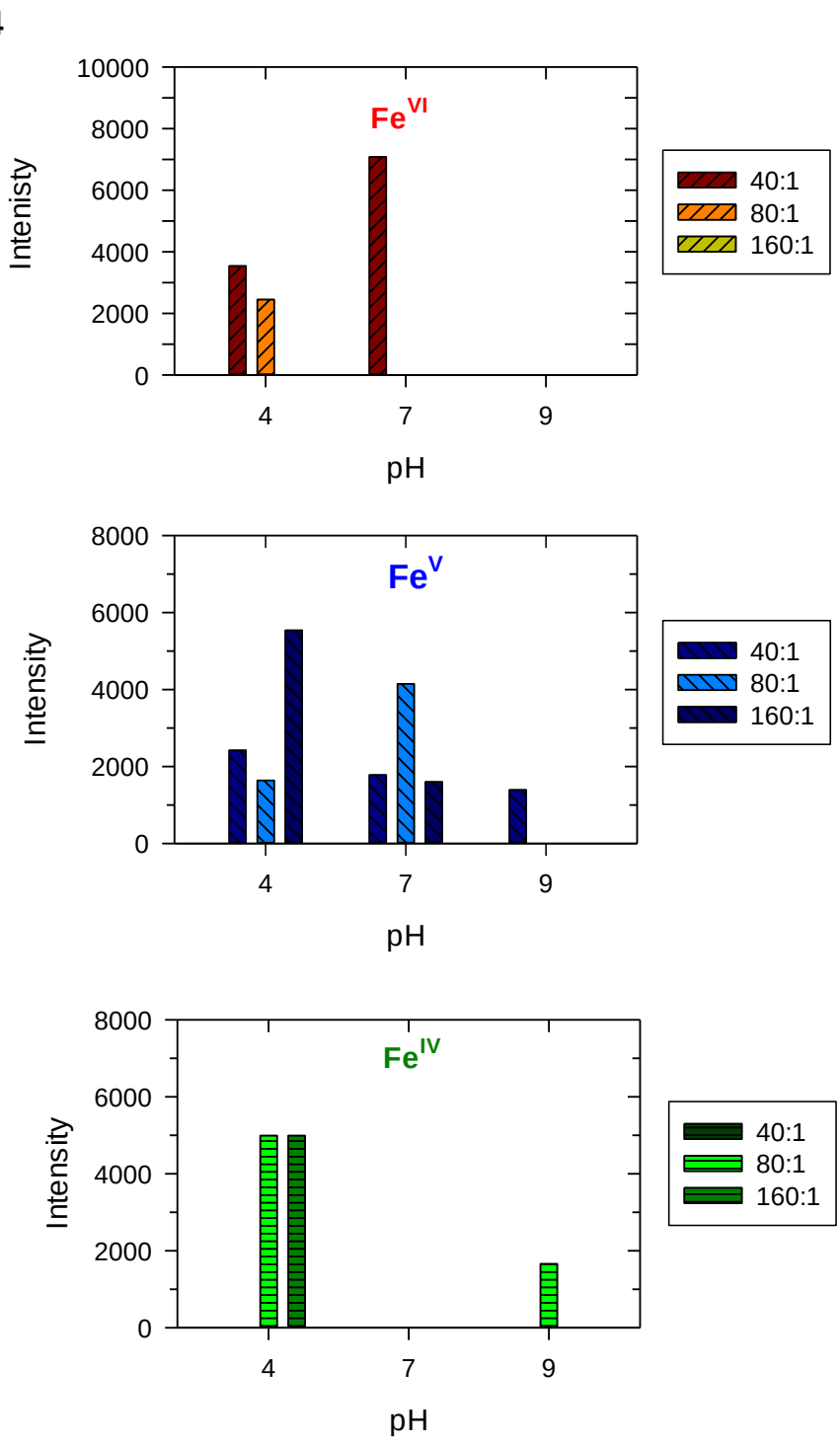

Fig. 3.18. Intensity of P_744 during the oxidation of MC-LR by Fe^{VI}, Fe^{V}, and Fe^{IV} at different molar ratios of ferrates to MC-LR ([Ferrates] = 200-800 µM and [MC-LR] = 5 µM).

4. OXIDATION OF SULFADIAZINE BY FERRATE(VI): KINETICS AND OXIDIZED PRODUCTS

4.1. Introduction

Pharmaceuticals in water and wastewater have emerged as one of the most important public and ecological health concerns (Cizmas, et al., 2015; Carvalho and Santos, 2016). The consumption of pharmaceuticals has increased because of an increase in the world population and of the aging population in industrialized countries (aus der Beek, et al., 2016; Cizmas, et al., 2015). An overuse of pharmaceuticals has caused growing concern because their release into the environment presents potential risks to human health and ecosystems (Carraro, et al., 2016; Hu, et al., 2017). Generally, pharmaceuticals are only slightly degraded or even unchanged as the parent compounds are released into wastewater treatment plants and subsequently enter into the aquatic environment (Cizmas, et al., 2015; Hu, et al., 2017). In addition, the direct input by the use of drugs in aquaculture facilities and the indirect input through manure application during agricultural activities as well as release from manufacturing sites, hospitals, and nursing homes have greatly contributed to the widespread occurrence of pharmaceuticals in natural waters (Bu et al., 2013; Carraro, et al., 2016). Recent studies also indicated that many pharmaceuticals are persistent or pseudo-persistent in the environment, which ultimately lead to their bioaccumulation in aquatic organisms of different trophic levels. This has resulted in the exertion of adverse effects on non-target organisms (Bu, et al., 2013; Sharma, et al., 2016b).

Antibiotics are among various pharmaceuticals that have received a great deal of attention in the last two decades (Carvalho and Santos, 2016; Kim, et al., 2013; Meng, et al., 2016). The occurrence of antibiotics in the environment has resulted in the growth of antibiotic resistant bacteria (ARBs) and antibiotic resistant genes (ARGs) (Ben, et al., 2017; Sharma, et al., 2016b). According to the World Health Organization, ARBs are the one of the most important global health problems of this century (World Health Organization, 2014). Sulfonamides are among antibiotics which are widely used in veterinary and human medicines (Chen, et al., 2015; Hoff, et al., 2016). They may enter into the environment through leaching from manure and effluents of aquaculture ponds and wastewater. The present paper focuses on sulfadiazine (SDZ, 4-amino-N-(2-pyrimidinyl) benzenesulfonamide), which is extensively used as veterinary medicine and is considered as a high priority sulfonamide because of its great potential to enter into the environment (Feng, et al., 2016c). Notably, Bu et al. (2013) recently reviewed the existing studies and occurrence data of SDZ in China, and reported its concentrations ranging from ND (not detected) to 505 ng/L in surface waters.

Many studies have been forthcoming to effectively treat antibiotics in water before their release into the environment. The treatment techniques include biological treatment, adsorption, membrane processes, chlorination, electrochemical means, and advanced oxidation technology (Barbosa, et al., 2016; Ganiyu, et al., 2015; Haddad, et al., 2015; Moreira, et al., 2016; Oturan and Aaron, 2014; Polesel, et al., 2016; Pérez, et al., 2017; Verlicchi, et al., 2015; Yu, et al., 2016). Of these approaches, oxidative technologies are promising because the treatment also eliminates antibiotic activities of

the parent compound. In the current paper, we explore the use of an iron-based oxidant, ferrate(VI) ($Fe^{VI}O_4^{2-}$, Fe^{VI}), to oxidize SDZ in water. Fe^{VI} has been investigated as a green chemical to transform pharmaceuticals including sulfonamides (Jiang, 2014; Karlesa, et al., 2014; Kralchevska, et al., 2016; Machalová Šišková, et al., 2016; Sharma, et al., 2008, 2016a; Yang, et al., 2016; Zhou and Jiang, 2015b). Most of the studies of sulfonamides were performed on sulfamethoxazole (SMX, 4-amino-*N*-(5-methylisoxazole-3-yl)-benzenesulfonamide), but no detailed studies were conducted on the oxidation of SDZ by Fe^{VI}. Products obtained were from the attacks on the aniline and isoxazole moieties as well as the breakage of the S-N bond (Kim, et al., 2015; Sharma, et al., 2015; Sharma, et al., 2006a; Zhou and Jiang, 2015b). Particularly, a pathway involving the extrusion of SO_2 has not been shown in the oxidation of sulfonamides by Fe^{VI}. In this paper, we demonstrate for the first time the products identified after SO_2 extrusion from the transformation of SDZ by Fe^{VI}.

Objectives of the paper are: (i) to study the kinetics of the reaction between Fe^{VI} and SDZ as a function of pH and to determine the species-specific rate constants, and (ii) to identify the transformation products of the oxidation of SDZ by Fe^{VI} by a liquid chromatography-mass spectrometry/mass spectrometry (LC-MS/MS) technique.

4.2. Materials and methods

4.2.1 Chemicals and reagents

Sulfadiazine, sodium dihydrogen phosphate, and sodium borate phosphate were obtained either from Fisher-Scientific (Austin, TX, USA) or Sigma-Aldrich (St. Louis, MO, USA). The purity of the chemicals was greater than 97%, and they were used

without further purification. Organic solvents of methanol and acetonitrile used in the high-performance liquid chromatography (HPLC) were obtained from Fisher-Scientific. Solid potassium ferrate (K_2FeO_4) of ~98% purity was synthesized by the wet chemical technique (Luo, et al., 2011). Solutions of Fe^{VI} were prepared by dissolving solid K_2FeO_4 in 1 mM $Na_2B_4O_7 \cdot 10H_2O$/5 mM Na_2HPO_4 at pH 9.0. In this solution, Fe(VI) is sufficiently stable to perform experiments. Absorbance of Fe^{VI} solutions was conducted at a wavelength of 510 nm using a UV-Visible spectrophotometer. An extinction coefficient, ε_{510nm} = 1150 M^{-1} cm^{-1}, was used to determine the concentration of Fe^{VI}. All solutions were made in water that was obtained from a purification system (18 MΩ cm Milli-Q Millipore, Waters Alliance, Milford, MA, USA). In kinetic experiments, the solution of sulfadiazine was prepared by dissolving the solid compounds in a 10 mM Na_2HPO_4 buffer-acetone (85:15) solution. The pH of the solution was adjusted by adding either NaOH or phosphoric acid. In the product analysis of the oxidation of SDZ by Fe^{VI}, the solution of SDZ was in the buffer solution at pH 9.0.

4.2.2. Stopped-flow experiments

Experiments were conducted under pseudo-first-order conditions to perform the kinetics of the reactions between Fe^{VI} and SDZ. Under this condition, the concentrations of SDZ was higher than the Fe(VI) concentration. The kinetic measurement was performed using a stopped-flow spectrophotometer (SX-20 MV, Applied Photophysics, Surrey, UK). Kinetic traces were monitored at a wavelength of 510 nm. Results from the stopped-flow spectrophotometer were analyzed using the nonlinear least-square algorithm of the SX-20 MV Global Software (Applied Photophysics, Surrey, UK). Six

replicate runs were made to determine averaged rate constants. The pseudo-first-order rate constants were evaluated by subtracting the observed rate constants for the reaction from the rate constants of the control (i.e., Fe(VI) decay without SDZ) at each studied pH).

4.2.3 Oxidized product experiments

The oxidized products (OPs) of SDZ by Fe(VI) were determined using solid phase extraction-liquid chromatograph mass spectrometry (SPE-LC-MS) (Feng, et al., 2016a). Chromatographic separation was carried out by a Thermo BDS Hypersil C_{18} column (2.1 mm × 100 mm, particle size 2.4 μm) (Thermo Fisher Scientific, Waltham, MA, USA) at a flow rate of 200 μL/min and 30 °C. The mobile phase consisted of 0.3% formic acid in water (A) and methanol (B). The linear gradient started with 90% A, which was held for 2 min, decreased to 10% in 1 min, maintained for 23 min, returned to the initial condition in 1 min, and followed by an 8 min equilibration. The injection volume of each sample was 10 μL, and the total elution time was 35 min.

MS detection was performed using an Agilent 1260 Infinity HPLC coupled with a hybrid quadrupole time-of-flight mass spectrometer (LC-MS-Triple TOF 5600, AB Sciex, Foster City, CA) operating in positive ion mode using an electrospray interface (ESI) source. The mass range of the TOF MS was *m/z* 70 to 700. The other experimental parameters were set as follows: nebulizer gas (gas 1), 55 psi; heater gas (gas 2), 55 psi; curtain gas, 35 psi; temperature, 550 °C; ionspray voltage floating, 5500 V; declustering potential, 80 V; and collision energy, 10 V. All gases used were nitrogen. Following the MS analysis, the protonated molecular ions $[M + H]^+$ of certain OPs were chosen as the

parent ions to yield the characteristic MS/MS fragments using the product ion mode. Additionally, the Q-TOF MS was automatically calibrated using an APCI positive calibration solution delivered via a calibration delivery system (AB Sciex, Concord, ON, Canada). The LC-MS data were acquired by Analyst TF software (Version 1.6, AB Sciex, Concord, ON, Canada) and processed by PeakView software (Version 1.2, AB Sciex, Concord, ON, Canada).

4.3. Results and discussion

4.3.1. Kinetics

Initially, the reaction between Fe^{VI} and SDZ was studied at pH 8.94 by observing the decay of Fe^{VI} as a function of time under pseudo-order conditions in which SDZ was in excess. As shown in Fig. 4.1, the decrease in the absorbance of Fe^{VI} with time follows nicely the exponential decay. This suggests that the rate of the reaction is first-order with respect to the concentration of Fe^{VI}. The kinetic traces of Fe^{VI} were repeated five more times, and the first-order rate constant (k_1) at pH 9.0 was obtained as $(3.78\pm0.34)\times10^{1}$ $M^{-1}s^{-1}$.

Next, similar experiments were conducted at pH 7.00 by varying the concentrations of SDZ. Decay curves of Fe^{VI} with time at different levels of SDZ were evaluated for values of k_1. Fig. 4.2 shows the plot of k_1 at various concentrations of SDZ. The linearity of the plot indicates that the rate of the reaction between Fe^{VI} and SDZ was first-order with respect to the concentrations of SDZ, and it can be expressed as

$$-d[Fe(VI)]/dt = k[Fe(VI)][SDZ] \quad (4.1)$$

where *k* is the second-order rate constant of the reaction. The value of *k* at pH 7.00 was $(8.44\pm0.24)\times10^2$ $M^{-1}s^{-1}$. This increase in value of *k* at pH 7.0 from the value at pH 9.0 has been observed in the reactions of Fe^{VI} with several inorganic and organic compounds (Karlesa, et al., 2014; Kralchevska, et al., 2016; Lee and von Gunten, 2012; Sharma, et al., 2015).

The value of *k* at pH 7.0 can be used to learn the half-life ($t_{1/2}$) of the elimination of SDZ by Fe^{VI}. A calculated value of $t_{1/2}$ was determined as 66 s if the concentration of Fe^{VI} is in excess over SDZ at a dose of [Fe] = 1 mg L^{-1} or [FeO_4^{2-}] = 2.2 mg L^{-1}. Because the values of *k* are pH dependent, the half-lives for the elimination of SDZ by Fe(VI) would also vary with pH. Additionally, variation in the dose of Fe^{VI} would also change the $t_{1/2}$ to remove SDZ by Fe^{VI}.

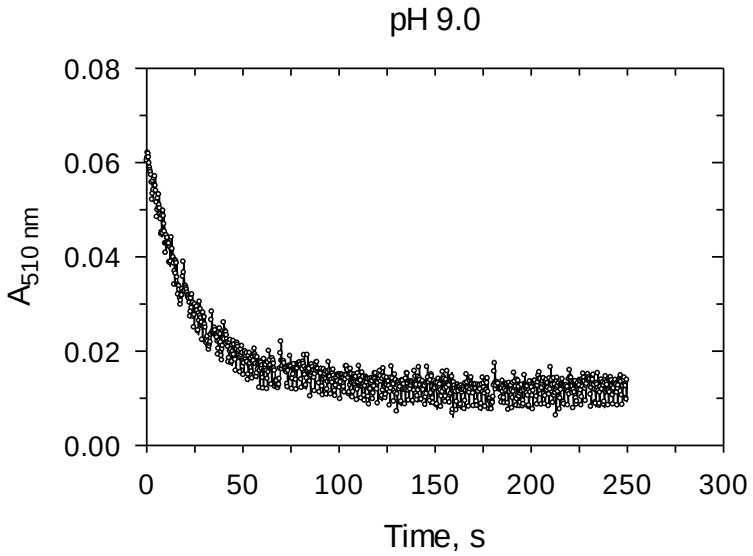

Fig. 4.1. Kinetic traces of the decay of Fe^{VI} at 510 nm in the reaction between Fe^{VI} and SDZ at pH 9.0 and at 25 °C. ([Fe^{VI}] = 50 μM and [SDZ] = 500 μM)

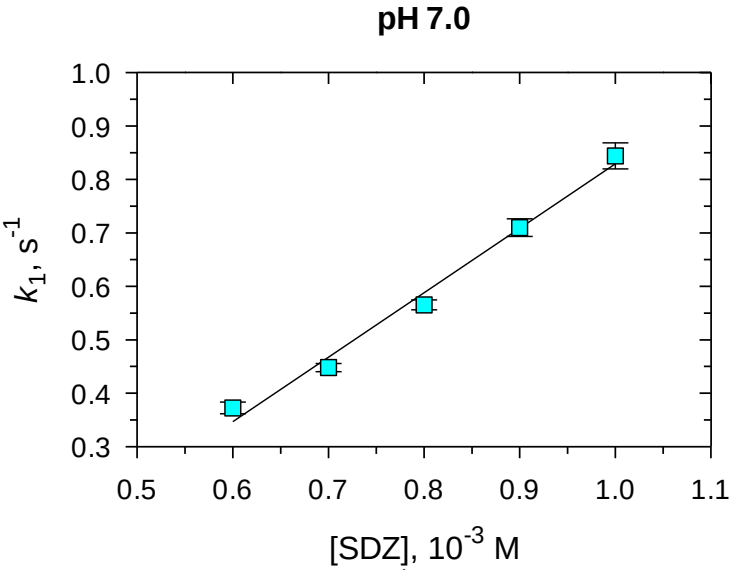

Fig. 4.2. Pseudo first-order rate constant (k_1, s^{-1}) for the oxidation of SDZ by Fe^{VI} at pH 9.0 and at 25 °C. ([Fe^{VI}] = 50 µM)

Finally, values of *k* at other pHs were determined in the pH range from pH 4.5 to 10.0. Results shown in Fig. 4.3 give the dependence of *k* on the pH. In the pH range from 4.0 to 7.0, rates slowly decreased with an increase in pH. However, a sharp decrease in the rate constants was observed when the pH increased from 7.0 to 10.0. Similar trends in the values of *k* with pH in the acidic to basic pH range were observed in the oxidation of other sulfonamides (Kim, et al., 2015; Lee, et al., 2009; Sharma, et al., 2006a; Sharma, et al., 2006b).

The variation in the values of *k* with pH was analyzed quantitatively using acid-base equilibria of Fe^{VI} and SDZ (X) (Eqns. 4.2-4.6) (Boreen, et al., 2005; Boreen, et al., 2005; Sharma, et al., 2006a).

$$H_3FeO_4^+ \rightleftharpoons H^+ + H_2FeO_4 \qquad pK_{a1} = 1.6 \qquad (4.2)$$

$$H_2FeO_4 \rightleftharpoons H^+ + HFeO_4^- \qquad pK_{a2} = 3.5 \qquad (4.3)$$

$$HFeO_4^- \rightleftharpoons H^+ + FeO_4^{2-} \qquad pK_{a3} = 7.23 \qquad (4.4)$$

$$H_2X^+ \rightleftharpoons H^+ + HX \qquad pK_{a1} = 2.69 \qquad (4.5)$$

$$HX \rightleftharpoons H^+ + X^- \qquad pK_{a2} = 6.59 \qquad (4.6)$$

In the pH range of 4.0 to 10.0, the four species of Fe^{VI} (i.e., $H_3FeO_4^+$, H_2FeO_4, $HFeO4^-$, and FeO_4^{2-}) can possibly react with the three species of X (H_2X^+, HX, and X^-). The dependence of k on the pH can be modeled by Eq. 4.7.

$$-d[X]/dt = k\,[Fe(VI)]_{tot}\,[X]_{tot} = \Sigma\, k_{ij}\,\alpha_i\,\beta_j\,[Fe(VI)]_{tot}\,[X]_{tot} \qquad (4.7)$$
$$i = 1, 2, 3, 4,$$
$$j = 1, 2, 3$$

where $[Fe^{VI}]_{tot} = [H_3FeO_4^+] + [H_2FeO_4] + [HFeO_4^-] + [FeO_4^{2-}]$; $[X]_{tot} = [H_2X^+] + [HX] + [X^-]$; α_i and β_j represent the species fractions of Fe(VI) and SDZ, respectively; i and j are each of the species of Fe(VI) and SDZ respectively; and k_{ij} is the species-specific second-order rate constant for the reaction between the Fe(VI) species i and the X species j. Overall, twelve reactions could possibly contribute to Eq. (4.7).

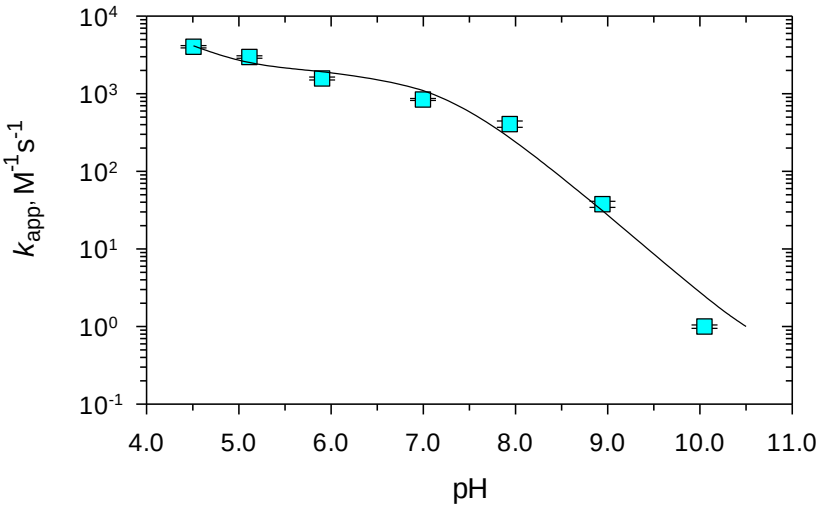

Fig. 4.3. Dependence of second-order rate constants (k_{app}, $M^{-1}s^{-1}$) on pH for the oxidation of SDZ by Fe^{VI} at 25 °C.

Eq. 4.7 was applied to fit the kinetic data from the oxidation of SDZ by Fe^{VI}. Initially, the experimental values of *k* at different pHs were statistically fit by involving sixteen reactions. In this approach, the fit obtained was very poor. In this empirical fit, some values of rate constants were negative. Therefore, only reactions those gave positive values of the rate constants were included in the model. This approach was based on earlier studies on the oxidation of sulfur-containing pharmaceuticals (e.g. sulfonamides) by Fe(VI) in both acid and alkaline medium (Kim, et al., 2015; Sharma, et al., 2006a). Only three of the possible reactions were needed to fit the results of Fig. 4.3. The experimental results could be described reasonably using the Eqs. 4.8-4.10. (a solid line in Fig. 4.3). Values of contributed species-specific rate constants are given in Eqs. 4.8-4.10.

$H_2FeO_4 + SH \rightarrow Fe(III) + Products$ $\quad k_8 = (2.7\pm0.5)\times10^4\ M^{-1}s^{-1}$ (4.8)

$HFeO_4^- + SH \rightarrow Fe(III) + Products$ $\quad k_9 = (2.0\pm0.3)\times10^3\ M^{-1}s^{-1}$ (4.9)

$HFeO_4^- + S^- \rightarrow Fe(III) + Products$ $\quad k_{10} = (1.6\pm0.5)\times10^3\ M^{-1}s^{-1}$ (4.10)

The result suggests that the reactions of Fe^{VI} with the protonated species of SDZ (Eqs. 4.8 and 4.9) follow the order of reactivity as $H_2FeO_4 > HFeO_4^-$. This order in the rate constants is the same for the fractions of Fe^{VI} species at low pH and therefore involve in determining the overall rates of the reaction between Fe(VI) and SDZ in the acidic to neutral pH range, causing the increase in the rates of oxidation of SDZ by Fe^{VI} (Fig. 4.3). In the neutral to basic pH range, the fraction of $HFeO_4^-$ decreases sharply with an increase in pH and likewise with the rate constants (see Fig. 4.3). The trend seen in Fig. 4.3 is consistent with the predicted variation in rates with an increase in pH using density functional theory calculations (Kamachi, et al., 2005).

4.3.2 Identification of the OPs of SDZ by Fe(VI)

In this study, the OPs, generated via the oxidation of SD (100 μM) by Fe(VI) (500-2000 μM) overnight at pH 7.0, were characterized using LC-TOF-MS (ESI pos). Structural assignments of a total of eleven identified OPs were carried out by a product ion scan. This is based on the corresponding MS/MS spectra and their proposed fragmentation patterns (Fig. 4.4). The data and suggested structures of the OPs and their MS/MS fragments are shown in Table 4.1 and Fig. 4.4 For the scientific identification of the possible OPs, it is necessary to analyze the mass spectrum of the parent compound and the fragment losses generated, which may also be detected in the structural identification of the OPs (Feng, et al., 2016a). Regarding SDZ (*m/z* 251.0578 and R_t at 2.74 min), five main product ions at *m/z* 185.0807, 158.0006, 156.0102, 108.0440 and 92.0499 corresponded to individual losses of SO_2 and 2H (66 Da from SDZ), C_6H_5 and NH_2 (93 Da from SDZ), $C_4H_5N_3$ (95 Da from SDZ), C_6H_5 (77 Da from 185.0807), and SO_2 (64 Da from 156.0102), respectively (Fig. 4.4A). Similar MS/MS fragments of SDZ were also reported during its catalytic peroxymonosulfate (PMS) oxidation by $CuFeO_2$ rhombphedral crystals (Feng, et al., 2016c).

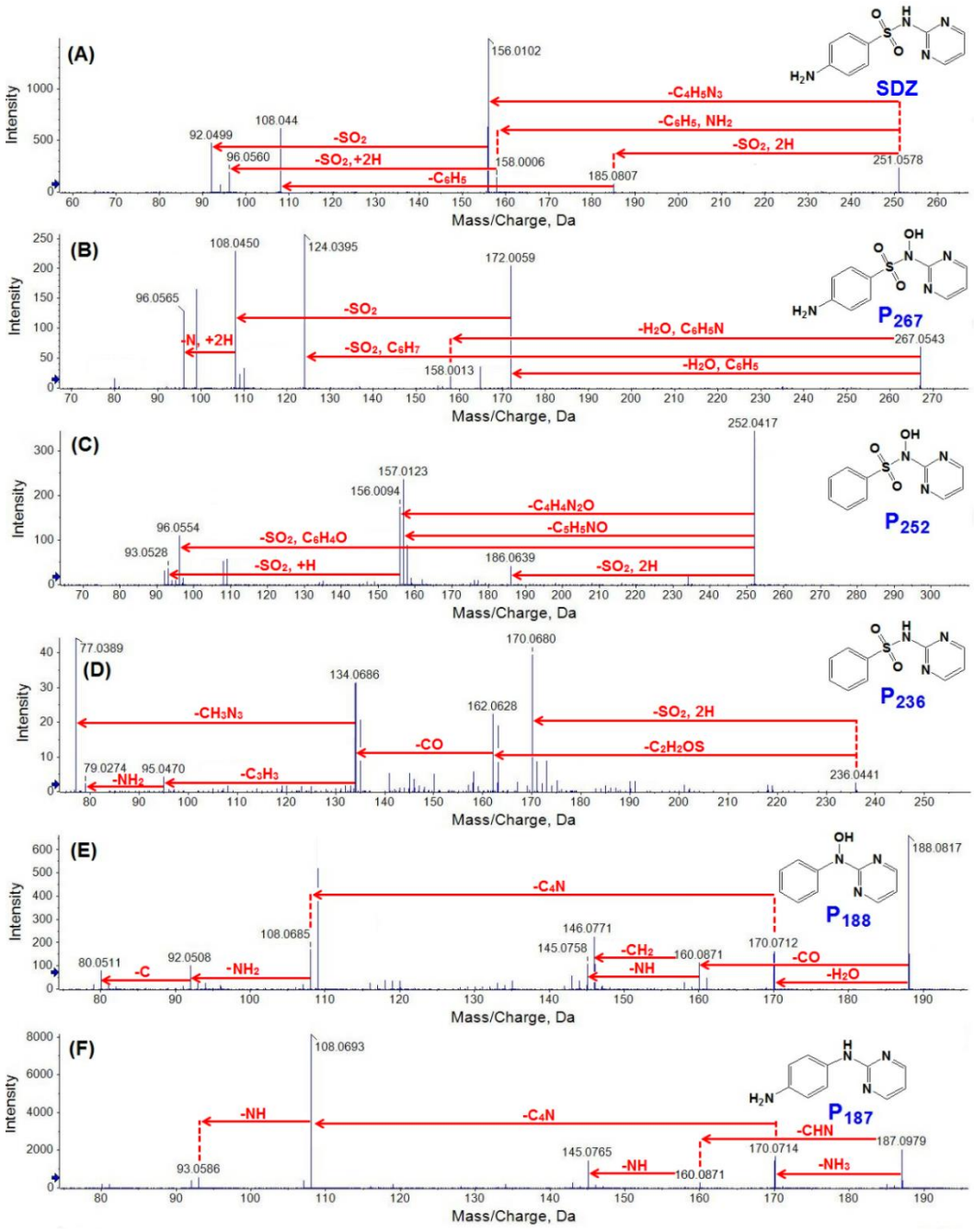

Fig. 4.4. Product ion spectra of SDZ and its degradation products by Fe(VI), measured by LC-HR-MS/MS (ESI pos), and their proposed fragmentation pathways. (Experimental conditions: $[SDZ]_0$ = 100 μM, $[Fe(VI)]_0$ = 500-2000 μM, pH = 7.0).

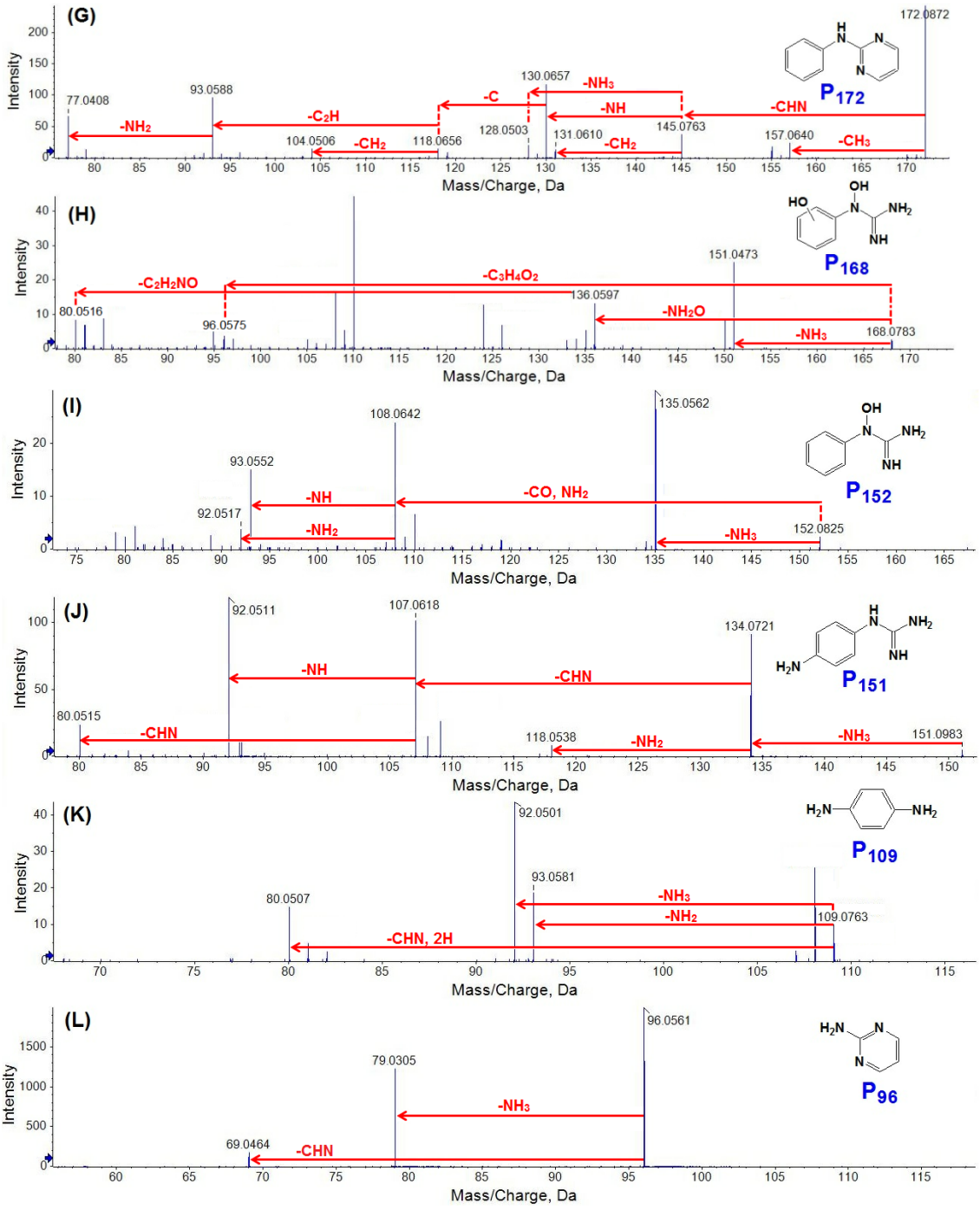

Fig. 4.4. Continued.

Although the MS/MS information regarding the degradation products of SDZ by Fe^{VI} oxidation is still lacking, references could be found in several transformation studies of sulfonamides to facilitate the structural identification of these OPs (Feng, et al., 2016c; Kim, et al., 2015). Representatively, in this work, P_{267} with a protonated form at *m/z* 267.0543 and chromatographic retention time at 2.56 min was proposed as the product generated from the hydroxylation at the N atom between two rings of the SDZ molecule (Table 4.1 and Fig. 4.4B). This structure was confirmed by the product ions at *m/z* 172.0059, 158.0013, 124.0395 and 108.0450, which correspond to the separate losses of fragments as H_2O and C_6H_5 (95 Da from 267.0543), H_2O and C_6H_5N (109 Da from 267.0543), SO_2 and C_6H_7 (143 Da from 267.0543), and SO_2 (64 Da from 172.0059), respectively. As another typical OP with a chromatograph retention time of 3.42 min and two major product ions at *m/z* 134.0721 and 107.0618 (Table 1), P_{151} (*m/z* 151.0983) resulted from the ring cleavage of the SDZ molecule. This structure was suggested mainly by the product ions at *m/z* 134.0721, 118.0538, 107.0618, 92.0511 and 80.0515, which individually corresponded to the losses of such fragments as NH_3 (17 Da from 151.0983), NH_2 (16 Da from 134.0721), CHN (27 Da from 134.0721), NH (15 Da from 107.0618), and CHN (27 Da from 107.0618) (Fig. 4.4). Similarly, in view of the repeated MS/MS fragments and proposed fragmentation patterns of the OPs of SDZ, the individual structures of P_{252}, P_{236}, P_{188}, P_{187}, P_{172}, P_{168}, P_{152}, P_{109} and P_{96} were proposed, and the detailed fragmentation pathways are shown in Fig. 4.4.

Table 4.1. Accurate mass measurements of SDZ and its transformation products by Fe(VI), which were determined by LC-HR-MS/MS (ESI pos).

Compound	R_t (min)	Formula $[M + H]^+$	Experimental mass (*m/z*)	Calculated mass (*m/z*)	Error (ppm)	DBE [a]
SDZ	2.74	$C_{10}H_{11}N_4O_2S$	251.0578	251.0603	-9.96	8
		$C_6H_6NO_2S$	156.0102	156.0119	-10.90	5
		$C_4H_4N_4$	108.0442	108.0436	5.55	5
P_{267}	2.56	$C_{10}H_{11}N_4O_3S$	267.0543	267.0552	-3.37	8
		$C_4H_4N_4O_2S$	172.0059	172.0055	2.33	5
		$C_4H_4N_4O$	124.0395	124.0385	8.06	5
P_{252}	4.15	$C_{10}H_{10}N_3O_3S$	252.0417	252.0443	-10.32	8
		$C_{10}H_8N_3O$	186.0639	186.0667	-15.05	9
		$C_5H_5N_2O_2S$	157.0123	157.0072	32.48	5
P_{236}	11.06	$C_{10}H_{10}N_3O_2S$	236.0441	236.0494	-22.45	8
		$C_{10}H_8N_3$	170.0680	170.0718	-22.34	9
		$C_7H_8N_3$	134.0686	134.0718	-23.87	6
P_{188}	7.08	$C_{10}H_{10}N_3O$	188.0817	188.0824	-3.72	8
		$C_{10}H_8N_3$	170.0712	170.0718	-3.53	9
		$C_4H_5N_4$	109.0534	109.0514	18.34	5
P_{187}	6.64	$C_{11}H_{10}N_4$	187.0979	187.0987	-4.28	9
		$C_{10}H_8N_3$	170.0714	170.0718	-2.35	9
		$C_6H_8N_2$	108.0693	108.0687	5.55	4
P_{172}	13.11	$C_{10}H_{10}N_3$	172.0872	172.0875	-1.74	8
		C_9H_8N	130.0657	130.0657	0.00	7
		C_6H_7N	93.0588	93.0578	10.75	4
P_{168}	2.06	$C_7H_{10}N_3O_2$	168.0783	168.0773	5.95	5
		$C_7H_7N_2O_2$	151.0473	151.0508	-23.17	6
		$C_4H_6N_4$	110.0574	110.0592	-16.35	4
P_{152}	2.50	$C_7H_{10}N_3O$	152.0825	152.0824	0.66	5
		$C_7H_7N_2O$	135.0562	135.0558	2.96	6
		$C_4H_4N_4$	108.0456	108.0436	18.51	5
P_{151}	3.42	$C_7H_{11}N_4$	151.0983	151.0984	-0.66	5
		$C_7H_8N_3$	134.0721	134.0718	2.24	6
		$C_6H_7N_2$	107.0618	107.0609	8.41	5
P_{109}	2.25	$C_6H_9N_2$	109.0763	109.0766	-2.75	4
		C_6H_6N	92.0501	92.0500	1.09	5
		C_5H_6N	80.0507	80.0500	8.74	4
P_{96}	2.47	$C_4H_6N_3$	96.0561	96.0562	-1.04	4
		$C_4H_3N_2$	79.0305	79.0296	11.39	5
		$C_3H_5N_2$	69.0464	69.0453	15.93	3

[a] DBE, double bond equivalent.

4.3.3. Plausible reaction pathways

The suggested transformation pathways of SDZ by Fe^{VI} at pH 7.0 are illustrated in Fig. 4.5. Three initial attack sites of SDZ by Fe^{VI} are indicated, including the SO_2 extrusion, deamination, and hydroxylation. In pathway I, SDZ could be oxidized by Fe^{VI} via SO_2 extrusion to generate P_{187}. Notably, SO_2 extrusion has also been indicated during different transformation processes of sulfonamides, such as the catalytic PMS degradation of SDZ by $CuFeO_2$ (Feng, et al., 2016c), the catalytic persulfate oxidation of sulfamonomethoxine by Fe_3O_4 (Yan, et al., 2011), and the triplet-sensitized photodegradation of sulfa drugs (Boreen, et al., 2004; Boreen, et al., 2008). Subsequently, the oxidation of P_{187} proceeded by three different patterns to form P_{151} (cleavage of six-membered heterocyclic ring, which could be further transformed to be P_{109}), P_{96} (bond cleavage) and P_{172} (deamination), respectively. The generation of P_{96} has recently been demonstrated during the catalytic PMS degradation of SDZ by $CuFeO_2$ (Feng, et al., 2016c) and its aerobic degradation by *Arthrobacter spp.* (Deng, et al., 2016). Pathway II was initiated by deamination at the aromatic ring of SDZ, with the resultant product of P_{236}. Because of the electron-rich moiety of an SDZ molecule, the amide group is susceptible to chemical attacks of Fe^{VI} via an electrophilic oxidation mechanism. Afterwards, pathway II continued via two sequential reaction patterns, i.e., SO_2 extrusion and bond cleavage, to yield P_{172} and P_{96}. Meanwhile, hydroxylation could occur for P_{236} to form P_{252}. In pathway III, hydroxylation takes place on the N atom between two rings of SD, resulting in the formation of P_{267}, which was also detected during the catalytic PMS degradation of SDZ by $CuFeO_2$ (Feng, et al., 2016c). The

hydroxylation process of organic pollutants during Fe^{VI} treatment has also been demonstrated in recent investigations on other antibiotics such as trimethoprim (Anquandah, et al., 2011), sulfamethoxazole (Kim, et al., 2015), ciprofloxacin and enrofloxacin (Zhou and Jiang, 2015a), as well as flumequine (Feng, et al., 2016a). With the reaction progressing, P_{252}, P_{188}, P_{152} and P_{168} were generated, mainly via deamination, SO_2 extrusion, opening of the six-membered heterocyclic ring, and further hydroxylation, respectively. Overall, eleven identified OPs allowed the enhanced understanding of oxidation of sulfonamides by Fe^{VI}.

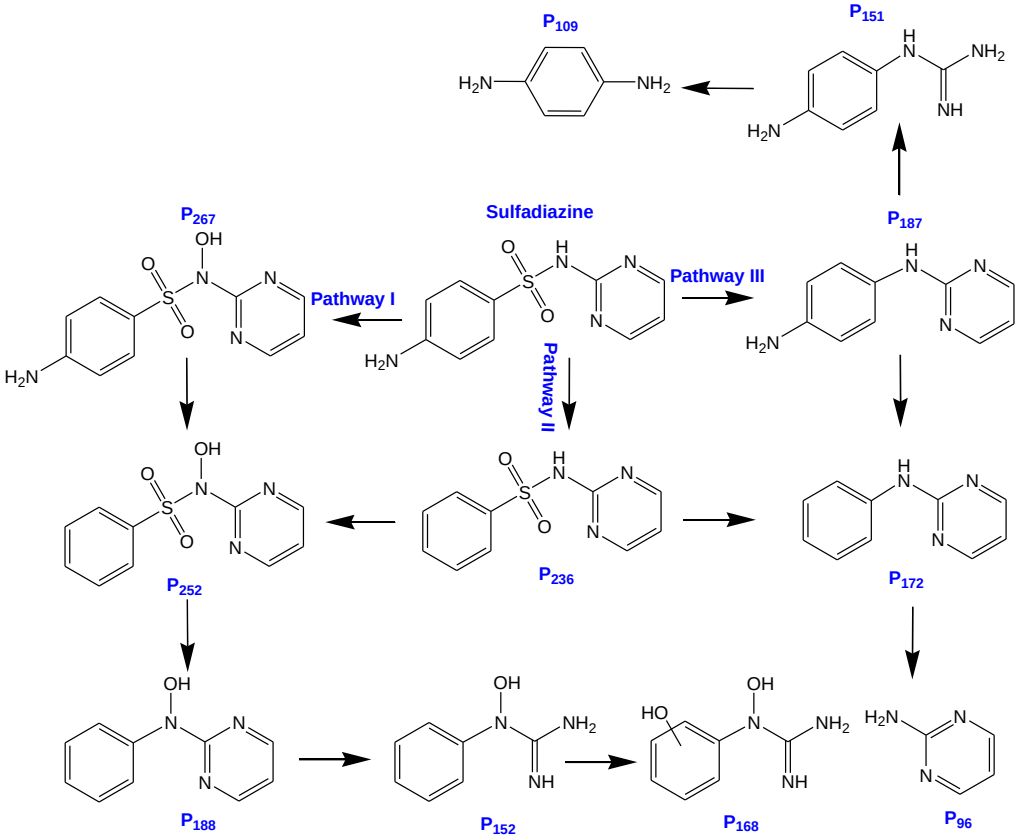

Fig. 4.5. Proposed transformation pathways of SDZ by Fe(VI). (Experimental conditions: $[SDZ]_0$ = 100 μM, $[Fe(VI)]_0$ = 500-2000 μM, pH = 7.0).

5. OXIDATION OF FLUMEQUINE BY FERRATE(VI), FERRATE(V), AND FERRATE(IV): EFFECT OF AMMONIA ON DEGRADATION PRODUCTS

5.1. Introduction

Since their discovery in the 1940s, antibiotics have been widely developed and increasingly used as the most important pharmaceuticals for improving human health, treating bacterial infection, and promoting growth in animal farming (Martinez, 2009; Lewis, 2013). During human and veterinary applications, antibiotics are less metabolized due to their chemical stability. Antibiotics are thus mainly discharged through human and animal excretion in which their pharmaceutically active forms remain intact in wastewater and soil (Homem and Santos, 2011). Notably, antibiotics even at environmentally relevant concentrations could trigger adverse ecological consequences, including the inhibition of microbial species (Ebert, et al., 2011; González-Pleiter et al., 2013), the development of antibiotics resistant bacteria (ARB) and antibiotics resistant genes (ARG) with public health concerns (Ben, et al., 2017; Sharma, et al., 2016b), and chronic inhibitory effects on the growth and reproduction of various aquatic organisms (Corcoran et al., 2010; Brausch, et al., 2012). Therefore, the presence of antibiotics in the aquatic environment has led to the emergence of a global environmental pollution problem.

Fluoroquinolone antibiotics (FQs) are the potent and broad-spectrum antimicrobial agents increasingly used in hospitals, households and veterinary applications for treating severe or resistant bacterial infections since the late 1980s (Chen, et al., 2015; Dorival-García, et al., 2013). Four generations of FQs have been

developed and examples include flumequine (FLU), norfloxacin (NOR), ofloxacin (OFL), lomefloxacin (LOM), and enrofloxacin (ENR) (Chen, et al., 2015; Janecko, et al., 2016; Khetan and Collins, 2007). After cephalosporin antibiotics, FQs have become the largest antibiotic drugs in the market (Hamad, 2010). FQs treat effectively both human and animal infections, but only a small percentage of them are retained by the body (Barbosa, et al., 2016; Van Doorslaer, et al., 2014). The bactericidal action of FQs is based on the inhibition of bacterial growth by interfering with key cellular processes including DNA metabolism and inhibiting the enzymes topoisomerase II (DNA-gyrase) in gram-negative bacteria and topoisomerase IV in gram-positive bacteria (Sukul and Spiteller, 2007; Janecko, et al., 2016). These processes could result in the impaired DNA transcription and replication (at lower concentrations) and even cell death (at lethal concentrations) (Sukul and Spiteller, 2007; Janecko, et al., 2016). Approximately 90% of the pharmaceuticals are usually released in the form of either urine or excrement (Tran, et al., 2016; Wang, et al., 2016). Conventional wastewater treatment technologies are not adequate to remove the FQs completely (Wu, et al., 2016). More and more FQs are entering into the environment (Chen, et al., 2015). Studies have shown their detection in surface water, groundwater, and soil (Chen, et al., 2015; Dekker, et al., 2015; Peixoto, et al., 2016). In the aquatic environment, FQs inhibit the growth of certain organisms, hence affecting the ecological system (Cizmas, et al., 2015). Additionally, the release of antibiotics leads to the development of antibiotic resistant bacteria and antibiotic resistant genes, an important health problem around the world (Osinska, et al., 2017; Proia, et al., 2016; Sharma, et al., 2016b).

Many treatment technologies are being investigated to remove FQs in water and during wastewater treatment. These removal techniques include adsorption on nanomaterials, reverse osmosis, smart membranes, electro-Fenton process, advanced oxidation processes, chlorination, ozonation, and permanganate oxidation (Dodd, et al., 2005; Feng, et al., 2015; Feng, et al., 2016a; Feng, et al., 2016b; Guo, et al., 2017; Guo, et al., 2016; Jiang, et al., 2016; Jojoa-Sierra, et al., 2017; Kim, et al., 2014; Maia, et al., 2014; Qin, et al., 2014; Santoke, et al., 2009; Sharma, et al., 2015; Wang, et al., 2010). Most of these methods generally give good performance in removing FQs in the laboratory set-up. This chapter focuses on the use of tetraoxy high-valent iron species in +6, +5, and +4 ($Fe^{VI}O_4^{2-}$ (Fe^{VI}), $Fe^{V}O_4^{3-}$ (Fe^{V}), and $Fe^{IV}O_4^{4-}$ (Fe^{IV})), which are generally called ferrates, to remove a particular FQs, namely FLU.

A recent study showed that removal of most of the studied FQs were degraded within 2 min at [Fe(VI)]:[FQ] ≤ 20.0, except FLU (Feng, et al., 2016a). A molar ratio of 100:1 was needed to achieve more complete removal of FLU in water in 2 min (Feng, et al., 2016a). A more recent study on the removal of FLU by Fe^{VI} demonstrated the enhanced removal of FLU in the presence of ammonia ($NH_4^+ + NH_3$) (Feng, et al., 2017). Some of the research in this chapter was stimulated by this surprising finding in which ammonia could activate Fe^{VI} to oxidize FLU so that the removal of FLU took place in a shorter time than without ammonia in the reaction solution (Feng, et al., 2017). This study postulated a formation of the intermediate highly reactive Fe^{V}-ammonia and Fe^{IV}-ammonia complexes during the oxidation of FLU by Fe^{VI} to cause the increased removal of FLU in the presence of ammonia. This chapter aimed to test this hypothesis

by conducting independently the oxidation of FLU by only Fe^{V} and Fe^{IV} species. Initially, removal of FLU by Fe^{VI}, Fe^{V}, and Fe^{IV} species with and without ammonia was performed, followed by the identification of transformation products (or oxidized products (OPs)). Amounts of OPs were used to elucidate the role of intermediate iron species in the oxidation of FLU by Fe^{VI} in the presence of ammonia.

5.2. Materials and methods

5.2.1. Chemicals

FLU (purity 98%) was obtained from Sigma-Aldrich (St. Louis, Mossouri, USA). Salts of ammonium ion (NH_4Cl) and buffers (sodium dihydrogen phosphate (Na_2HPO_4) and sodium tetraborate decahydrate ($Na_2B_4O_7{\cdot}10H_2O$)) were purchased from Sigma-Aldrich (St. Louis, Mossouri, USA). Methanol and formic acid of HPLC grade were acquired from Merck (Darmstadt, Germany). A wet chemical method was applied to synthesize solid potassium ferrate (K_2FeO_4, purity > 95%) (Luo, et al., 2011). Solid salts of Fe^{IV} (Na_4FeO_4) and Fe^{V} (K_3FeO_4) were prepared using thermal techniques (Kralchevska, et al., 2016; Machalová Šišková, et al., 2016). The purities of these salts were evaluated by ^{57}Fe Mössbauer spectroscopy (Sharma, et al., 2015). The purity of Na_4FeO_4 was high (> 90%) (Sharma, et al., 2015). In the salt of K_3FeO_4, 75% was Fe^{V} and 25% was Fe^{VI}. The water used in preparing solutions throughout the experiments was ultrapure (> 18.2 MΩ cm), which was produced from a Milli Q Plus system (Millipore, Bedford, USA). Solutions of FLU with and without ammonia (NH_4^+) were prepared in a 0.01 M phosphate buffer solution. The pH of the buffer solution was adjusted using phosphoric acid. An Orion 710A pH meter system equipped with an

Accumet pH probe (± 0.05 pH at 25 °C) was used for all pH measurements.

5.2.2. Removal of FLU by Fe^{VI}, Fe^{V}, and Fe^{IV} and the influence of ammonia

The removal experiments at pH 7.0 were performed in a Coy glove box with a vinyl anaerobic chamber under dry N_2 atmosphere in order to prevent the decay of ferrates to iron(III) by ambient air humidity. A batch of 20 mL solutions containing 30 µM FLU with and without 10 mM ammonia was prepared, and the pH was adjusted at pH 7.0 using phosphoric acid. After the preparation of the 30 µM FLU solution, solid compounds of Fe^{VI}, Fe^{V}, and Fe^{IV} were directly added to the FLU solution. The final concentrations of Fe^{VI}, Fe^{V}, and Fe^{IV} in the mixed solutions were 300 µM, 600 µM, 1500 µM, and 3000 µM. In the case of the reaction of FLU with Fe^{VI}, the disappearance of the characteristic color of Fe^{VI} in the mixture indicated that the reaction was complete. This was also confirmed by performing absorbance measurement that showed the disappearance of an absorbance peak at 510 nm for Fe^{VI}. In studying the reactions of FLU with Fe^{VI} and Fe^{IV}, after adding solid salts to the 30 µM FLU solution, reactions were immediately stopped (within 10 s) by adding excessive hydroxylamine as an quenching reagent. The concentration of hydroxylamine in the reaction mixture was 30 mM. Hydroxylamine reacted rapidly with Fe^{VI}, hence no significant reaction of Fe^{VI} with FLU could occur (Johnson and Hornstein, 2003). As written in section 2.1, a salt of Fe^{V} had an impurity of Fe^{VI}, which could possibly interfere with the reaction of Fe^{V} with FLU. Furthermore, both Fe^{V} and Fe^{IV} species also simultaneously decay themselves in water (Menton and Bielski, 1990; Rush and Bielski, 1989; Rush and Bielski, 1994) to give Fe^{VI} ion (Yates, et al., 2014). A rapid addition of hydroxylamine to the mixed

solutions of Fe^{V}-FLU and Fe^{IV}-FLU avoided any interference from the oxidation of FLU by Fe^{VI}. This experimental approach studied only the products from the reaction of Fe^{V} and FLU and Fe^{IV}-FLU.

5.2.3. Analytical procedures

Concentrations of FLU were determined by an Agilent 1200 high performance liquid chromatograph (HPLC) (Agilent Technologies, Palo Alto, CA, USA), which was equipped with a quaternary pump and a diode array detector at 248 nm. Chromatographic analysis was performed at a flow rate of 1.0 mL/min on a Zorbax Eclipse XDB-C_{18} analytical column (4.6 mm × 150 mm, particle size 5 μm) (Agilent Technologies, Palo Alto, CA, USA) at 30 °C. The mobile phase applied to obtain the chromatographic peak was 0.3% formic acid in water (A) and methanol (B) with an isocratic elution of 50/50 (v/v). The elution time of the peak was 5.5 min. The injected volume was 20 μL.

The transformation products in the oxidation of FLU by Fe^{VI} and Fe^{V} in the presence or absence of ammonia were identified by solid phase extraction-liquid chromatography-high-resolution mass spectrometry (SPE-LC-HRMS) (Feng, et al., 2016a). The protonated molecular ions $[M + H]^{+}$ of certain products were chosen as the parent ions to obtain the characteristic MS/MS fragments, which facilitated their structural identification. An error of < 3 ppm between the observed mass measurements and the proposed molecular formulas was utilized to identify accurate evaluations of the fragments and their elemental compositions.

5.3. Results and discussion

5.3.1. Removal

In this set of experiments, different amounts of Fe^{VI}, Fe^{V}, and Fe^{IV} were added into 30 μM FLU at pH 7.0. The varied molar ratios of oxidants to FLU were in the range from 10:1 to 100:1. Results of the remaining FLU with and without ammonia at different molar ratios are presented in Fig. 5.1. Fe^{VI} fully removed FLU at a molar ratio of 100:1 ($[Fe^{VI}]$:[FLU]) in the absence of ammonia. However, ammonia's presence in the reaction solution decreased the required molar ratio to 50:1 for completely removing FLU (Fig. 5.1). Comparatively, Fe^{V} could remove only 8% at the highest molar ratio of 100:1. Importantly, the presence of ammonia achieved the same removal of FLU of 8% at a molar ratio of 50:1. Furthermore, when a molar ratio was increased to 100:1 in the presence of ammonia, removal of FLU increased to 20% by Fe^{V}. In the case of Fe^{IV}, no removal of FLU was observed with or without ammonia in the reaction solution. Similar efficiencies of ferrate species were seen in removing estrogens in water (Machalová Šišková, et al., 2016).

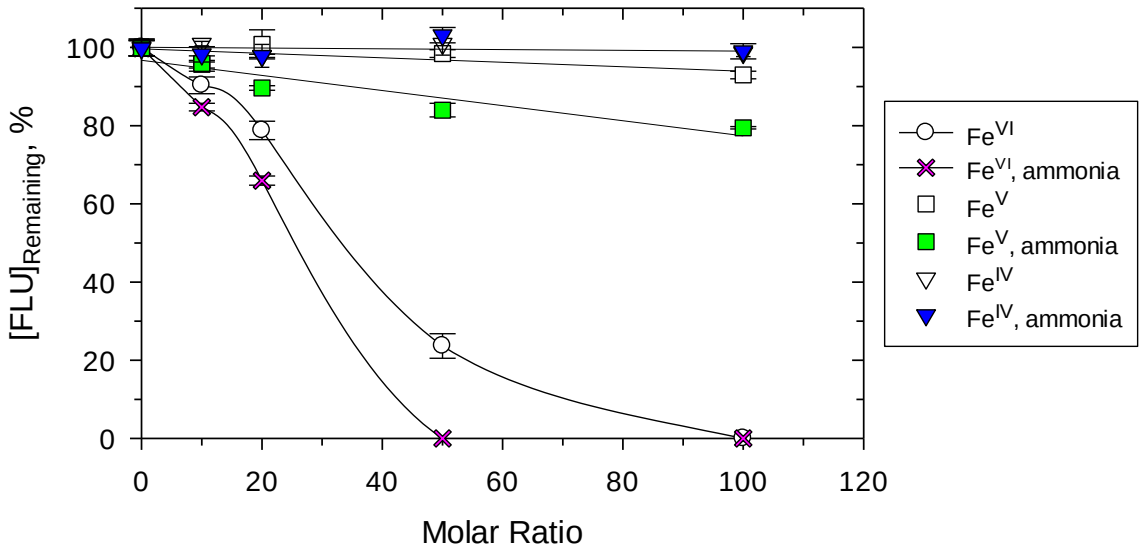

Fig. 5.1. Oxidation of FLU by Fe^{VI}, Fe^{V}, and Fe^{IV} species with and without ammonia at pH 7.0. ([FLU] = 30 µM).

5.3.2. Identification of oxidized products

In this study, OPs of the reactions between Fe^{VI}/Fe^{V} with FLU at pH 7.0 in the absence and presence of ammonia were determined. When Fe^{VI} was applied as an oxidant, OPs were identified at the molar ratios of 50:1 and 100:1 ([Fe^{VI}]:[FLU]) with and without ammonia. At these molar ratios, high percentages of FLU removal (80-100 %) with and without ammonia were obtained (Fig. 5.1). OPs were identified by LC-HRMS (ESI pos) (Table 5.1). As shown in Figs. 5.2-5.19, seventeen OPs were characterized, and their formulas and structures were assigned using extracted ion chromatograms (XIC) and MS/MS spectra. The identified OPs were named, based on the proposed reaction schemes, as *Scheme I*: P_{312}, P_{296}, P_{278}', P_{234}, P_{220}, P_{312}, P_{268}, P_{224}, *Scheme II*: P_{294}, P_{250}, P_{236}, P_{222}, P_{208}, P_{266}, P_{238}, and P_{210} and *Scheme III*: P_{278}'' and P_{276}

(Fig. 5.20). Similar OPs were seen during the oxidation of FLU by Fe^{VI} without ammonia (Feng, et al., 2016a).

Scheme I represents the hydroxylation at the C12=C13 double bond due to its high electron-cloud density (i.e., hydroxylation of the quinolone ring). P_{234} and P_{296} were obtained from the ring cleavage of the product, P_{278}'. The formation of P_{234} occurred from the decarboxylation of P_{278}'. The demethylation of P_{234} yielded P_{220}. When P_{296} cleaved, it generated P_{224}, P_{312}, and P_{268} (Scheme *I*). In the *Scheme II*, a ring opening happened in which Fe^{VI} attacked the double bond of the quinolone ring via a 1,3-dipolar cycloaddition to produce P_{294}. P_{250} and P_{266} were produced from the further reactions of P_{294}. Steps of decarboxylation, decarbonylation, hydroxylation, and demethylation of P_{250} and P_{266} produced P_{236}, P_{208}, P_{222}, P_{238} and P_{210} (Scheme *II*). The simple addition of a hydroxyl group at the C10 position of FLU gave P_{278}'', which on further oxidation resulted in P_{276}.

Table 5.1. Accurate mass measurements of FLU and its transformation products by Fe(VI), which were determined by LC-HR-MS/MS (ESI pos).

Compound	R_t (min)	Formula $[M + H]^+$	Experimental mass (*m/z*)	Calculated mass (*m/z*)	Error (ppm)	DBE [a]
FLU	13.51	$C_{14}H_{13}FNO_3$	262.0873	262.0879	-2.29	9
		$C_{14}H_{11}FNO_2$	244.0769	244.0774	-2.05	10
		$C_{11}H_5FNO_2$	202.0299	202.0304	-2.47	10
P_{312}	11.90	$C_{14}H_{15}FNO_6$	312.0865	312.0883	-5.77	8
		$C_{14}H_{13}FNO_5$	294.0764	294.0778	-4.76	9
		$C_{14}H_{11}FNO_4$	276.0659	276.0672	-4.71	10
P_{296}	11.15	$C_{14}H_{15}FNO_5$	296.0927	296.0934	-2.36	8
		$C_{14}H_{13}FNO_4$	278.0823	278.0829	-2.16	9
		$C_{14}H_{11}FNO_3$	260.0717	260.0723	-2.31	10
P_{294}	12.48	$C_{14}H_{13}FNO_5$	294.0769	294.0778	-3.06	9
		$C_{14}H_{11}FNO_4$	276.0663	276.0672	-3.26	10
		$C_{14}H_9FNO_3$	258.0556	258.0566	-3.88	11
P_{278}', P_{278}''	12.16,	$C_{14}H_{13}FNO_4$	278.0823	278.0829	-2.16	9
	12.44	$C_{14}H_{11}FNO_3$	260.0714	260.0723	-3.46	10
		$C_{14}H_9FNO_2$	242.0612	242.0617	-2.07	11
P_{276}	10.75	$C_{14}H_{11}FNO_4$	276.0662	276.0672	-3.62	10
		$C_{14}H_9FNO_3$	258.0557	258.0566	-3.49	11
		$C_{14}H_{11}FNO_2$	244.0762	244.0774	-4.92	10
P_{268}	11.94	$C_{13}H_{15}FNO_4$	268.0950	268.0985	-13.05	7
		$C_{13}H_{13}FNO_3$	250.0879	250.0879	0.00	8
		$C_{12}H_{13}FNO_2$	222.0915	222.0930	-6.75	7
P_{266}	10.79	$C_{13}H_{13}FNO_4$	266.0825	266.0829	-1.50	8
		$C_{12}H_{13}FNO_3$	238.0871	238.0879	-3.36	7
		$C_{12}H_{11}FNO_2$	220.0766	220.0774	-3.64	8
P_{250}	11.88	$C_{13}H_{13}FNO_3$	250.0872	250.0879	-2.80	8
		$C_{12}H_{13}FNO_2$	222.0921	222.0930	-4.05	7
		$C_{10}H_7FNO_3$	208.0401	208.0410	-4.33	8
P_{238}	10.62	$C_{12}H_{13}FNO_3$	238.0875	238.0879	-1.68	7
		$C_{12}H_{11}FNO_2$	220.0772	220.0774	-0.91	8
		$C_{11}H_{13}FNO_2$	210.0930	210.0930	0.00	6
P_{236}	12.82	$C_{12}H_{11}FNO_3$	236.0716	236.0723	-2.97	8
		$C_{12}H_9FNO_2$	218.0609	218.0617	-3.67	9
		$C_{11}H_7FNO_2$	204.0456	204.0461	-2.45	9
P_{234}	14.27	$C_{13}H_{13}FNO_2$	234.0924	234.0930	-2.56	8
		$C_{11}H_7FNO_2$	204.0457	204.0461	-1.96	9
		$C_{10}H_7FNO_2$	192.0455	192.0461	-3.12	8
P_{224}	17.23	$C_{12}H_{15}FNO_2$	224.1079	224.1087	-3.57	6
		$C_{11}H_{11}FNO$	192.0819	192.0825	-3.12	7
		$C_{10}H_{11}FN$	164.0869	164.0876	-4.27	6

Table 5.1. Continued.

Compound	R_t (min)	Formula $[M + H]^+$	Experimental mass (*m/z*)	Calculated mass (*m/z*)	Error (ppm)	DBE [a]
P_{222}	12.84	$C_{12}H_{13}FNO_2$	222.0925	222.0930	-2.25	7
		$C_{12}H_{11}FNO$	204.0814	204.0825	-5.39	8
		$C_{11}H_{13}FNO$	194.0972	194.0981	-4.64	6
P_{220}	10.75	$C_{12}H_{11}FNO_2$	220.0769	220.0774	-2.27	8
		$C_{10}H_7FNO_2$	192.0459	192.0461	-1.04	8
		$C_9H_5FNO_2$	178.0302	178.0304	-1.12	8
P_{210}	12.36	$C_{11}H_{13}FNO_2$	210.0926	210.0930	-1.90	6
		$C_{11}H_{11}FNO$	192.0818	192.0825	-3.64	7
		$C_{10}H_{11}FN$	164.0869	164.0876	-4.27	6
P_{208}	14.05	$C_{11}H_{11}FNO_2$	208.0764	208.0774	-4.81	7
		$C_{11}H_9FNO$	190.0657	190.0668	-5.79	8
		$C_{10}H_9FNO$	178.0655	178.0668	-7.30	7

[a] DBE: double bond equivalent.

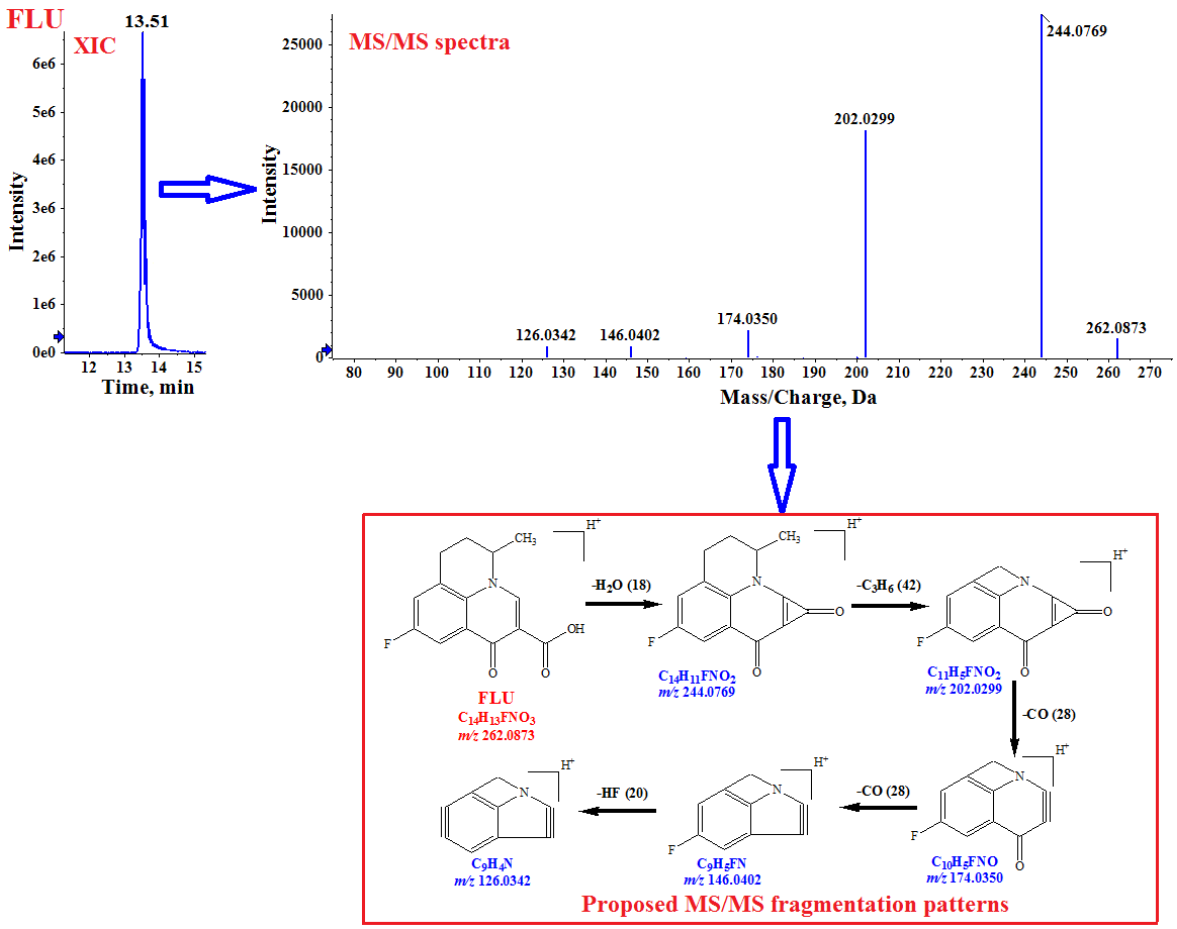

Fig. 5.2. Extracted ion chromatogram (XIC), MS/MS spectra, and proposed MS/MS fragmentation patterns of FLU (*m/z* 262.0873).

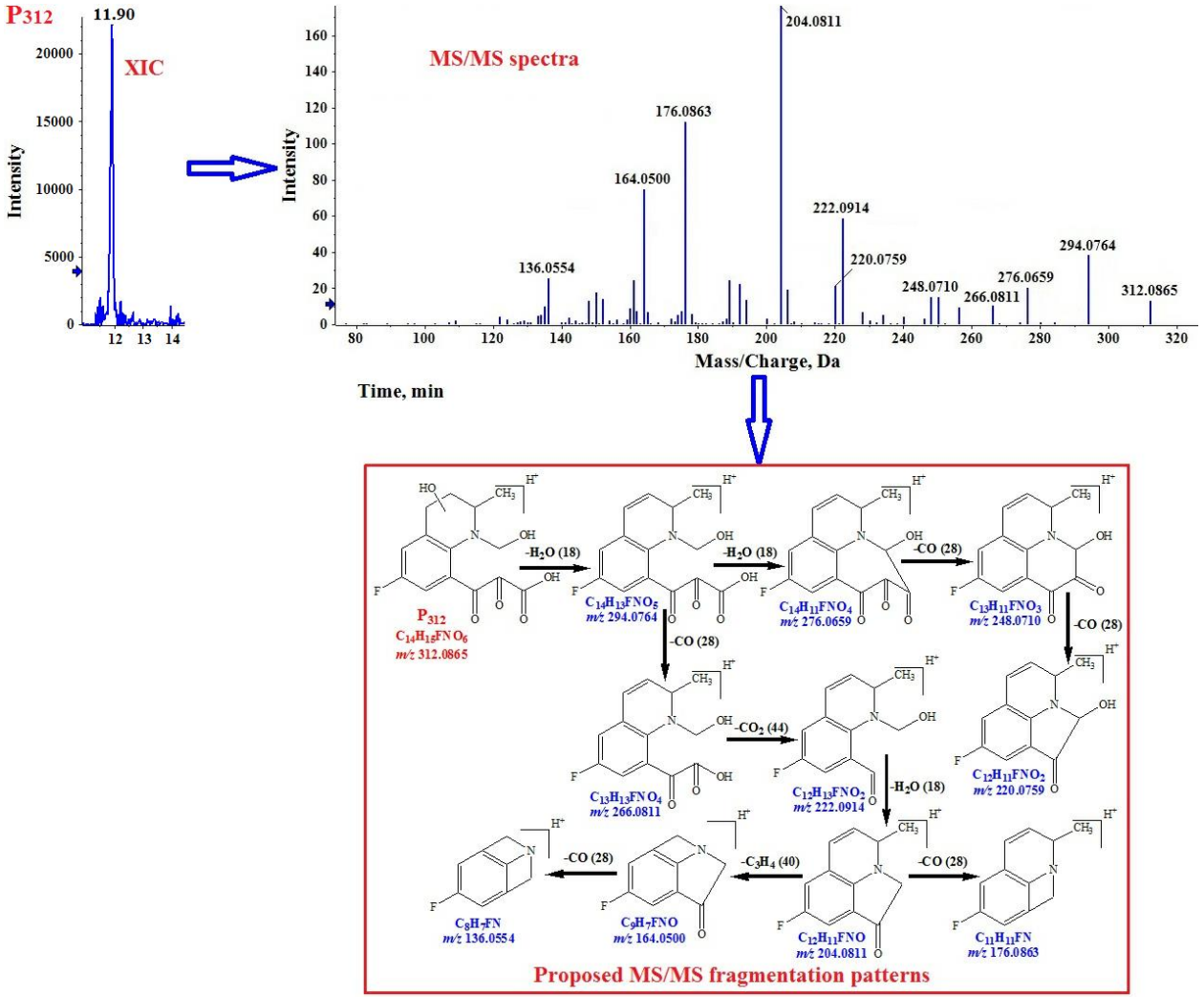

Fig. 5.3. Extracted ion chromatogram (XIC), MS/MS spectra, and proposed MS/MS fragmentation patterns of P_{312} (*m/z* 312.0865).

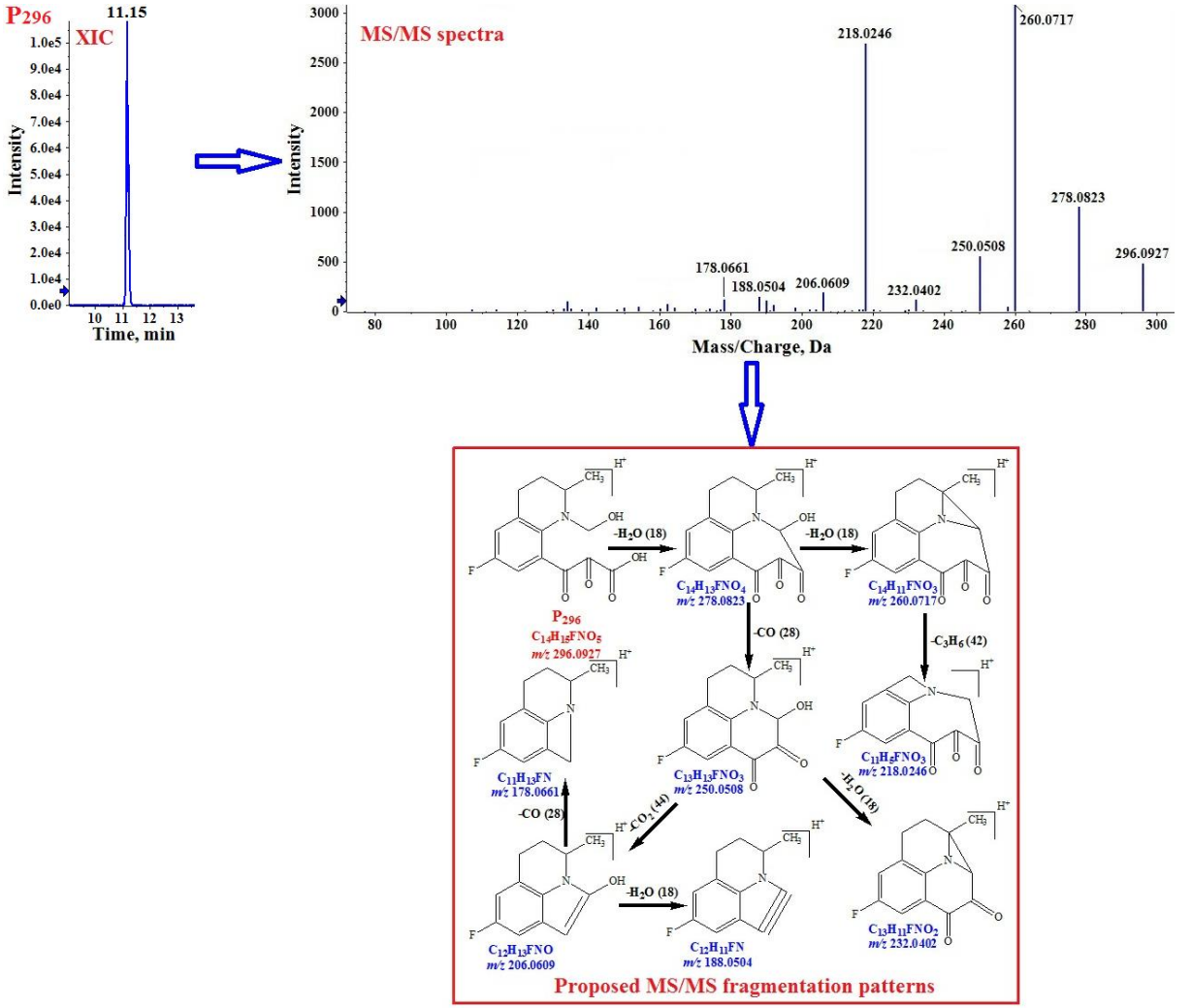

Fig. 5.4. Extracted ion chromatogram (XIC), MS/MS spectra, and proposed MS/MS fragmentation patterns of P_{296} (*m/z* 296.0927).

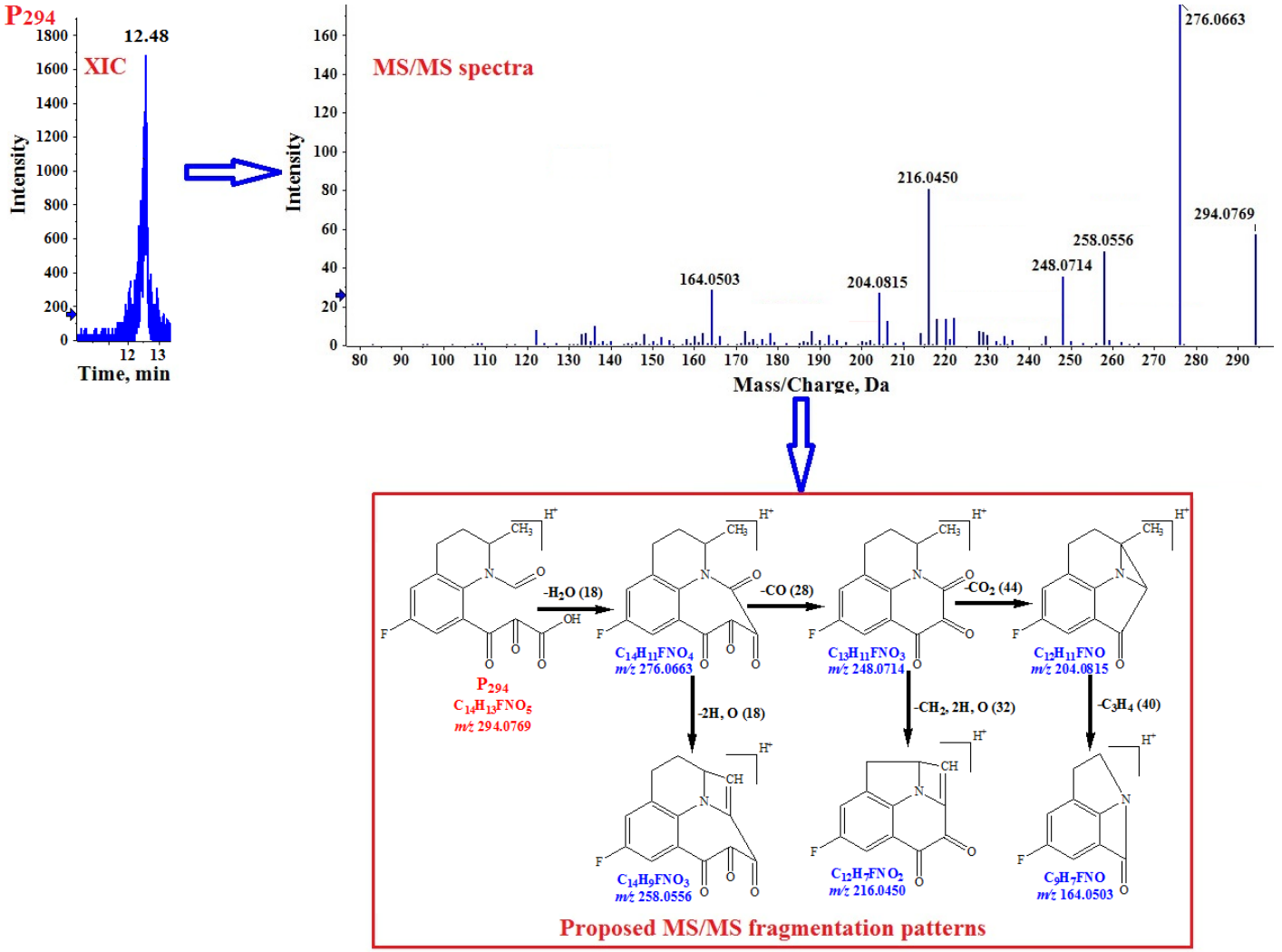

Fig. 5.5. Extracted ion chromatogram (XIC), MS/MS spectra, and proposed MS/MS fragmentation patterns of P_{294} (*m/z* 294.0769).

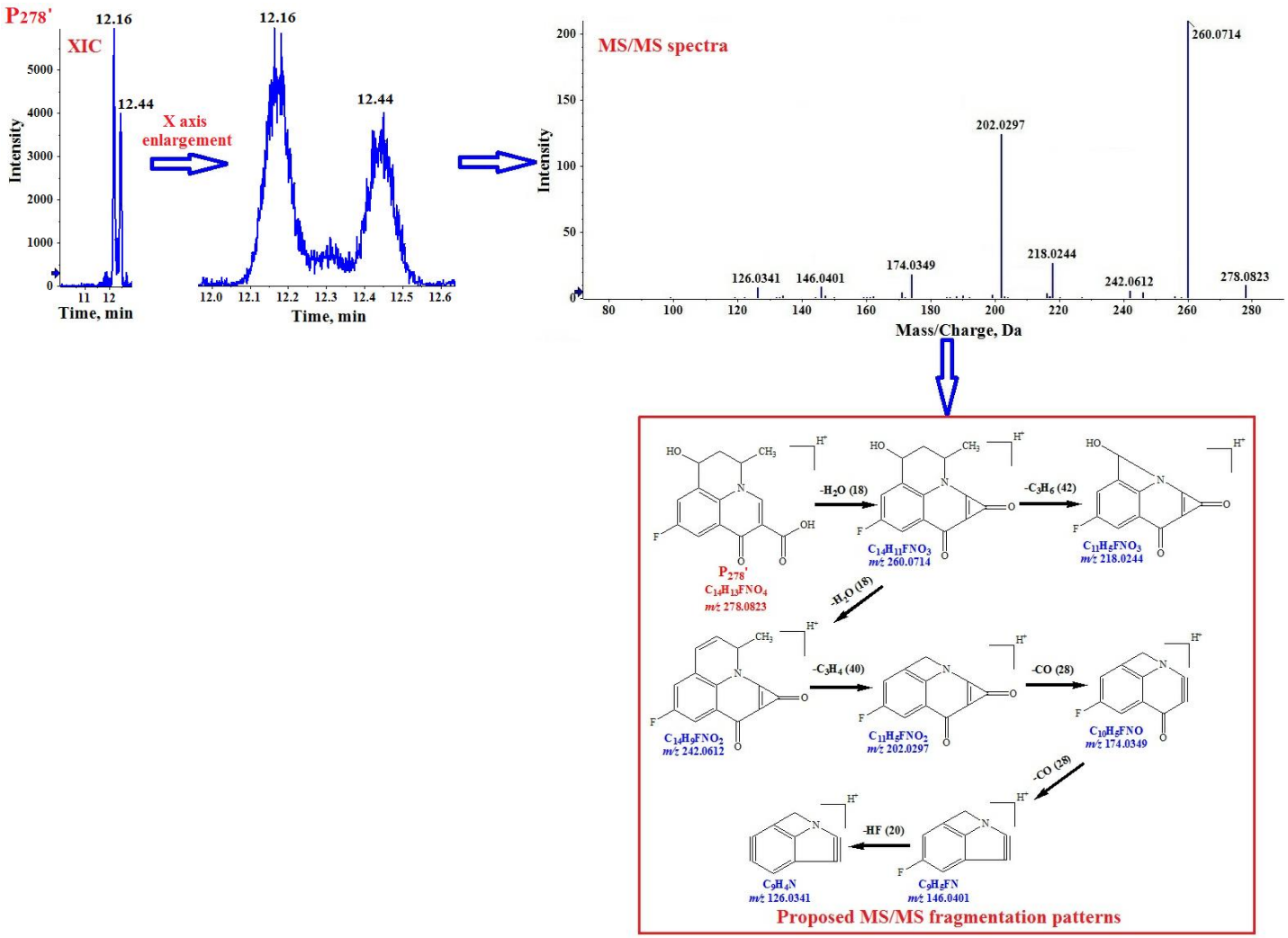

Fig. 5.6. Extracted ion chromatogram (XIC), MS/MS spectra, and proposed MS/MS fragmentation patterns of P_{278}' (*m/z* 278.0823).

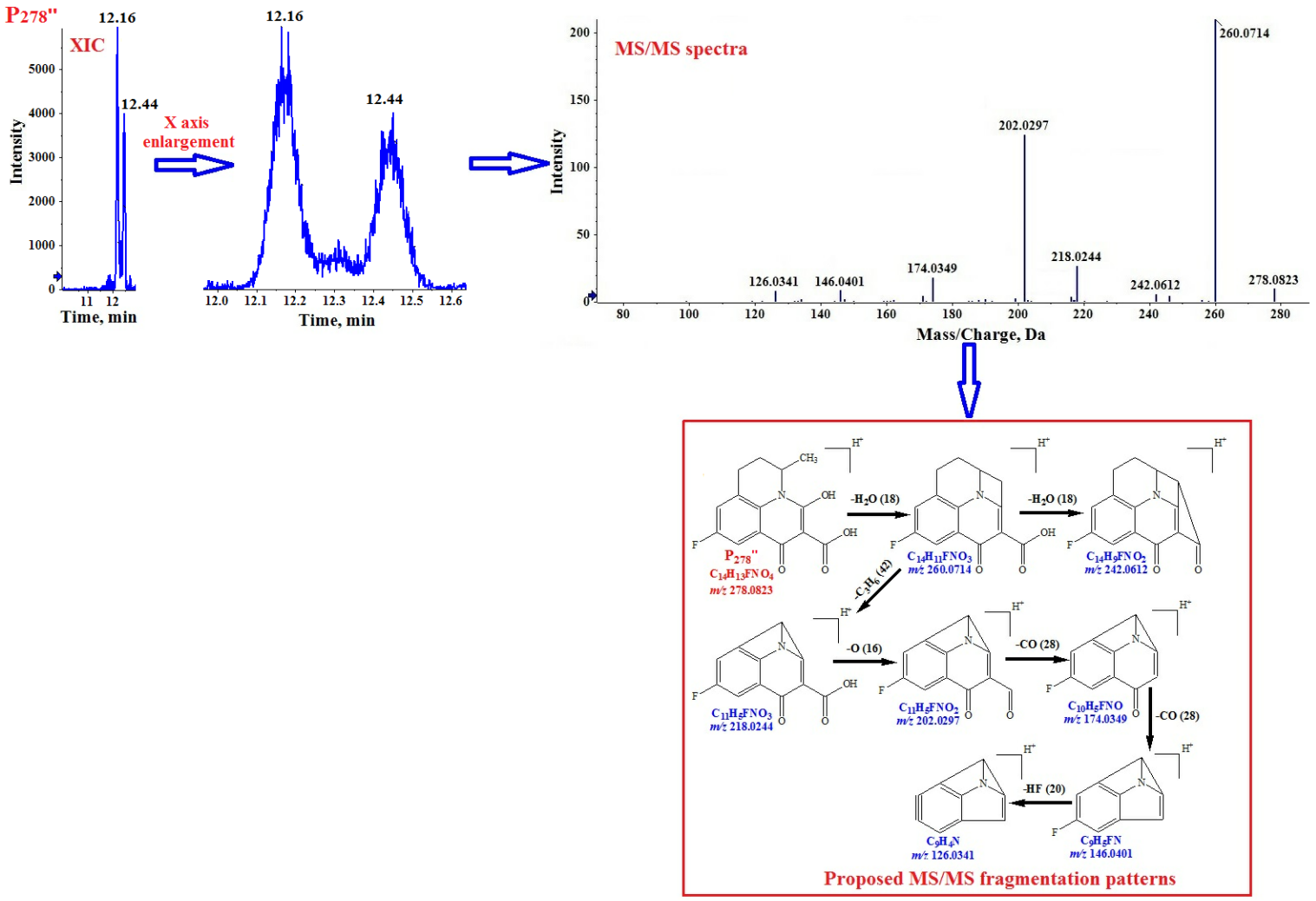

Fig. 5.7. Extracted ion chromatogram (XIC), MS/MS spectra, and proposed MS/MS fragmentation patterns of P_{278}'' (*m/z* 278.0823).

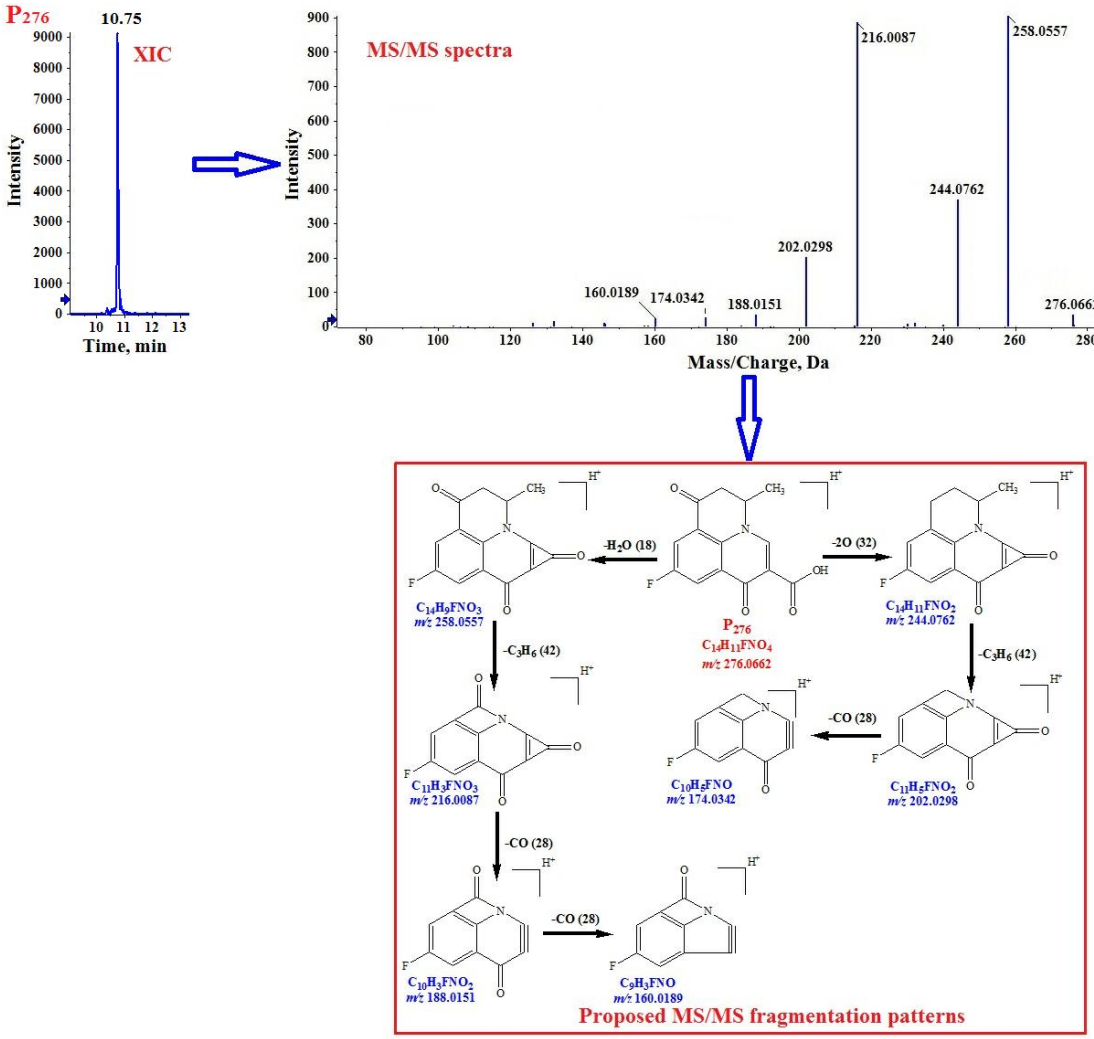

Fig. 5.8. Extracted ion chromatogram (XIC), MS/MS spectra, and proposed MS/MS fragmentation patterns of P_{276} (*m/z* 276.0662).

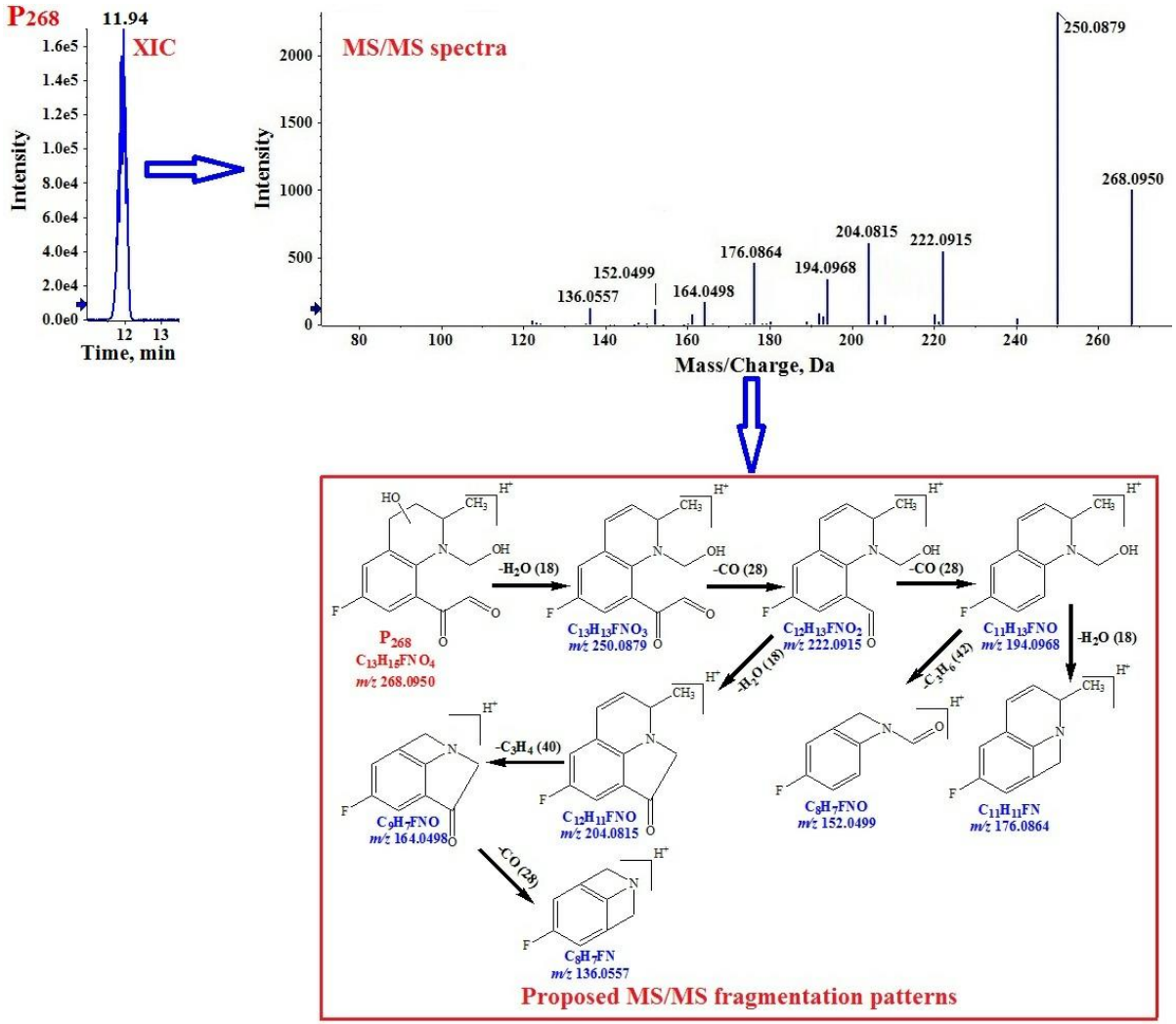

Fig. 5.9. Extracted ion chromatogram (XIC), MS/MS spectra, and proposed MS/MS fragmentation patterns of P_{268} (*m/z* 268.0950).

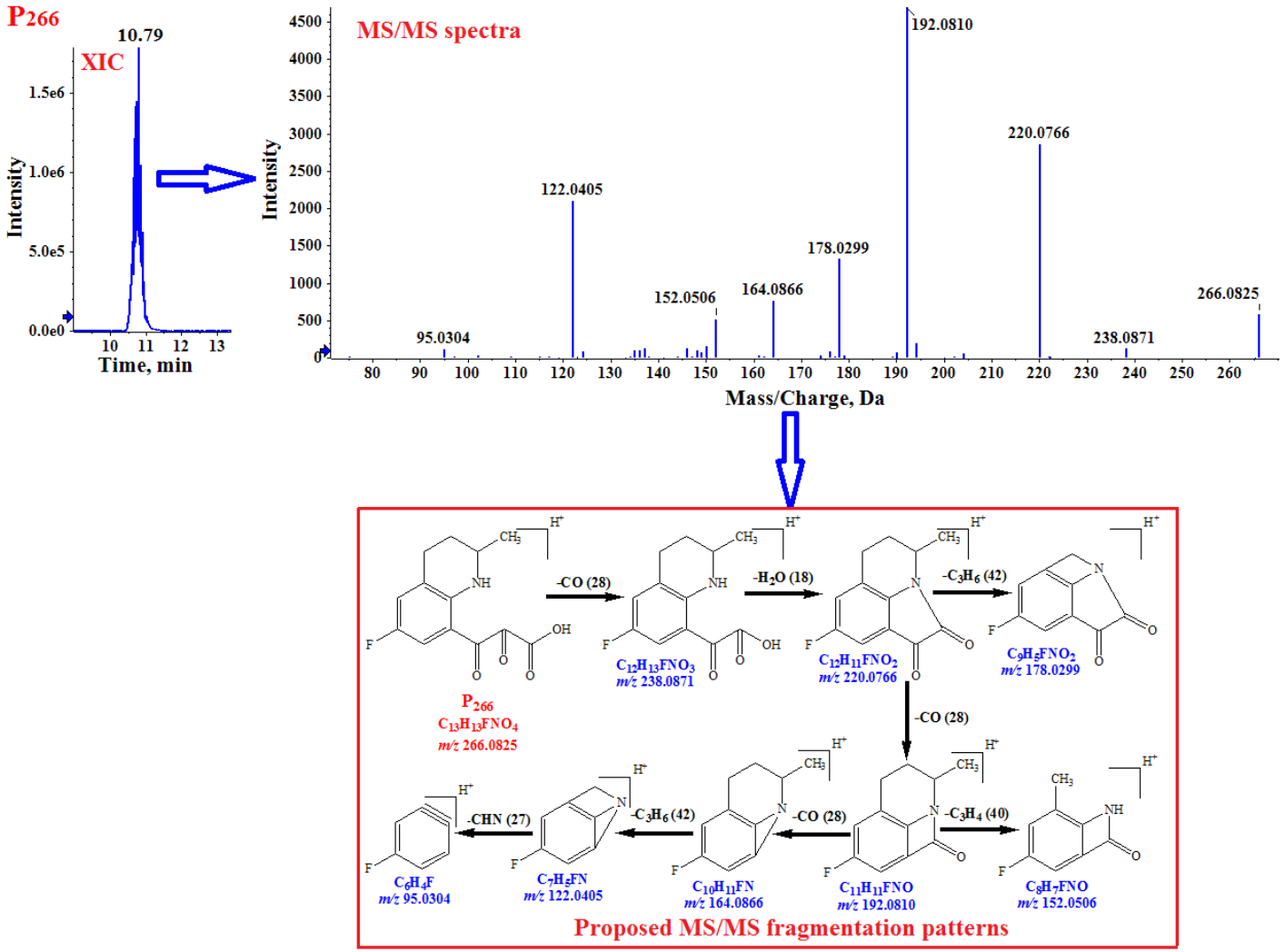

Fig. 5.10. Extracted ion chromatogram (XIC), MS/MS spectra, and proposed MS/MS fragmentation patterns of P_{266} (*m/z* 266.0825).

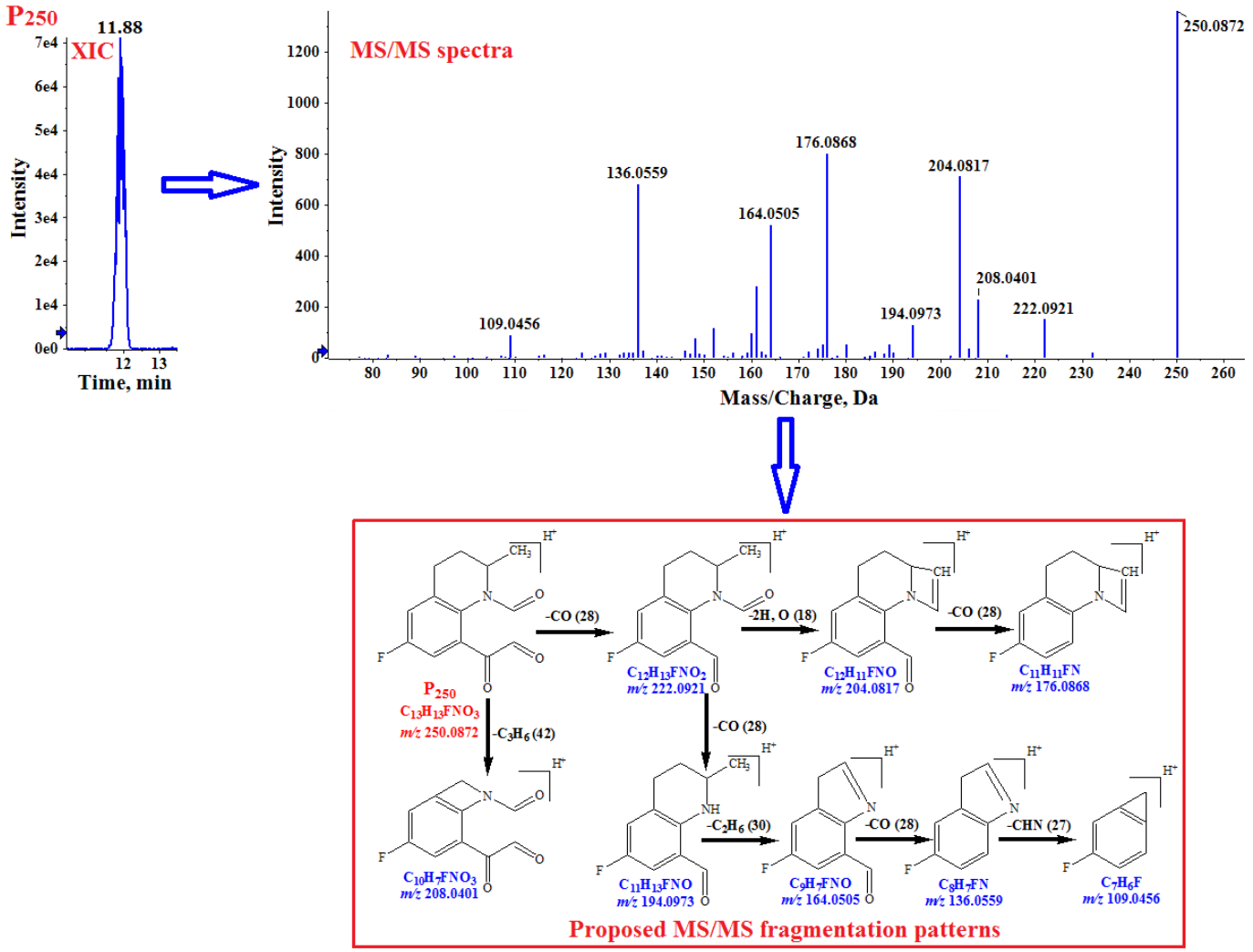

Fig. 5.11. Extracted ion chromatogram (XIC), MS/MS spectra, and proposed MS/MS fragmentation patterns of P_{250} (*m/z* 250.0872).

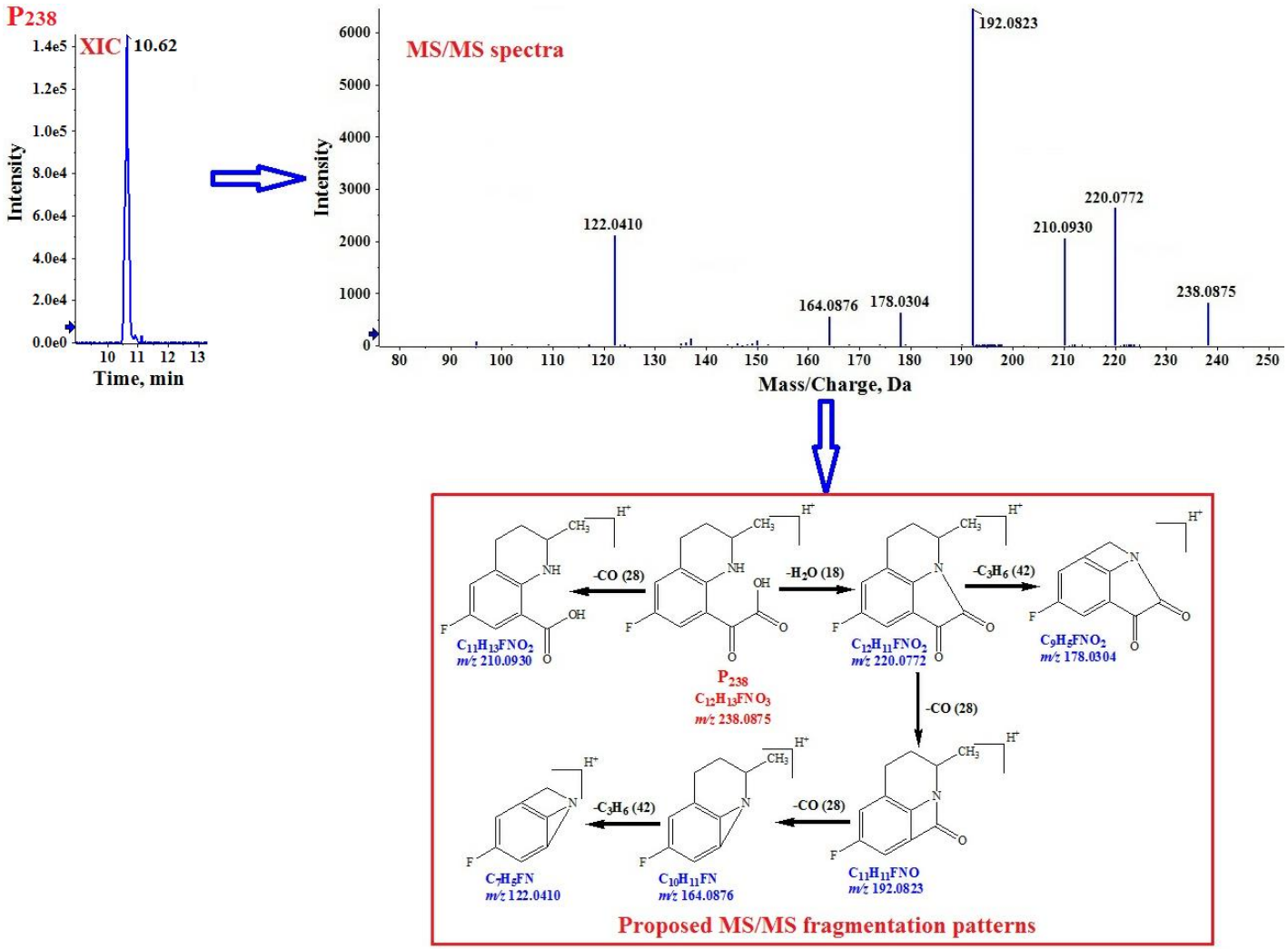

Fig. 5.12. Extracted ion chromatogram (XIC), MS/MS spectra, and proposed MS/MS fragmentation patterns of P_{238} (*m/z* 238.0875).

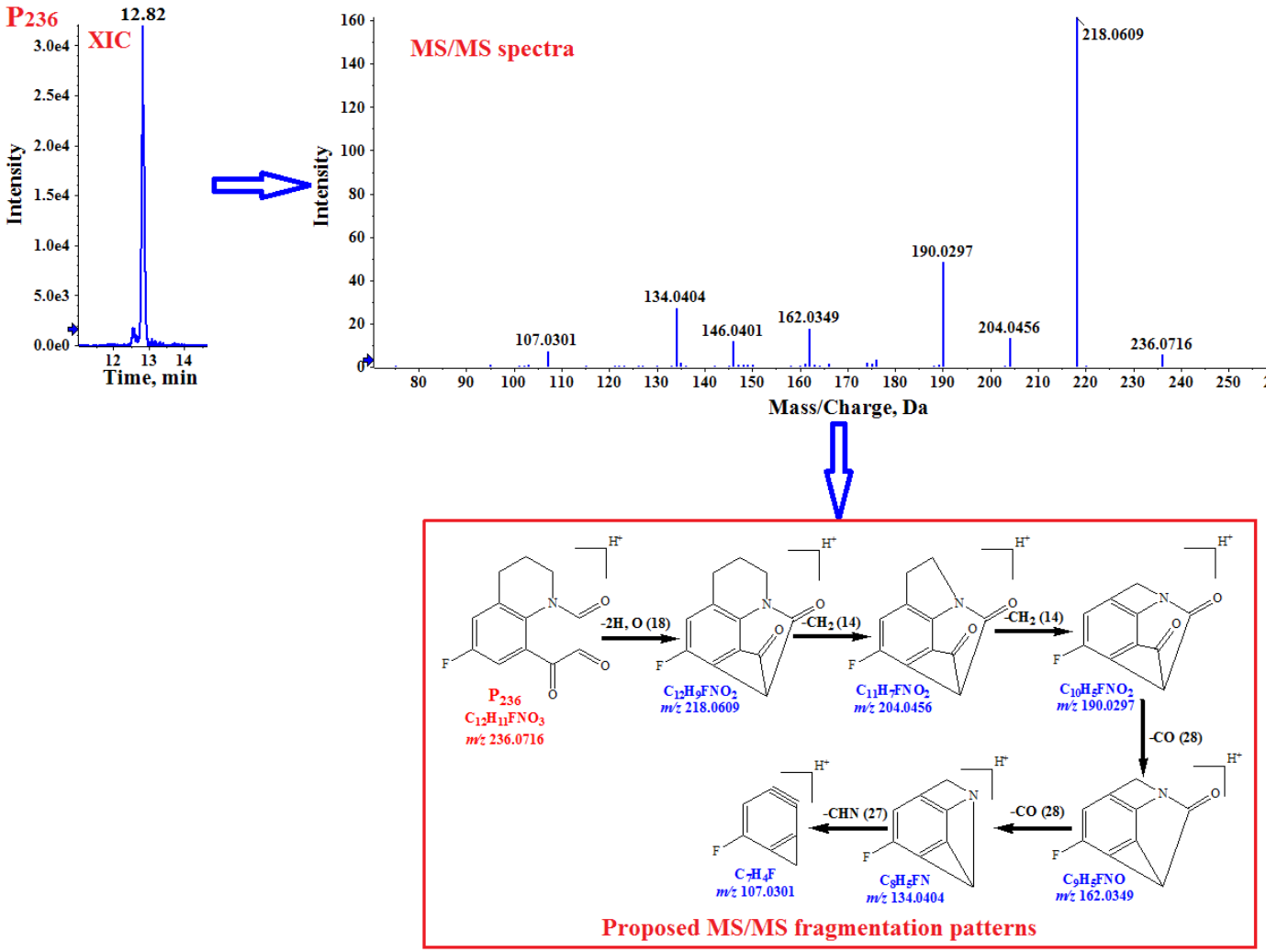

Fig. 5.13. Extracted ion chromatogram (XIC), MS/MS spectra, and proposed MS/MS fragmentation patterns of P_{236} (*m/z* 236.0716).

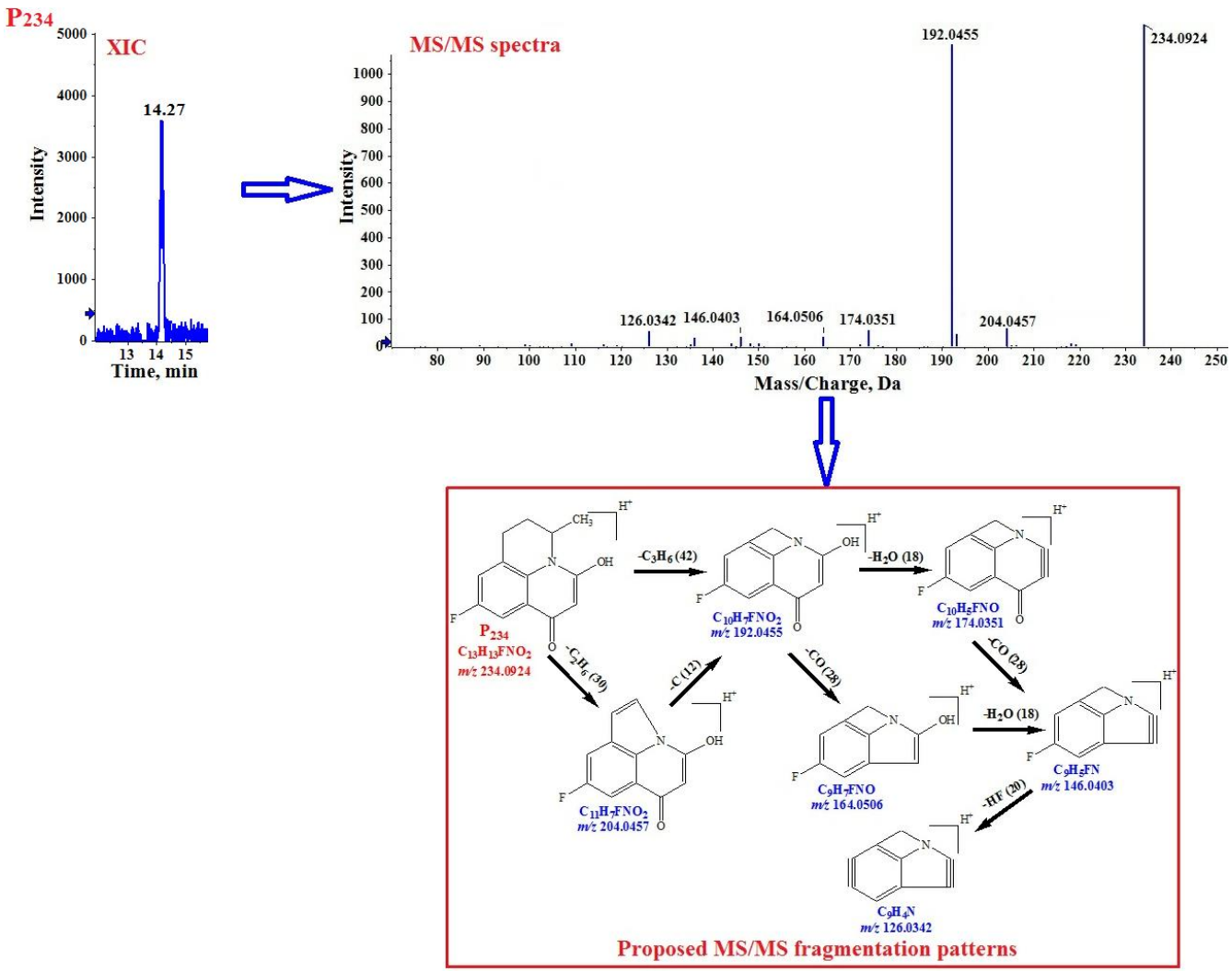

Fig. 5.14. Extracted ion chromatogram (XIC), MS/MS spectra, and proposed MS/MS fragmentation patterns of P_{234} (*m/z* 234.0924).

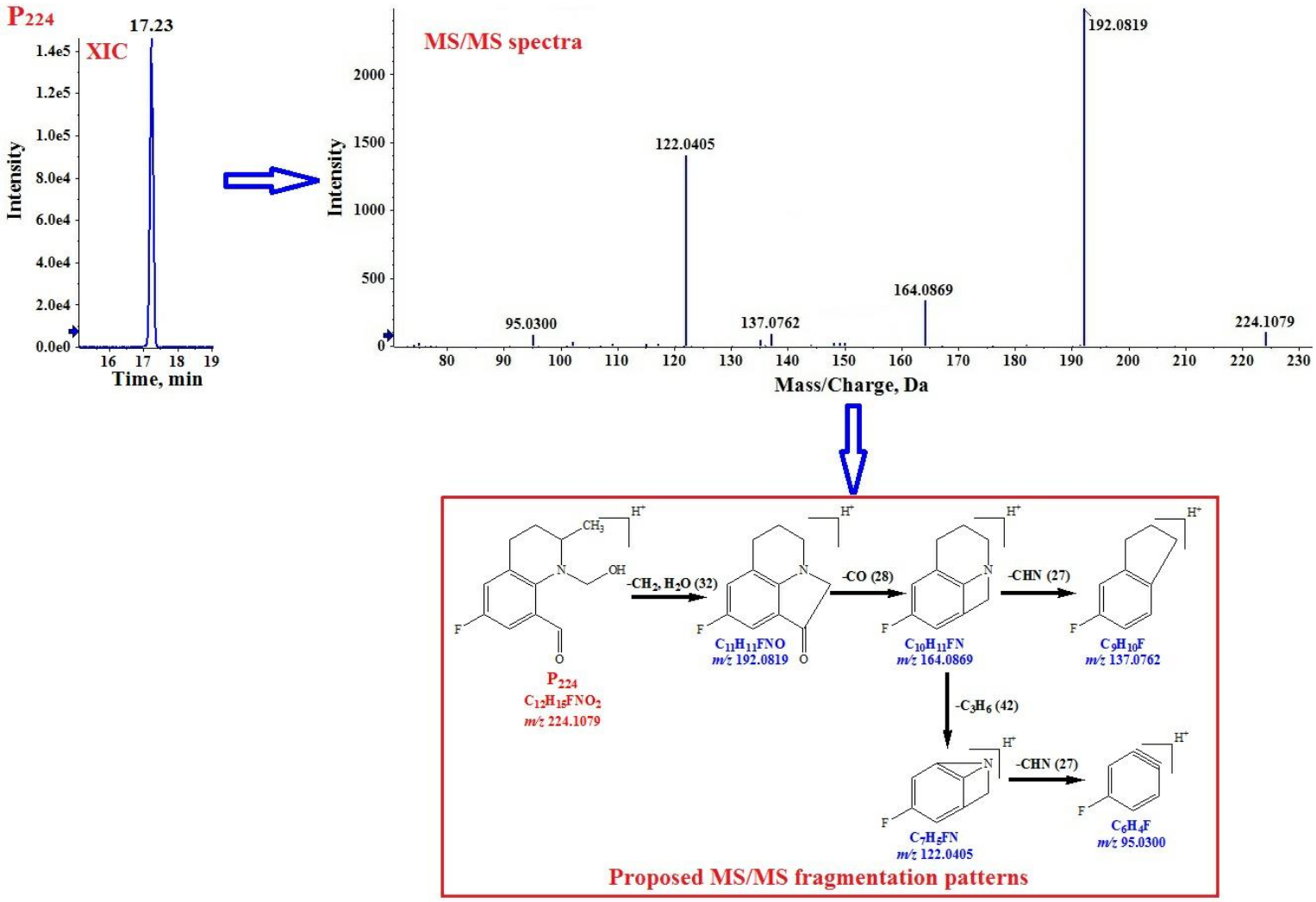

Fig. 5.15. Extracted ion chromatogram (XIC), MS/MS spectra, and proposed MS/MS fragmentation patterns of P_{224} (*m/z* 224.1079).

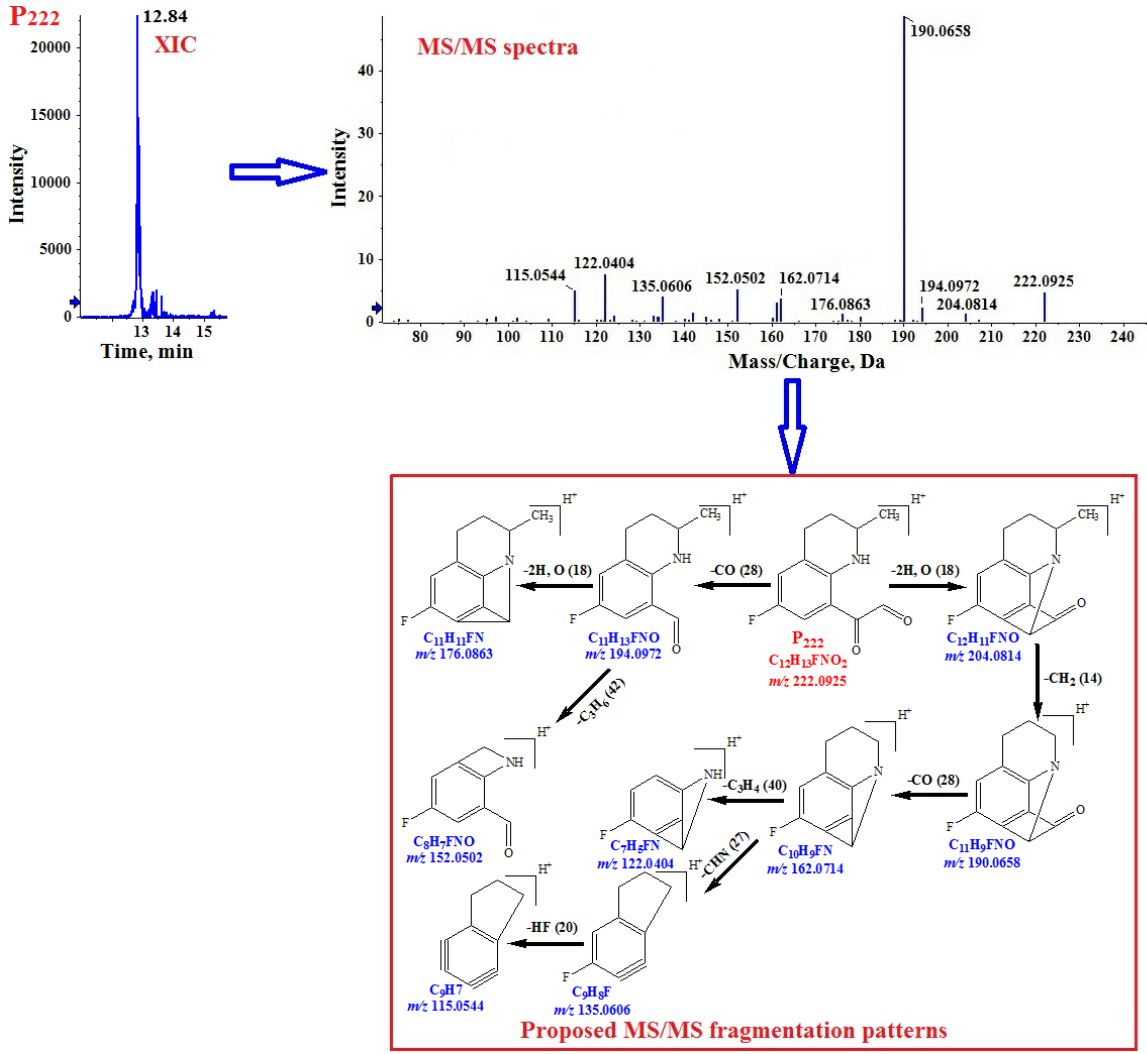

Fig. 5.16. Extracted ion chromatogram (XIC), MS/MS spectra, and proposed MS/MS fragmentation patterns of P_{222} (*m/z* 222.0925).

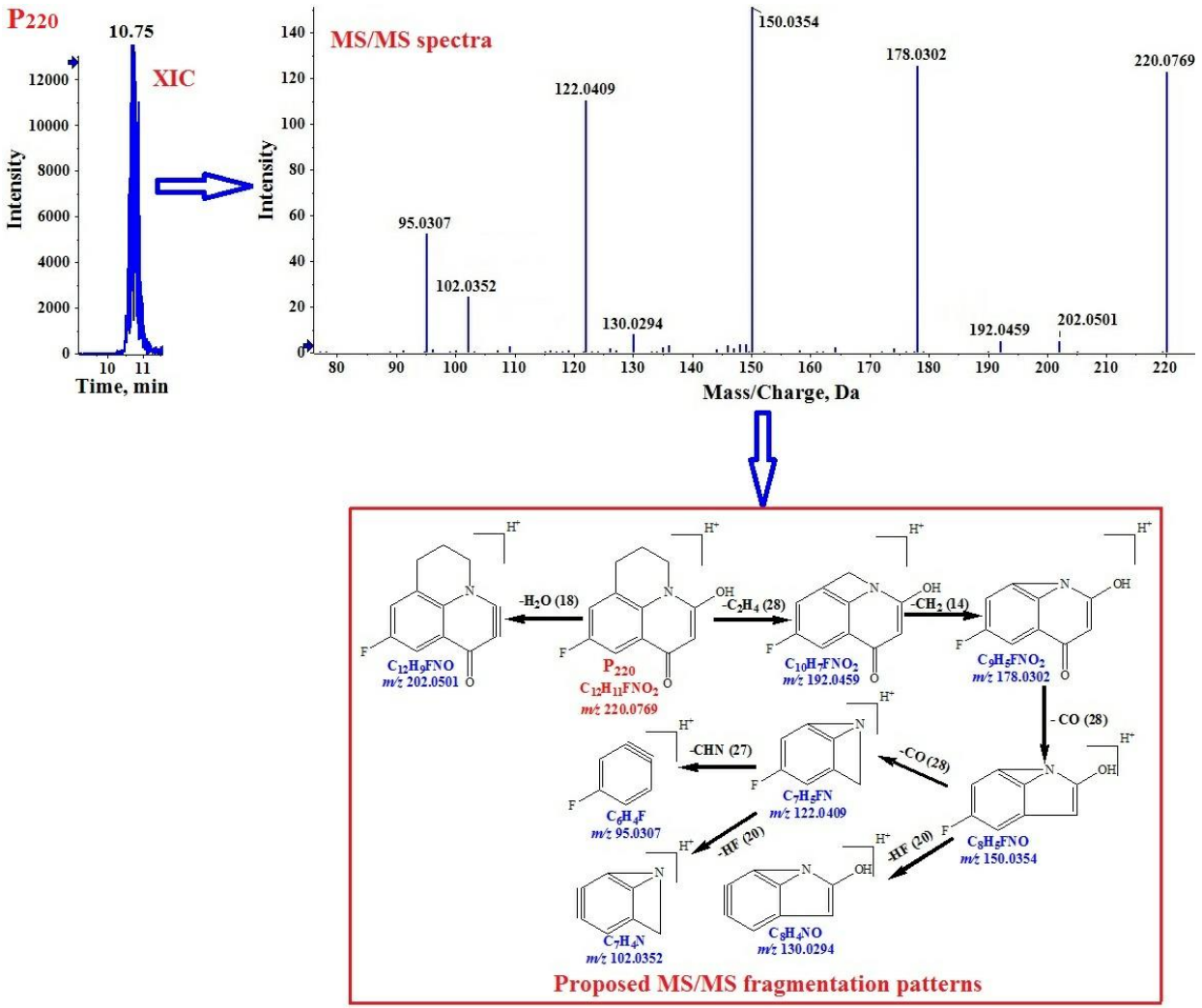

Fig. 5.17. Extracted ion chromatogram (XIC), MS/MS spectra, and proposed MS/MS fragmentation patterns of P_{220} (*m/z* 220.0769).

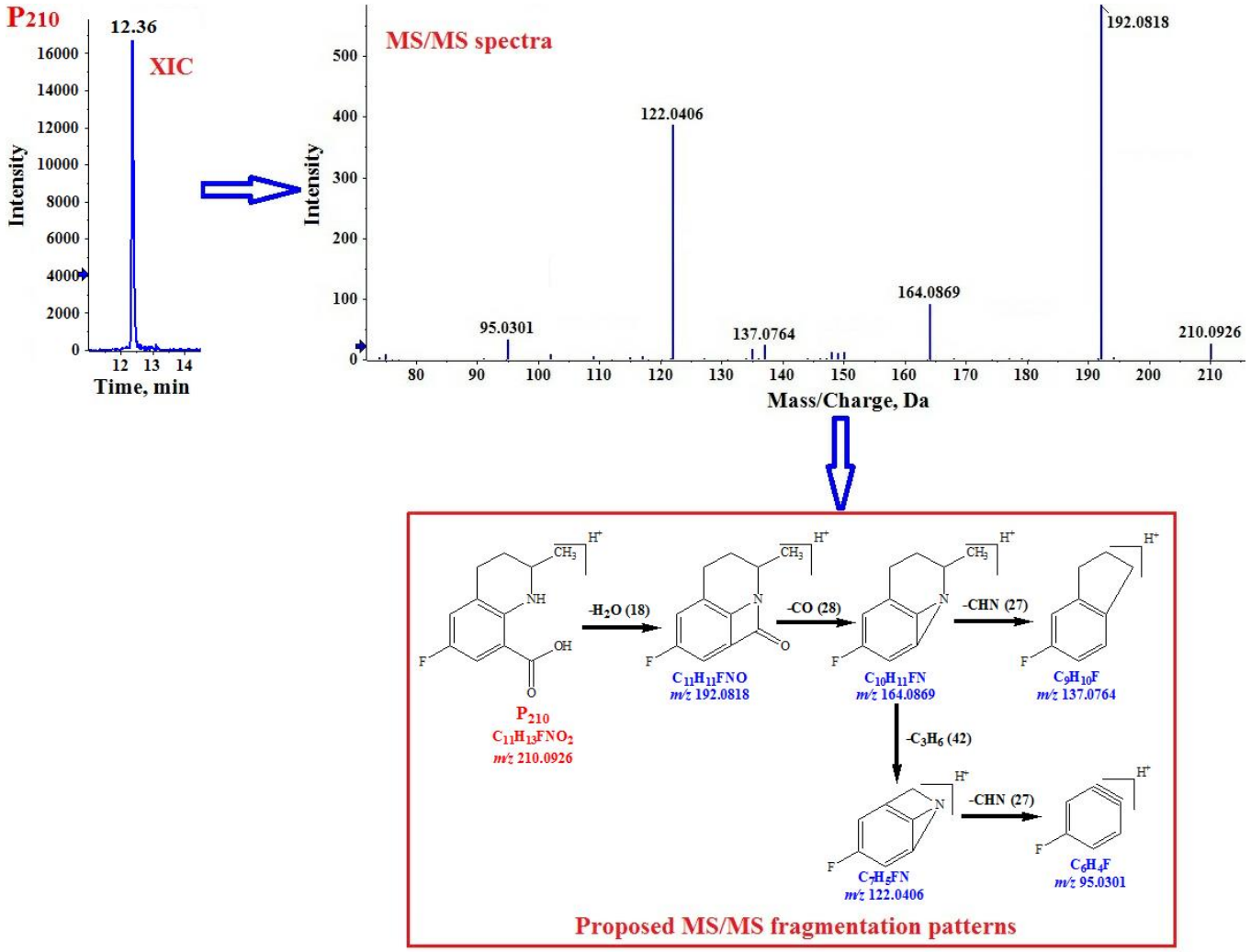

Fig. 5.18. Extracted ion chromatogram (XIC), MS/MS spectra, and proposed MS/MS fragmentation patterns of P_{210} (*m/z* 210.0926).

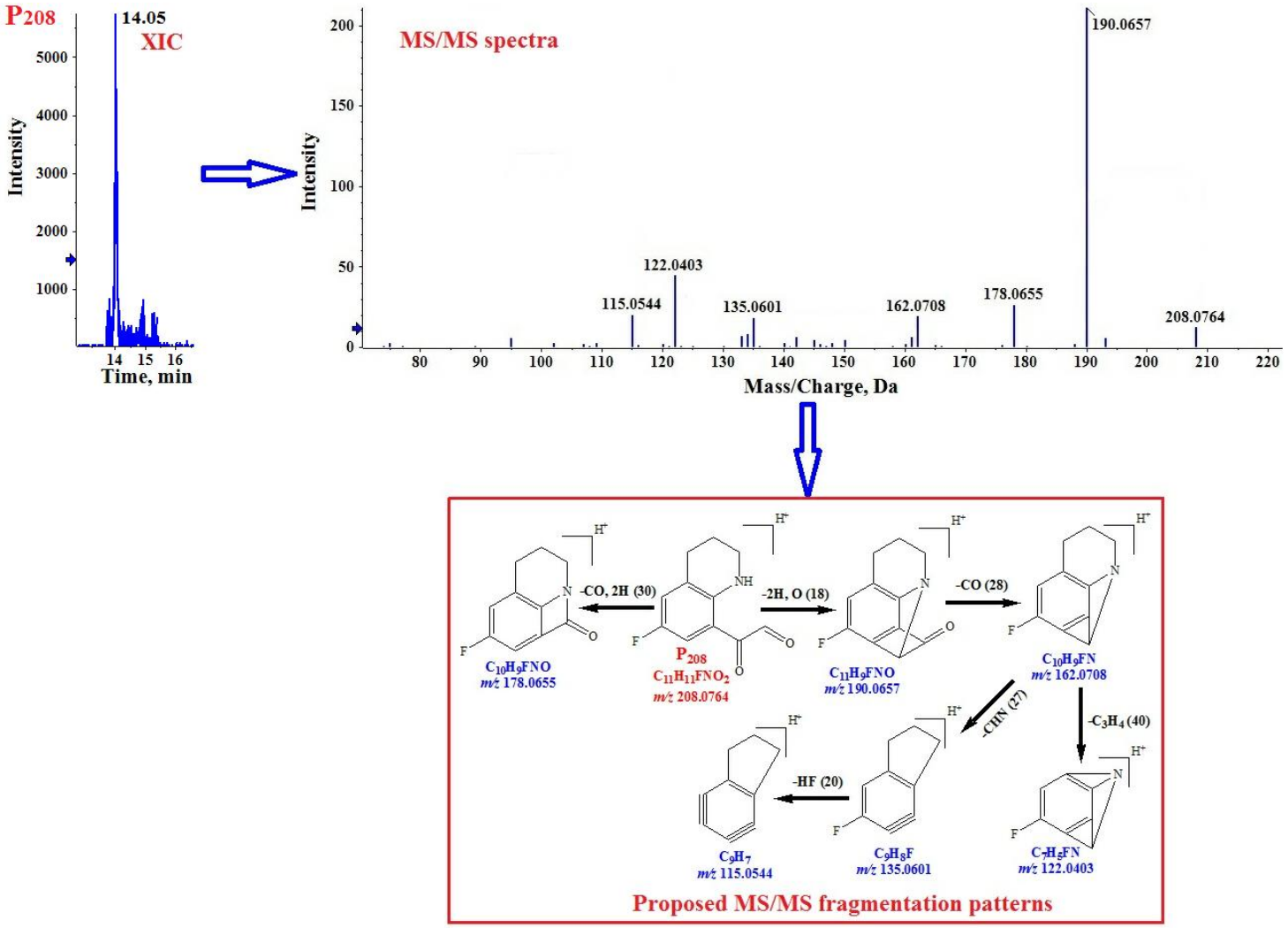

Fig. 5.19. Extracted ion chromatogram (XIC), MS/MS spectra, and proposed MS/MS fragmentation patterns of P_{208} (*m/z* 208.0764).

Scheme I

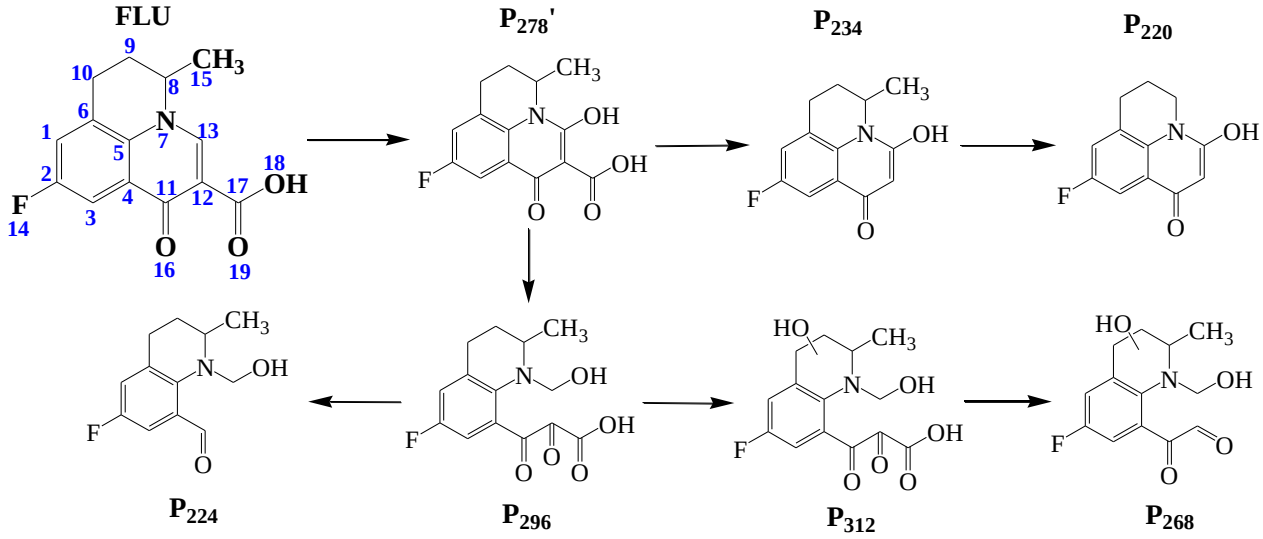

Fig. 5.20. Proposed reaction schemes of the oxidation of FLU by Fe^{VI} and Fe^{V} in the presence of 10 mM ammonia at pH 7.0 and 25 °C.

Scheme II

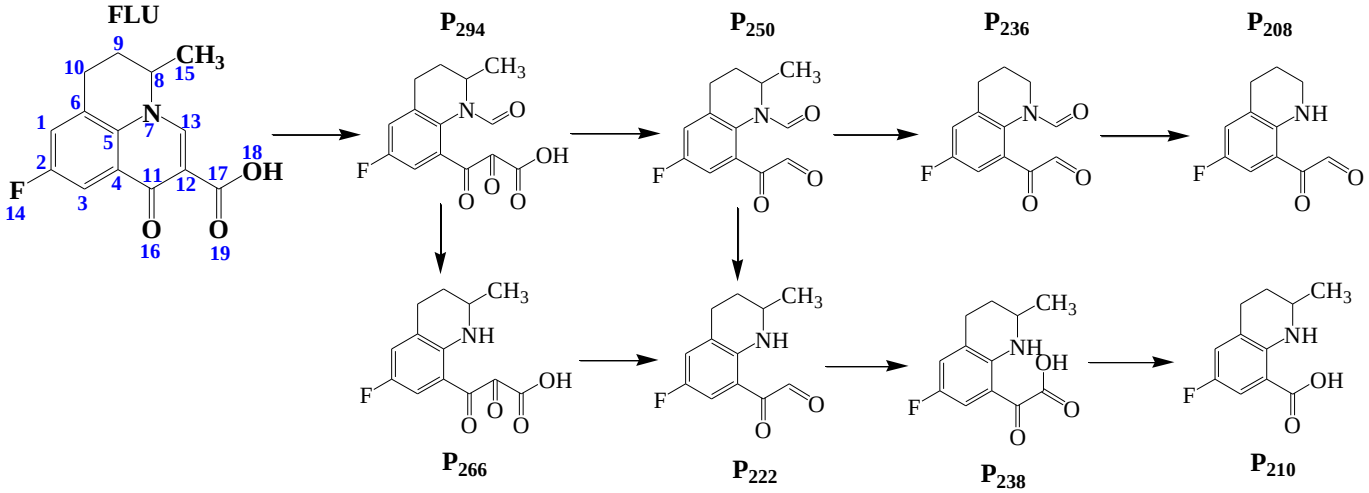

Scheme III

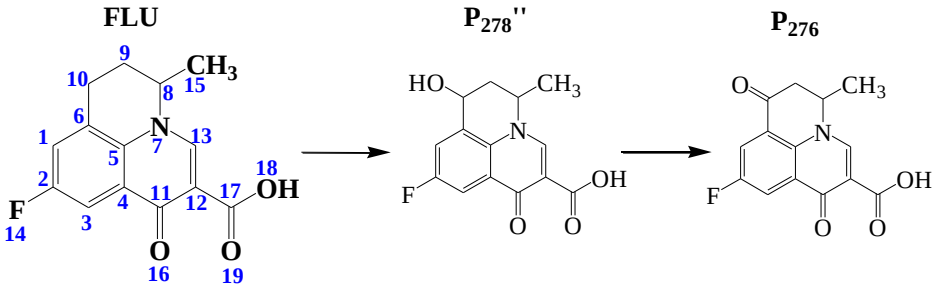

Fig. 5.20. Continued.

The influence of ammonia on enhanced removal of FLU by Fe^{VI} and Fe^{V} was understood by comparing the peak areas of the obtained OPs at molar ratios of 50:1 and 100:1 with and without ammonia (Figs. 5.21 and 5.22). As shown in *Scheme I* of Fig. 5.21, the presence of ammonia resulted in higher peak areas of products P_{234}, P_{312}, and P_{268}. These products suggest that ammonia in a reaction solution of Fe^{VI}-FLU could increase the attack on the double bond of C12=C13. This phenomenon of Fe^{VI} due to the presence of ammonia was also observed in the *Scheme II* of Fig. 20, which had higher peak areas of the products P_{294} and P_{250} in the presence of ammonia than in the absence of ammonia. Again, both of these products were obtained by the enhanced attack of oxidant(s) in the presence of ammonia on the double bond of the quinolone ring of FLU. These oxidants could be either Fe^{VI}-ammonia or Fe^{V}-ammonia or both species. The reasons for such possibility are based on available literatures on the high reactivity of high-valent iron compounds containing nitrogen-containing ligands (Ansari, et al., 2013; Berry, et al., 2006; McDonald and Que, 2013; Mills, et al., 2016; Scepaniak, et al., 2011). The peak areas of Fig. 5.21 suggest that Fe^{VI}-ammonia and Fe^{V}-ammonia complexes reacted faster at the double bond moiety of FLU than the un-complexed Fe^{VI} and Fe^{V} species. Furthermore, the peak areas of the products of *Scheme III* of Fig. 5.20 in the presence of ammonia were lower than those in the absence of ammonia. This further suggests the preference of Fe^{VI}-ammonia and Fe^{V}-ammonia complexes to produce OPs by involving the C12=C13 double bond of FLU.

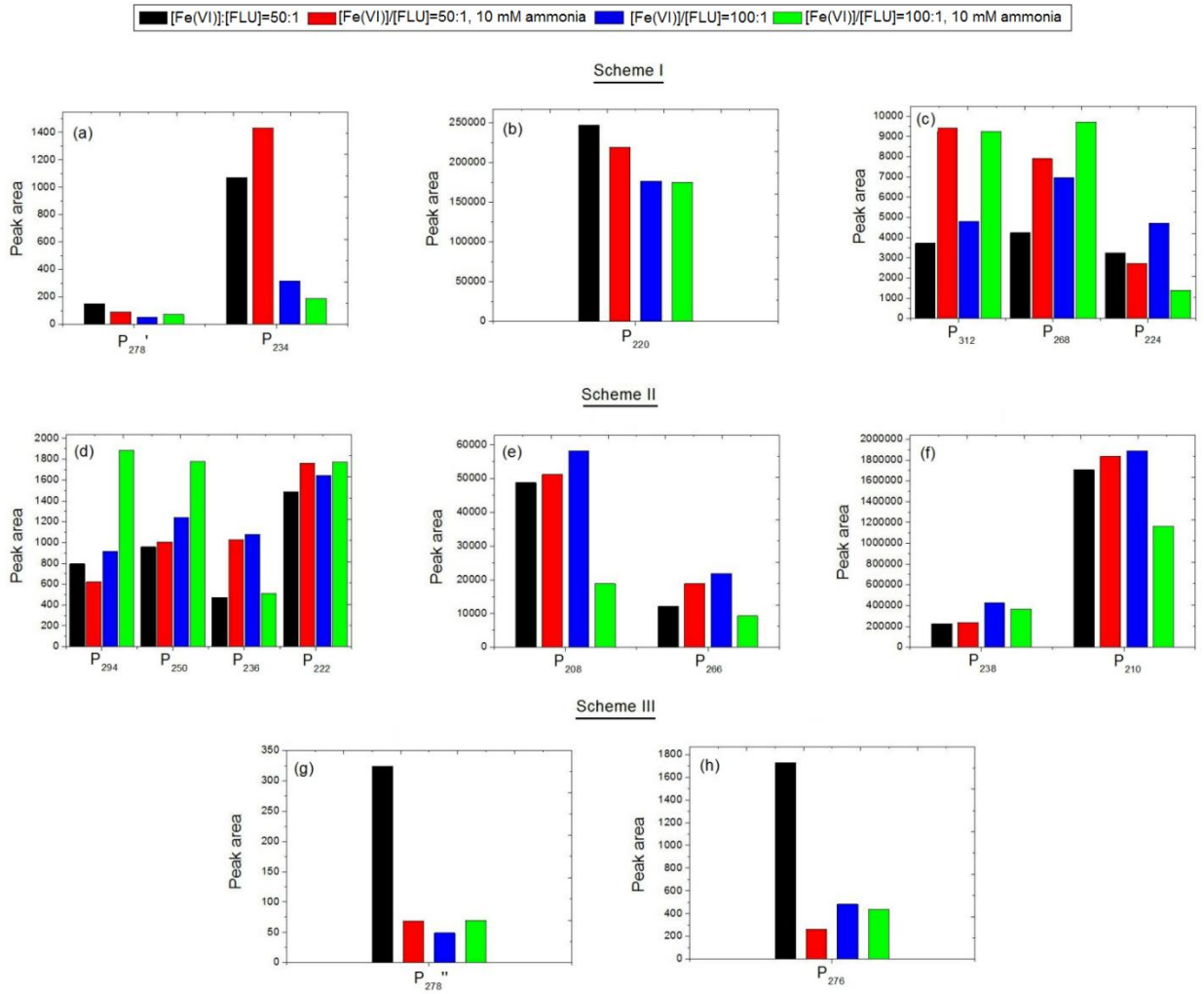

Fig. 5. 21. Peak areas of oxidized products in different schemes in reactions of Fe^{VI} with FLU with and without ammonia.

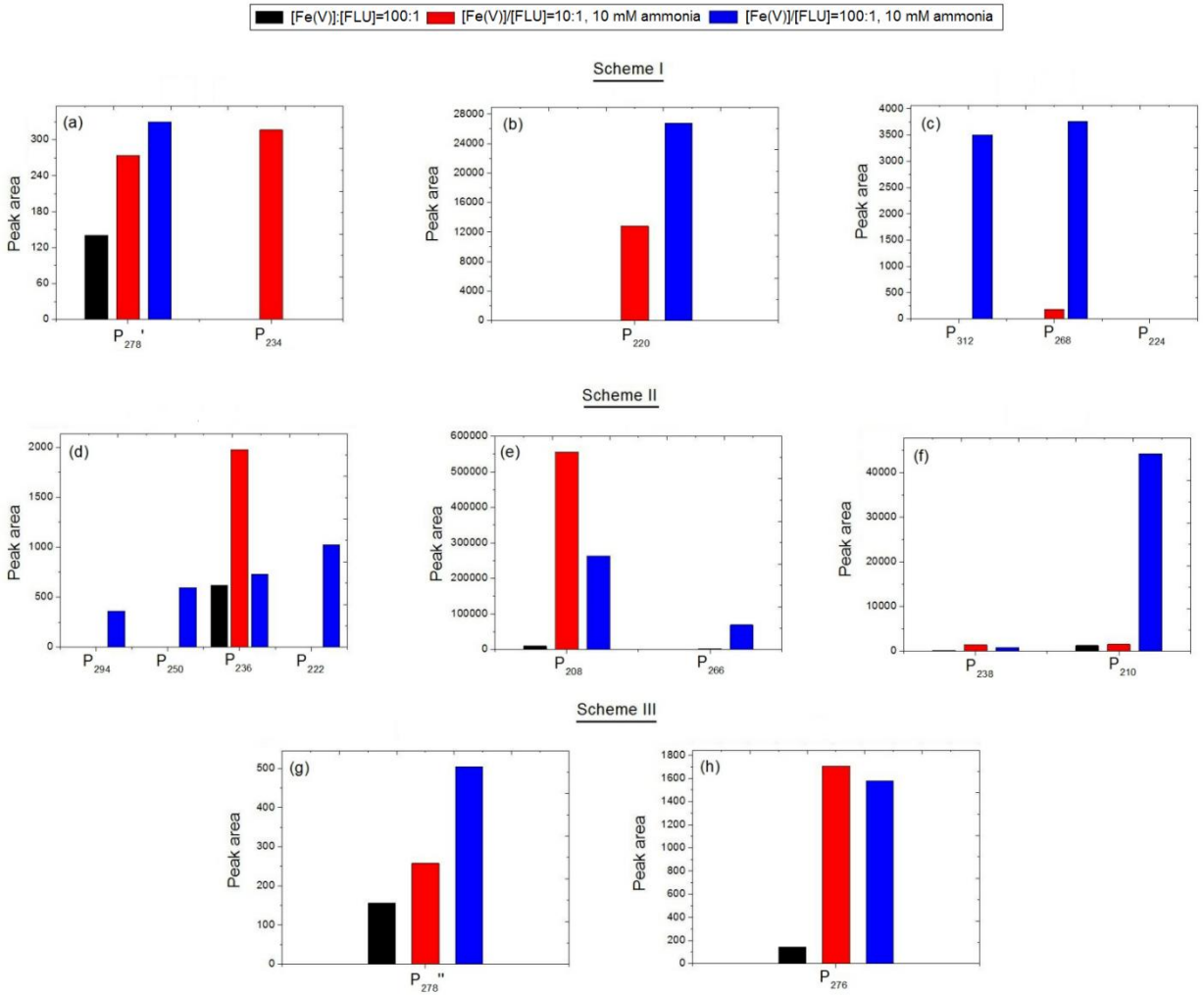

Fig. 5.22. Peak areas of oxidized products in different schemes in reactions of Fe^{V} with FLU with and without ammonia.

The involvement of Fe^{V} species in the oxidation of FLU by Fe^{VI} was observed in results of experiments carried out by using only Fe^{V} in the absence and presence of ammonia (Fig. 5.21). Black and red bars represent the same percentages of removal of FLU by Fe^{V} in the absence and presence of ammonia, respectively. However, peaks areas of OPs of the reaction schemes of Fig. 5.20 were greater with ammonia than without ammonia in the reaction solution of Fe^{V}-FLU. Significantly, the observation of similar OPs using only Fe^{V} supports the participation of Fe^{V} species in the degradation of FLU by Fe^{V}. Furthermore, enhanced peak areas due to the presence of ammonia again provide evidence that the Fe^{V}-ammonia complex may also be causing the enhanced oxidation at the C12=C13 double bond of FLU (see peak areas of *Schemes I* and *II* of Fig. 5.21). Similarly, such Fe^{V}-ammonia complexes could also increase hydroxylation at the C10 site of the FLU (see peak areas of *Scheme III* of Fig. 5.21). It appears from the results of peak areas of OPs in the absence and presence of ammonia that the nature of the reactive high-valent iron oxidant species in Fe^{VI}/Fe^{V}-ammonia-FLU mixtures were different from that present in Fe^{VI}/Fe^{V}-FLU solutions.

6. CONCLUSIONS

6.1. Summary

In this dissertation, aqueous transformations of three emerging micro-pollutants, including MC-LR (a representative cyclic heptapeptide toxin produced by cyanobacterial species), SDZ and FLU (two typical antibiotics of sulfonamides and fluoroquinolones), by high-valent iron species (Fe^{VI}, Fe^{V}, and Fe^{IV}) were carried out. Specifically, the additions and concentration effects of these three ferrates as well as those of the solution pH values on the transformation products and mechanisms of MC-LR were investigated. Regarding SDZ, the kinetics of the reaction between Fe^{VI} and SDZ as a function of pH were studied to determine the species-specific rate constants, while the products and pathways of SDZ by Fe^{VI} were first-measured and proposed. Additionally, the effects of ammonia on the oxidation of FLU by three ferrate species in the reaction solution were also investigated. The main conclusions of these studies are as follows:

(i) Based on seventeen identified products of MC-LR by Fe^{VI}, Fe^{V} and Fe^{IV} species at varying concentrations of 200 μM, 400 μM and 850 μM at pH 7.0, three reaction mechanisms were proposed, including hydroxylation at the Adda diene, elimination of the methoxy group of the Adda diene, and hydroxylation at the diene bond of the Mdha. Notably, the results demonstrated the hydroxylation of the aromatic ring of MC-LR by all these ferrate species, while hydroxylation and breakage of the peptide ring were also involved. The increasing concentrations of these oxidants for MC-LR oxidation showed that the product distribution may be not only related to differences in the nature of high-valent iron species, but also to their tendency in water to perform oxidation reactions.

Fe^{VI} is much more stable than Fe^{V} and Fe^{IV} species in water; therefore, Fe^{VI} would have a prolonged presence to yield OPs with lower molecular weight.

In addition, the influence of the solution pH (4.0, 7.0, and 9.0) on the oxidation of MC-LR by Fe^{VI}, Fe^{V} and Fe^{IV} was also investigated. The results indicated that the hydroxylation of the Adda diene and at the diene bond of the Mdha of MC-LR by all these ferrate species was greatly favored by acidic conditions compared to neutral and basic pH environments. In the initial step by MC-LR, the elimination of the methoxy moiety was seen only in the oxidation by Fe^{V} and Fe^{IV}, which was independent of the solution pH. Furthermore, the final products of the elimination of the methoxy processes were also independent of the pH.

(ii) The oxidation kinetic investigation of SDZ by Fe^{VI} indicated that the reaction followed the second-order kinetics, i.e., first-order with respect to each reactant. The measured values of the second-order rate constants decreased along with ~~the~~ increasing pH from 4.0 to 10.0, which can be successfully modeled by using equilibrium species of Fe^{VI} and SDZ, i.e., the protonation of Fe^{VI} increased the reactivity with the neutral species of SDZ. Based on eleven identified OPs of SDZ by LC-TOF-MS (ESI pos) in a product ion scan, the transformation pathways of SDZ by Fe^{VI} oxidation included three initial attacks, including SO_2 extrusion, deamination, and hydroxylation. Notably, the presence of Fe^{VI} resulted in SO_2 extrusion for the first time during the transformation of SDZ. Meanwhile, some other reactions such as opening of the six-membered heterocyclic ring were also involved.

(iii) The removal studies indicated that, at the test concentrations of three ferrate species, only Fe^{VI} could remove FLU completely at pH 7.0, followed by Fe^{V} (~20% removal of FLU) and Fe^{IV} (no removal of FLU). It appears that the self-decomposition rates of Fe^{V} and Fe^{IV} species in water were faster than their reactions with FLU at pH 7.0, since they possess a higher reactivity to pollutants than Fe^{VI}. In the presence of ammonia, the removal of FLU by Fe^{VI} and Fe^{V} species was enhanced, and this may be attributed to the formation of higher reactive Fe^{VI}-ammonia and Fe^{V}-ammonia complexes rather than to un-complexed Fe^{VI} and Fe^{V} species. The peak areas of the identified products and the proposed mechanisms indicated that the former complexes reacted faster at the double bond moiety of the quinolone ring of FLU than the latter species, leading to the larger amounts of certain OPs in the presence of ammonia than in the absence of ammonia.

6.2. Outlook

The current studies presented some detailed investigations regarding the transformation processes and mechanisms of three typical micro-pollutants (MC-LR, SDZ and FLU) by three ferrate species (Fe^{VI}, Fe^{V}, and Fe^{IV}) in water. Based on these findings, future research~~es~~ may be performed aimed at the following aspects:

(i) As can be learned from MC-LR, other microcystins such as microcystin-LA, microcystin-RR, and microcystin-YR can be further investigated and compared to learn if amino acids have any influence on kinetics and products after treatment~~s~~ by three high-valent iron species, i.e., Fe^{VI}, Fe^{V}, and Fe^{IV}. In addition, the possible influences of more environmental factors, such as solution pH, co-existing cations and anions, natural

organic matters and even different water matrices, could be studied to learn the efficiency and practicality of ferrate technologies for removing these kinds of toxins from the real water environment.

(ii) Regarding SDZ, it is noteworthy that SO_2 extrusion occurred during its oxidation by Fe^{VI} in water. In future degradation studies, we could explore any other sulfonamides to determine if SO_2 extrusion is also happening in those molecules during aqueous transformation by three different ferrate species, and therefore, more detailed mechanisms for this reaction should be investigated. In addition, the formation of the resultant products should be further structurally demonstrated by comparing them with the corresponding standard chemicals or by using more systematical analytical approaches such as FT-IR and NMR. Meanwhile, some quantum chemical methods, including the frontier molecular orbitals, transition states, and reaction energy barriers, may be applied to provide theoretical guidelines and confirmations for the reaction mechanisms.

(iii) Notably, it is observed that the removal percentage of FLU could be improved by the use of ammonia-activated Fe^{VI} and Fe^{V}. In subsequent studies, similar enhanced effects of ammonia should be investigated for other FQs to learn if ferrate technologies could be used as the preferential and alternative treatments for the remediation of ammonia-containing wastewaters polluted by FQ residues.

(iv) Overall, the removal experiments of micro-pollutants by ferrates in the present thesis were performed using lab-scale methods. In future, efforts should be made to facilitate their practical applications in water and wastewater treatment. Generally, the

superior oxidation/disinfection and coagulation properties of ferrates over conventional treatment chemicals can meet the new challenges confronting the water industry in treating effectively both organic and inorganic contaminants. Additionally, concerns related to toxic by-products (e.g., chlorinated by-products from chlorination, nitrosoamines from chloramination, and bromate formation from the ozonation of bromide-containing water) can be addressed successfully using ferrate technology. Any practical application of ferrate in real water treatment settings (i.e., plant scale facilities) would require detailed investigation of the stability of ferrates species in the wastewater matrices. A cost effectiveness of the use of ferrates also needs to be evaluated in order to apply ferrates as an environmental friendly technology to remediate pollutants in water and wastewater.

REFERENCES

Acero, J.L., RodriÌguez, E., Majado, M.E., Sordo, A., Meriluoto, J., 2008. Oxidation of microcystin-LR with chlorine and permanganate during drinking water treatment. J. Water Supply: Res. Technol. - AQUA. 57, 371-380.

Adamovsky, O., Moosova, Z., Pekarova, M., Basu, A., Babica, P., Svihalkova Sindlerova, L., Kubala, L., Blaha, L., 2015. Immunomodulatory potency of microcystin, an important water-polluting cyanobacterial toxin. Environ. Sci. Technol. 49, 12457-12464.

Anquandah, G.A.K., Sharma, V.K., Knight, D.A., Batchu, S.R., Gardinali, P.R., 2011. Oxidation of trimethoprim by ferrate(VI): kinetics, products, and antibacterial activity. Environ. Sci. Technol. 45, 10575-10581.

Ansari, A., Kaushik, A., Rajaraman, G., 2013. Mechanistic insights on the *ortho*-hydroxylation of aromatic compounds by non-heme iron complex: A computational case study on the comparative oxidative ability of ferric-hydroperoxo and high-valent Fe^{IV}=O and Fe^{V}=O intermediates. J. Am. Chem. Soc. 135, 4235-4249.

Antoniou, M.G., de la Cruz, A.A., Dionysiou, D.D., 2010. Intermediates and reaction pathways from the degradation of microcystin-LR with sulfate radicals. Environ. Sci. Technol. 44, 7238-7244.

Antoniou, M.G., Shoemaker, J.A., de la Cruz, A.A., Dionysiou, D.D., 2008. Unveiling new degradation intermediates/pathways from the photocatalytic degradation of microcystin-LR. Environ. Sci. Technol. 42, 8877-8883.

aus der Beek, T., Weber, F.A., Bergmann, A., Hickmann, S., Ebert, I., Hein, A., Küster, A., 2016. Pharmaceuticals in the environment-global occurrences and perspectives. Environ. Toxicol. Chem. 35, 823-835.

Backer, L.C., Manassaram-Baptiste, D., LePrell, R., Bolton, B., 2015. Cyanobacteria and algae blooms: Review of health and environmental data from the harmful algal bloom-related illness surveillance system (HABISS) 2007–2011. Toxins 7, 1048-1064.

Barbosa, M.O., Moreira, N.F.F., Ribeiro, A.R., Pereira, M.F.R., Silva, A.M.T., 2016. Occurrence and removal of organic micropollutants: An overview of the watch list of EU Decision 2015/495. Water Res. 94, 257-279.

Ben, W., Wang, J., Cao, R., Yang, M., Zhang, Y., Qiang, Z., 2017. Distribution of antibiotic resistance in the effluents of ten municipal wastewater treatment plants in China and the effect of treatment processes. Chemosphere 172, 392-398.

Bernasconi, L., Louwerse, M.J., Baerends, E.J., 2007. The role of equatorial and axial ligands in promoting the activity of non-heme oxidoiron(IV) catalysts in alkane hydroxylation. Eur. J. Inorg. Chem. 19, 3023-3033.

Berry, J.F., Bill, E., Bothe, E., George, S., Mienert, B., Neese, F., Wieghardt, K., 2006. An octahedral coordination complex of iron(VI). Science 312, 1937-1941.

Bielski, B.H.J., Sharma, V.K., Czapski, G., 1994. Reactivity of ferrate(V) with carboxylic acids: a pre-mix pulse radiolysis study. Radiat. Phys. Chem. 44, 479-484.

Boreen, A.L., Arnold, W.A., McNeill, K., 2004. Photochemical fate of sulfa drugs in then aquatic environment: sulfa drugs containing five-membered heterocyclic groups. Environ. Sci. Technol. 38, 3933-3940.

Boreen, A.L., Arnold, W.A., McNeill, K., 2005. Triplet-sensitized photodegradation of sulfa drugs containing six-membered heterocyclic groups: Identification of an SO_2 extrusion photoproduct. Environ. Sci. Technol. 39, 3630-3638.

Boreen, A.L., Edhlund, B.L., Cotner, J.B., McNeill, K., 2008. Indirect photodegradation of dissolved free amino acids: The contribution of singlet oxygen and the differential reactivity of DOM from various sources. Environ. Sci. Technol. 42, 5492-5498.

Botana, L.M., 2016. Toxicological perspective on climate change: aquatic toxins. Chem. Res. Toxicol. 29, 619-625.

Boxall, A.B.A., Rudd, M.A., Brooks, B.W., Caldwell, D.J., Choi, K., Hickmann, S., Innes, E., Ostapyk, K., Staveley, J.P., Verslycke, T., 2012. Pharmaceuticals and personal care products in the environment: what are the big questions? Environ Health Perspect. 120, 1221-1229.

Brausch, J.M., Connors, K.A., Brooks, B.W., Rand, G.M., 2012. Human pharmaceuticals in the aquatic environment: A review of recent toxicological studies and considerations for toxicity testing. Rev. Environ. Contam. T. 218, 1-99.

Bu, Q.W., Wang, B., Huang, J., Deng, S.B., Yu, G., 2013. Pharmaceuticals and personal care products in the aquatic environment in China: A review. J. Hazard. Mater. 262, 189-211.

Buratti, F.M., Scardala, S., Funari, E., Testai, E., 2011. Human glutathione transferases catalyzing the conjugation of the hepatoxin microcystin-LR. Chem. Res. Toxicol. 24, 926-933.

Campinas, M., Rosa, M.J., 2010. Removal of microcystins by PAC/UF. Sep. Purif. Technol. 71, 114-120.

Carr, J.D., 2008. Kinetics and product identification of oxidation by ferrate(VI) of water and aqueous nitrogen containing solutes. ACS Symp. Ser. 985(Ferrates), 189-196.

Carraro, E., Bonetta, S., Bertino, C., Lorenzi, E., Bonetta, S., Gilli, G., 2016. Hospital effluents management: chemical, physical, microbiological risks and legislation in different countries. J. Environ. Manage. 168, 185-199.

Carvalho, I.T., Santos, L., 2016. Antibiotics in the aquatic environments: A review of the European scenario. Environ. Int. 94, 736-757.

Cataldo, F., Ragni, P., Iglesias-Groth, S., Manchado, A., 2011. Solid state radiolysis of sulphur-containing amino acids: Cysteine, cystine and methionine. J. Radioanal. Nucl. Chem. 287, 573-580.

Cavazza, C., Bochot, C., Rousselot-Pailley, P., Carpentier, P., Cherrier, M.V., Martin, L., Marchi-Delapierre, C., Fontecilla-Camps, J.C., Ménage, S., 2010. Crystallographic snapshots of the reaction of aromatic C-H with O_2 catalysed by a protein-bound iron complex. Nature Chem. 2, 1069-1076.

Chanda, A., Khetan, S.K., Banerjee, D., Ghosh, A., Collins, T.J., 2006. Total degradation of fenitrothion and other organophosphorus pesticides by catalytic oxidation employing Fe-TAML peroxide activators. J. Am. Chem. Soc. 128, 12058-12059.

Chen, G., Li, M., Liu, X., 2015. Fluoroquinolone antibacterial agent contaminants in soil/groundwater: A literature review of sources, fate, and occurrence. Water Air Soil Pollut. 226, 1-11.

Chen, L., Chen, J., Zhang, X., Xie, P., 2016. A review of reproductive toxicity of microcystins. J. Hazard. Mater. 301, 381-399.

Chen, L., Mendoza, I., Gardinali, P.R., O'Shea, K.E., Dionysiou, D.D., Zboril, R., Sharma, V.K., 2017. Oxidation of microcystin-LR by Fe^{VI}, Fe^{V}, and Fe^{IV}: Degradation pathways. Chem. Eng. J., Submitted.

Chierentin, L., Salgado, H.R.N., 2016. Review of properties and analytical methods for the determination of norfloxacin. Crit. Rev. Anal. Chem. 46, 22-39.

Cho, K.B., Hirao, H., Shaik, S., Nam, W., 2016. To rebound or dissociate? This is the mechanistic question in C-H hydroxylation by heme and nonheme metal-oxo complexes. Chem. Soc. Rev. 45, 1197-1210.

Cizmas, L., Sharma, V.K., Gray, C., McDonald, T.J., 2015. Pharmaceuticals and personal care products in waters: occurrence, toxicity, and risk. Environ. Chem. Lett. 13, 381-394.

Corcoran, J., Winter, M.J., Tyler, C.R., 2010. Pharmaceuticals in the aquatic environment: A critical review of the evidence for health effects in fish. Crit. Rev. Toxicol. 40, 287-304.

Craig, M., Luu, H.A., McCready, T.L., Williams, D., Andersen, R.J., Holmes, C.F.B., 1996. Molecular mechanisms underlying the interaction of motuporin and microcystins with type-1 and type-2A protein phosphatases. Biochem. Cell Biol. 74, 569-578.

Dawson, J.F., Holmes, C.F., 1999. Molecular mechanisms underlying inhibition of protein phosphatases by marine toxins. Front. Biosci. 4. D646-D658.

De Freitas, A.M., Sirtori, C., Lenz, C.A., Zamora, P.G.P., 2013. Microcystin-LR degradation by solar photo-Fenton, UV-A/photo-Fenton and UV-C/H_2O_2: A comparative study. Photochem. Photobiol. Sci. 12, 696-702.

de la Cruz, A.A., Antoniou, M.G., Hiskia, A., Pelaez, M., Song, W., O'Shea, K.E., He, X., Dionysiou, D.D., 2011. Can we effectively degrade microcystins? - Implications on human health. Anti-Cancer Agent. ME. 11, 19-37.

Dekker, D.M., Krumkamp, R., Sarpong, N., Frickmann, H., Boahen, K.G., Frimpong, M., Asare, R., Larbi, R., Hagen, R.M., Poppert, S., Rabsch, W., Marks, F., Sarkodie, Y.A., May, J., 2015. Drinking water from dug wells in rural Ghana — *Salmonella* contamination, environmental factors, and genotypes. Int. J. Environ. Res. Public Health. 12, 3535-3546.

Deng, Y., Mao, Y., Li, B., Yang, C., Zhang, T., 2016. Aerobic degradation of sulfadiazine by *arthrobacter spp.*: Kinetics, pathways, and genomic characterization. Environ. Sci. Technol. 50, 9566-9575.

Dodd, M.C., Shah, A.D., Von Gunten, U., Huang, C.H., 2005. Interactions of fluoroquinolone antibacterial agents with aqueous chlorine: Reaction kinetics, mechanisms, and transformation pathways. Environ. Sci. Technol. 39, 7065-7076.

Dorival-García, N., Zafra-Gómez, A., Cantarero, S., Navalón, A., Vílchez, J.L., 2013. Simultaneous determination of 13 quinolone antibiotic derivatives in wastewater samples using solid-phase extraction and ultra performance liquid chromatography-tandem mass spectrometry. Microchem. J. 106, 323-333.

Drobac, D., Tokodi, N., Lujic, J., Marinovic, Z., Subakov-Simic, G., Dulic, T., Važic, T., Nybom, S., Meriluoto, J., Codd, G.A., Svircev, Z., 2016. Cyanobacteria and cyanotoxins in fishponds and their effects on fish tissue. Harmful Algae 55, 66-76.

Ebert, I., Bachmann, J., Kühnen, U., Küster, A., Kussatz, C., Maletzki, D., Schlüter, C., 2011. Toxicity of the fluoroquinolone antibiotics enrofloxacin and ciprofloxacin to photoautotrophic aquatic organisms. Environ. Toxicol. Chem. 30, 2786-2792.

Eskandarian, M.R., Choi, H., Fazli, M., Rasoulifard, M.H., 2016. Effect of UV-LED wavelengths on direct photolytic and TiO_2 photocatalytic degradation of emerging contaminants in water. Chem. Eng. J. 300, 414-422.

Fagan, R., McCormack, D.E., Dionysiou, D.D., Pillai, S.C., 2016. A review of solar and visible light active TiO_2 photocatalysis for treating bacteria, cyanotoxins and contaminants of emerging concern. Mater. Sci. Semicond. Process. 42, 2-14.

Feng, M., Cizmas, L., Wang, Z., Sharma, V.K., 2017. Activation of ferrate(VI) by ammonia in oxidation of flumequine: Kinetics, transformation products, and antibacterial activity assessment. Chem. Eng. J. Submitted.

Feng, M., Qu, R., Zhang, X., Sun, P., Sui, Y., Wang, L., Wang, Z., 2015. Degradation of flumequine in aqueous solution by persulfate activated with common methods and polyhydroquinone-coated magnetite/multi-walled carbon nanotubes catalysts. Water Res. 85, 1-10.

Feng, M., Wang, X., Chen, J., Qu, R., Sui, Y., Cizmas, L., Wang, Z., Sharma, V.K., 2016a. Degradation of fluoroquinolone antibiotics by ferrate(VI): Effects of water constituents and oxidized products. Water Res. 103, 48-57.

Feng, M., Yan, L., Zhang, X., Sun, P., Yang, S., Wang, L., Wang, Z., 2016b. Fast removal of the antibiotic flumequine from aqueous solution by ozonation: Influencing factors, reaction pathways, and toxicity evaluation. Sci. Total Environ. 541, 167-175.

Feng, Y., Wu, D., Deng, Y., Zhang, T., Shih, K., 2016c. Sulfate radical-mediated degradation of sulfadiazine by $CuFeO_2$ rhombohedral crystal-catalyzed peroxymonosulfate: Synergistic effects and mechanisms. Environ. Sci. Technol. 50, 3119-3127.

Ferrão-Filho, A.D.S., Kozlowsky-Suzuki, B., 2011. Cyanotoxins: Bioaccumulation and effects on aquatic animals. Mar. Drugs. 9, 2729-2772.

Flores, C., Caixach, J., 2015. An integrated strategy for rapid and accurate determination of free and cell-bound microcystins and related peptides in natural blooms by liquid chromatography-electrospray-high resolution mass spectrometry and matrix-assisted laser desorption/ionization time-of-flight/time-of-flight mass spectrometry using both positive and negative ionization modes. J. Chromatogr. A. 1407, 76-89.

Fotiou, T., Triantis, T.M., Kaloudis, T., O'Shea, K.E., Dionysiou, D.D., Hiskia, A., 2016. Assessment of the roles of reactive oxygen species in the UV and visible light photocatalytic degradation of cyanotoxins and water taste and odor compounds using C-TiO_2. Water Res. 90, 52-61.

Fotiou, T., Triantis, T.M., Kaloudis, T., Pastrana-Martínez, L.M., Likodimos, V., Falaras, P., Silva, A.M.T., Hiskia, A., 2013. Photocatalytic degradation of microcystin-LR and off-odor compounds in water under UV-A and solar light with a nanostructured

photocatalyst based on reduced graphene oxide-TiO_2 composite. Identification of intermediate products. Ind. Eng. Chem. Res. 52, 13991-14000.

Freitas de Magalhães, V., Moraes Soares, R., Azevedo, S.M.F.O., 2001. Microcystin contamination in fish from the Jacarepaguá Lagoon (Rio de Janeiro, Brazil): ecological implication and human health risk. Toxicon 39, 1077-1085.

Gan, W., Sharma, V.K., Zhang, X., Yang, L., Yang, X., 2015. Investigation of disinfection byproducts formation in ferrate(VI) pre-oxidation of NOM and its model comounds followed by chlorination. J. Hazard. Mater. 292, 197-204.

Ganiyu, S.O., Van Hullebusch, E.D., Cretin, M., Esposito, G., Oturan, M.A., 2015. Coupling of membrane filtration and advanced oxidation processes for removal of pharmaceutical residues: A critical review. Sep. Purif. Technol. 156, 891-914.

Ger, K.A., Hansson, L.A., Lürling, M., 2014. Understanding cyanobacteria-zooplankton interactions in a more eutrophic world. Freshw. Biol. 59, 1783-1798.

Gkelis, S., Zaoutsos, N., 2014. Cyanotoxin occurrence and potentially toxin producing cyanobacteria in freshwaters of Greece: A multi-disciplinary approach. Toxicon 78, 1-9.

Goldberg, J., Huang, H., Kwon, Y., Greengard, P., Nairn, A.C., Kuriyan, J., 1995. Three-dimensional structure of the catalytic subunit of protein serine/threonine phosphatase-1. Nature 376, 745-753.

González-Pleiter, M., Gonzalo, S., Rodea-Palomares, I., Leganés, F., Rosal, R., Boltes, K., Marco, E., Fernández-Piñas, F., 2013. Toxicity of five antibiotics and their mixtures towards photosynthetic aquatic organisms: Implications for environmental risk assessment. Water Res. 47, 2050-2064.

Gothwal, R., Shashidhar, T., 2015. Antibiotic pollution in the environment: A review. CLEAN - Soil, Air, Water 43, 479-489.

Guo, C., Gao, S., Lv, J., Hou, S., Zhang, Y., Xu, J., 2017. Assessing the photocatalytic transformation of norfloxacin by BiOBr/iron oxides hybrid photocatalyst: Kinetics, intermediates, and influencing factors. Appl. Catal. B Environ. 205, 68-77.

Guo, H., Gao, N., Yang, Y., Zhang, Y., 2016. Kinetics and transformation pathways on oxidation of fluoroquinolones with thermally activated persulfate. Chem. Eng. J. 292, 82-91.

Gurbuz, F., Uzunmehmetoglu, O.Y., Diler, Ö., Metcalf, J.S., Codd, G.A., 2016. Occurrence of microcystins in water, bloom, sediment and fish from a public water supply. Sci. Total Environ. 562, 860-868.

Haddad, T., Baginska, E., Kümmerer, K., 2015. Transformation products of antibiotic and cytostatic drugs in the aquatic cycle that result from effluent treatment and abiotic/biotic reactions in the environment: An increasing challenge calling for higher emphasis on measures at the beginning of the pipe. Water Res. 72, 75-126.

Hamad, B., 2010. The antibiotics market. Nat. Rev. Drug Discov. 9, 675-676.

Harke, M.J., Steffen, M.M., Gobler, C.J., Otten, T.G., Wilhelm, S.W., Wood, S.A., Paerl, H.W., 2016. A review of the global ecology, genomics, and biogeography of the toxic cyanobacterium, *Microcystis spp.* Harmful Algae 54, 4-20.

He, J., Li, G., Chen, J., Lin, J., Zeng, C., Chen, J., Deng, J., Xie, P., 2016. Prolonged exposure to low-dose microcystin induces nonalcoholic steatohepatitis in mice: a systems toxicology study. Arch. Toxicol. 91, 1-16.

He, X., de la Cruz, A.A., Hiskia, A., Kaloudis, T., O'Shea, K., Dionysiou, D.D., 2015. Destruction of microcystins (cyanotoxins) by UV-254 nm-based direct photolysis and advanced oxidation processes (AOPs): Influence of variable amino acids on the degradation kinetics and reaction mechanisms. Water Res. 74, 227-238.

Hernández, J.M., López-Rodas, V., Costas, E., 2009. Microcystins from tap water could be a risk factor for liver and colorectal cancer: A risk intensified by global change. Med. Hypotheses 72, 539-540.

Herrera, N.A., Echeverri, L.F., Ferrao-Filho, A.S., 2015. Effects of phytoplankton extracts containing the toxin microcystin-LR on the survival and reproduction of cladocerans. Toxicon 95, 38-45.

Hilborn, E.D., Carmichael, W.W., Soares, R.M., Yuan, M., Servaites, J.C., Barton, H.A., Azevedo, S.M.F.O., 2007. Serologic evaluation of human microcystin exposure. Environ. Toxicol. 22, 459-463.

Hoff, R., Pizzolato, T.M., Diaz-Cruz, M.S., 2016. Trends in sulfonamides and their by-products analysis in environmental samples using mass spectrometry techniques. Trends Environ. Anal. Chem. 9, 24-36.

Homem,V., Santos, L., 2011. Degradation and removal methods of antibiotics from aqueous matrices – A review. J. Environ. Manage. 92, 2304-2347.

Hu, W., Zhang, Y., Huang, B., Teng, Y., 2017. Soil environmental quality in greenhouse vegetable production systems in eastern China: Current status and management strategies. Chemosphere 170, 183-195.

Hu, Y., Chen, J., Fan, H., Xie, P., He, J., 2016. A review of neurotoxicity of microcystins. Environ. Sci. Pollut. Res. 23, 7211-7219.

Huang, T.L., Zhao, J.W., Chai, B.B., 2008. Mechanism studies on chlorine and potassium permanganate degradation of microcystin-LR in water using high-performance liquid chromatography tandem mass spectrometry. Water Sci. Technol. 58, 1079-1084.

Hudder, A., Song, W., O'Shea, K.E., Walsh, P.J., 2007. Toxicogenomic evaluation of microcystin-LR treated with ultrasonic irradiation. Toxicol. Appl. Pharmacol. 220, 357-364.

Ibelings, B.W., Bruning, K., De Jonge, J., Wolfstein, K., Dionisio Pires, L.M., Postma, J., Burger, T., 2005. Distribution of microcystins in a lake foodweb: No evidence for biomagnification. Microb. Ecol. 49, 487-500.

Janecko, N., Pokludova, L., Blahova, J., Svobodova, Z., Literak, I., 2016. Implications of fluoroquinolone contamination for the aquatic environment—A review. Environ. Toxicol. Chem. 35, 2647-2656.

Jiang, C., Ji, Y., Shi, Y., Chen, J., Cai, T., 2016. Sulfate radical-based oxidation of fluoroquinolone antibiotics: Kinetics, mechanisms and effects of natural water matrices. Water Res. 106, 507-517.

Jiang, J.Q., 2014. Advances in the development and application of ferrate(VI) for water and wastewater treatment. J. Chem. Technol. Biotechnol. 89, 165-177.

Jiang, J.Q., Zhou, Z., Sharma, V.K., 2013. Occurrence, transportation, monitoring and treatment of emerging micro-pollutants in waste water — A review from global views. Microchem. J. 110, 292-300.

Jiang, W., Chen, L., Batchu, S.R., Gardinali, P.R., Jasa, L., Marsalek, B., Zboril, R., Dionysiou, D.D., O'Shea, K.E., Sharma, V.K., 2014. Oxidation of microcystin-LR by ferrate(VI): Kinetics, degradation pathways, and toxicity assessment. Environ. Sci. Technol. 48, 12164-12172.

Johnson, M.D., Hornstein, B.J., 2003. The kinetics and mechanism of the ferrate(VI) oxidation of hydroxylamines. Inorg. Chem. 42, 6923-6928.

Johnson, M.D., Hornstein, B.J., Wischnewsky, J., 2008. Ferrate(VI) oxidation of nitrogenous compounds. ACS Symp. Ser. 985(Ferrates), 177-188.

Jojoa-Sierra, S.D., Silva-Agredo, J., Herrera-Calderon, E., Torres-Palma, R.A., 2017. Elimination of the antibiotic norfloxacin in municipal wastewater, urine and seawater by electrochemical oxidation on IrO_2 anodes. Sci. Total Environ. 575, 1228-1238.

Kamachi, T., Kouno, T., Yoshizawa, K., 2005. Participants of multioxidants in the pH dependence of the reactivity of ferrate(VI). J. Org. Chem. 70, 4380-4388.

Karlesa, A., De Vera, G.A.D., Dodd, M.C., Park, J., Espino, M.P.B., Lee, Y., 2014. Ferrate(VI) oxidation of ß-lactam antibiotics: Reaction kinetics, antibacterial activity changes, and transformation products. Environ. Sci. Technol. 48, 10380-10389.

Khetan, S.K., Collins, T.J., 2007. Human pharmaceuticals in the aquatic environment: A challenge to green chemistry. Chem. Rev. 107, 2319-2364.

Kim, C., Panditi, V.R., Gardinali, P.R., Varma, R.S., Kim, H., Sharma, V.K., 2015. Ferrate promoted oxidative cleavage of sulfonamides: kinetics and product formation under acidic conditions. Chem. Eng. J. 279, 307-316.

Kim, H., Hong, Y., Park, J., Sharma, V.K., Cho, S., 2013. Sulfonamides and tetracyclines in livestock wastewater. Chemosphere 91, 888-894.

Kim, H., Hwang, Y.S., Sharma, V.K., 2014. Adsorption of antibiotics and iopromide onto single-walled and multi-walled carbon nanotubes. Chem. Eng. J. 255, 23-27.

Kondo, F., Ikai, Y., Oka, H., Okumura, M., Ishikawa, N., Harada, K., Matsuuja, K., Murata, H., Suzuki, M., 1992. Formation, characterization, and toxicity of the glutathione and cysteine conjugates of toxic heptapeptide microcystins. Chem. Res. Toxicol. 5, 591-596.

Kopelev, N.S., 1997. Mossbauer effect studies of alkali metal ferrates(IV), (V) and (VI). In: VÃ©rtes, A., Homonnay, Z. (Eds.). Mossbauer Spectroscopy of Sophisticated Oxides. Academy Sci., Budapest, pp. 305-330.

Kralchevska, R.P., Sharma, V.K., Machala, L., Zboril, R., 2016. Ferrates (Fe^{VI}, Fe^{V}, and Fe^{IV}) oxidation of iodide: Formation of triiodide. Chemosphere 144, 1156-1161.

Kull, T.P.J., Backlund, P.H., Karlsson, K.M., Meriluoto, J.A.O., 2004. Oxidation of the cyanobacterial heptotoxin microcystin-LR by chlorine dioxide: Reaction kinetics, characterization, and toxicity of reaction products. Environ. Sci. Technol. 38, 6025-6031.

Lance, E., Brient, L., Carpentier, A., Acou, A., Marion, L., Bormans, M., Gérard, C., 2010. Impact of toxic cyanobacteria on gastropods and microcystin accumulation in a

eutrophic lake (Grand-Lieu, France) with special reference to *Physa* (= *Physella*) *acuta*. Sci. Total Environ. 408, 3560-3568.

Lee, J., Walker, H.W., 2008. Mechanisms and factors influencing the removal of microcystin-LR by ultrafiltration membranes. J. Membr. Sci. 320, 240-247.

Lee, Y., Cho, M., Kim, J.Y., Yoon, J., 2004. Chemistry of ferrate (Fe(VI)) in aqueous solution and its applications as a green chemical. J. Ind. Eng. Chem. 10, 161-171.

Lee, Y., von Gunten, U., 2012. Quantitative structure-activity relationships (QSARs) for the transformation of organic micropollutants during oxidative water treatment. Water Res. 46, 6177-6195.

Lee, Y., Yoon, J., von Gunten, U., 2005. Kinetics of the oxidation of phenols and phenolic endocrine disruptors during water treatment with ferrate (Fe(VI)). Environ. Sci. Technol. 39, 8978-8984.

Lee, Y., Zimmermann, S.G., Kieu, A.T., von Gunten, U., 2009. Ferrate (Fe(VI)) application for municipal wastewater treatment: A novel process for simultaneous micropollutant oxidation and phosphate removal. Environ. Sci. Technol. 43, 3831-3838.

Lewis, K., 2013. Platforms for antibiotic discovery. Nat. Rev. Drug Discov. 12, 371-387.

Li, W.C., 2014. Occurrence, sources, and fate of pharmaceuticals in aquatic environment and soil. Environ. Pollut. 187, 193-201.

Liao, W., Murugananthan, M., Zhang, Y., 2014. Electrochemical degradation and mechanistic analysis of microcystin-LR at boron-doped diamond electrode. Chem. Eng. J. 243, 117-126.

Lin, H., Liu, W., Zeng, H., Pu, C., Zhang, R., Qiu, Z., Chen, J.-., Wang, L., Tan, Y., Zheng, C., Yang, X., Tian, Y., Huang, Y., Luo, J., Luo, Y., Feng, X., Xiao, G., Feng, L., Li, H., Wang, F., Yuan, C., Wang, J., Zhou, Z., Wei, T., Zuo, Y., Wu, L., He, L., Guo, Y., Shu, W., 2016. Determination of environmental exposure to microcystin and aflatoxin as a risk for renal function based on 5493 rural people in Southwest China. Environ. Sci. Technol. 50, 5346-5356.

Liu, C., Chen, W., Sheng, Y., Li, L., 2009. Influence of pH on microcystins oxidation by chlorine. J. Xi'an University Arch. Technol. 41, 424-428.

Liu, I., Lawton, L.A., Robertson, P.K.J., 2003. Mechanistic studies of the photocatalytic oxidation of microcystin-LR: An investigation of byproducts of the decomposition process. Environ. Sci. Technol. 37, 3214-3219.

Liyanage, H.M., Arachchi, D.N.M., Abeysekara, T., Guneratne, L., 2016. Toxicology of freshwater cyanobacteria. J. Environ. Sci. Health Part C 34, 137-168.

Luo, Y.L., Guo, W.S., Ngo, H.H., Nghiem, L.D., Hai, F.I., Zhang, J., Liang, S., Wang, X.C., 2014. A review on the occurrence of micropollutants in the aquatic environment and their fate and removal during wastewater treatment. Sci. Total Environ. 473-474, 619-641.

Luo, Z., Strouse, M., Jiang, J.Q., Sharma, V.K., 2011. Methodologies for the analytical determination of ferrate(VI): A review. J. Environ. Sci. Health A 46, 453-460.

Machalová Šišková, K., Jancula, D., Drahoš, B., Machala, L., Babica, P., Alonso, P.G., Trávnícek, Z., Tucek, J., Maršálek, B., Sharma, V.K., Zboril, R., 2016. High-valent iron

(Fe^{VI}, Fe^{V}, and Fe^{IV}) species in water: Characterization and oxidative transformation of estrogenic hormones. Phys. Chem. Chem. Phys. 18, 18802-18810.

Maia, A.S., Ribeiro, A.R., Amorim, C.L., Barreiro, J.C., Cass, Q.B., Castro, P.M.L., Tiritan, M.E., 2014. Degradation of fluoroquinolone antibiotics and identification of metabolites/transformation products by liquid chromatography-tandem mass spectrometry. J. Chromatogr. A. 1333, 87-98.

Martinez, J.L., 2009. Environmental pollution by antibiotics and by antibiotic resistance determinants. Environ. Pollut. 157, 2893-2902.

Máthé, C., Beyer, D., M-Hamvas, M., Vasas, G., 2016. The effects of microcystins (Cyanobacterial heptapeptides) on the eukaryotic cytoskeletal system. Mini-Rev. Med. Chem. 16, 1063-1077.

McDonald, A.R., Que, L., 2013. High-valent nonheme iron-oxo complexes: Synthesis, structure, and spectroscopy. Coord. Chem. Rev. 257, 414-428.

Meneely, J.P., Elliott, C.T., 2013. Microcystins: Measuring human exposure and the impact on human health. Biomarkers 18, 639-649.

Meng, X.Z., Venkatesan, A.K., Ni, Y.L., Steele, J.C., Wu, L.L., Bignert, A., Bergman, A., Halden, R.U., 2016. Organic contaminants in Chinese sewage sludge: A meta-analysis of the literature of the past 30 years. Environ. Sci. Technol. 50, 5454-5466.

Menton, J.D., Bielski, B.H.J., 1990. Studies of the kinetics, spectral and chemical properties of Fe(IV) pyrophosphate by pulse radiolysis. Radiat. Phys. Chem. 36, 725-733.

Merel, S., Walker, D., Chicana, R., Snyder, S., Baurès, E., Thomas, O., 2013. State of knowledge and concerns on cyanobacterial blooms and cyanotoxins. Environ. Int. 59, 303-327.

Miao, H.F., Qin, F., Tao, G.J., Tao, W.Y., Ruan, W.Q., 2010. Detoxification and degradation of microcystin-LR and -RR by ozonation. Chemosphere 79, 355-361.

Mills, M.R., Weitz, A.C., Hendrich, M.P., Ryabov, A.D., Collins, T.J., 2016. NaClO-generated iron(IV)oxo ad iron(V)oxo TAML in pure water. J. Am. Chem. Soc. 138, 13866-13869.

Moreira, F.C., Soler, J., Alpendurada, M.F., Boaventura, R.A.R., Brillas, E., Vilar, V.J.P., 2016. Tertiary treatment of a municipal wastewater toward pharmaceuticals removal by chemical and electrochemical advanced oxidation processes. Water Res. 105, 251-263.

Nam, W., Lee, Y.M., Fukuzumi, S., 2014. Tuning reactivity and mechanism in oxidation reactions by mononuclear nonheme iron(IV)-oxo complexes. Acc. Chem. Res. 47, 1146-1154.

Nishiwaki-Matsushima, R., Nishiwaki, S., Ohta, T., Yoshizawa, S., Suganuma, M., Harada, K.I., Watanabe, M.F., Fujiki, H., 1991. Structure-function relationships of microcystins, liver tumor promoters, in interaction with protein phosphatase. Jpn. J. Cancer Res. 82, 993-996.

Noorhasan, N., Patel, B., Sharma, V.K., 2010. Ferrate(VI) oxidation of glycine and glycylglycine: Kinetics and products. Water Res. 44, 927-937.

Noorhasan, N.N., Sharma, V.K., Cabelli, D., 2008. Reactivity of ferrate(V) ($Fe^{V}O_4^{3-}$) with aminopolycarboxylates in alkaline medium: A premix pulse radiolysis. Inorg. Chim. Acta. 361, 1041-1046.

Osinska, A., Korzeniewska, E., Harnisz, M., Niestepski, S., 2017. The prevalence and characterization of antibiotic-resistant and virulent *Escherichia coli* strains in the municipal wastewater system and their environmental fate. Sci. Total Environ. 577, 367-375.

Oturan, M.A., Aaron, J.J., 2014. Advanced oxidation processes in water/wastewater treatment: Principles and applications. A review. Crit. Rev. Environ. Sci. Technol. 44, 2577-2641.

Pavagadhi, S., Tang, A.L.L., Sathishkumar, M., Loh, K.P., Balasubramanian, R., 2013. Removal of microcystin-LR and microcystin-RR by graphene oxide: Adsorption and kinetic experiments. Water Res. 47, 4621-4629.

Peixoto, P.S., Tóth, I.V., Segundo, M.A., Lima, J.L.F.C., 2016. Fluoroquinolones and sulfonamides: features of their determination in water. A review. Int. J. Environ. Anal. Chem. 96, 185-202.

Pérez, T., Sirés, I., Brillas, E., Nava, J.L., 2017. Solar photoelectro-Fenton flow plant modeling for the degradation of the antibiotic erythromycin in sulfate medium. Electrochim. Acta. 228, 45-56.

Pick, F.R., 2016. Blooming algae: a Canadian perspective on the rise of toxic cyanobacteria. Can. J. Fish. Aquatic Sci. 73, 1149-1158.

Polesel, F., Andersen, H.R., Trapp, S., Plósz, B.G., 2016. Removal of antibiotics in biological wastewater treatment systems - A critical assessment using the activated sludge modeling framework for xenobiotics (ASM-X). Environ. Sci. Technol. 50, 10316-10334.

Postigo, C., Richardson, S.D., 2014. Transformation of pharmaceuticals during oxidation/disinfection processes in drinking water treatment. J. Hazard. Mater. 279, 461-475.

Pouria, S., De Andrade, A., Barbosa, J., Cavalcanti, R.L., Barreto, V.T.S., Ward, C.J., Preiser, W., Poon, G.K., Neild, G.H., Codd, G.A., 1998. Fatal microcystin intoxication in haemodialysis unit in Caruaru, Brazil. Lancet. 352, 21-26.

Proia, L., Von Schiller, D., Sànchez-Melsió, A., Sabater, S., Borrego, C.M., Rodríguez-Mozaz, S., Balcázar, J.L., 2016. Occurrence and persistence of antibiotic resistance genes in river biofilms after wastewater inputs in small rivers. Environ. Pollut. 210, 121-128.

Prucek, R., Tucek, J., Kolarik, J., Huskova, I., Filip, J., Varma, R.S., Sharma, V.K., Zboril, R., 2015. Ferrate(VI)-prompted removal of metals in aqueous media: mechanistic delineation of enhanced efficiency via metal entrenchment in magnetic oxides. Environ. Sci. Technol. 49, 2319-2327.

Qi, Y., Bortoli, S., Volmer, D.A., 2014. Detailed study of cyanobacterial microcystins using high performance tandem mass spectrometry. J. Am. Soc. Mass Spectrom. 25, 1253-1262.

Qin, X., Liu, F., Wang, G., Weng, L., Li, L., 2014. Adsorption of levofloxacin onto goethite: Effects of pH, calcium and phosphate. Colloids Surf. B Biointerfaces 116, 591-596.

Rajasekhar, P., Fan, L., Nguyen, T., Roddick, F.A., 2012. A review of the use of sonication to control cyanobacterial blooms. Water Res. 46, 4319-4329.

Rastogi, R.P., Sinha, R.P., Incharoensakdi, A., 2014. The cyanotoxin-microcystins: Current overview. Rev. Environ. Sci. Biotechnol. 13, 215-249.

Ray, K., Heims, F., Schwalbe, M., Nam, W., 2015. High-valent metal-oxo intermediates in energy demanding processes: From dioxygen reduction to water splitting. Curr. Opin. Chem. Biol. 25, 159-171.

Rodríguez, E., Majado, M.E., Meriluoto, J., Acero, J.L., 2007. Oxidation of microcystins by permanganate: Reaction kinetics and implications for water treatment. Water Res. 41, 102-110.

Romero-Oliva, C.S., Contardo-Jara, V., Pflugmacher, S., 2015. Time dependent uptake, bioaccumulation and biotransformation of cell free crude extract microcystins from Lake Amatitlán, Guatemala by *Ceratophyllum demersum*, *Egeria densa* and *Hydrilla verticillata*. Toxicon. 105, 62-73.

Ruhi, A., Acuna, V., Barcelo, D., Huerta, B., Mor, J.R., Rodriguez-Mozaz, S., Sabater, S., 2016. Bioaccumulation and trophic magnification of pharmaceuticals and endorine disruptors in a Mediterranean river food web. Sci. Total Environ. 540, 250-259.

Rush, J.D., Bielski, B.H.J., 1986. Pulse radiolysis studies of alkaline Fe(III) and Fe(VI) solutions. Observation of transient iron complexes with intermediate oxidation states. J. Am. Chem. Soc. 108, 523-525.

Rush, J.D., Bielski, B.H.J., 1989. Kinetics of ferrate(V) decay in aqueous solution. A pulse-radiolysis study. Inorg. Chem. 28, 3947-3951.

Rush, J.D., Bielski, B.H.J., 1994. Decay of ferrate(V) in neutral and acidic solutions. A premix pulse radiolysis study. Inorg. Chem. 33, 5499-5502.

Rutgersson, C., Fick, J., Marathe, N., Kristiansson, E., Janzon, A., Angelin, M., Johansson, A., Shouche, Y., Flach, C.F., Larsson, D.G.J., 2014. Fluoroquinolones and *qnr* genes in sediment, water, soil, and human fecal flora in an environment polluted by manufacturing discharges. Environ. Sci. Technol. 48, 7825-7832.

Sandrini, G., Ji, X., Verspagen, J.M.H., Tann, R.P., Slot, P.C., Luimstra, V.M., Schuurmans, J.M., Matthijs, H.C.P., Huisman, J., 2016. Rapid adaptation of harmful cyanobacteria to rising CO_2. Proc. Natl. Acad. Sci. U.S.A. 113, 9315-9320.

Santoke, H., Song, W., Cooper, W.J., Greaves, J., Miller, G.E., 2009. Free-radical-induced oxidative and reductive degradation of fluoroquinolone pharmaceuticals: Kinetic studies and degradation mechanism. J. Phys. Chem. A 113, 7846-7851.

Scepaniak, J.J., Vogel, C.S., Khusniyarov, M.M., Heinemann, F.W., Meyer, K., Smith, J.M., 2011. Synthesis, structure, and reactivity of an iron(V) nitride. Science 331, 1049-1052.

Schmidt, J.R., Shaskus, M., Estenik, J.F., Oesch, C., Khidekel, R., Boyer, G.L., 2013. Variations in the microcystin content of different fish species collected from a Eutrophic Lake. Toxins 5, 992-1009.

Schmidt, J.R., Wilhelm, S.W., Boyer, G.L., 2014. The fate of microcystins in the environment and challenges for monitoring. Toxins 6, 3354-3387.

Šetlíková, I., Wiegand, C., 2009. Hepatic and branchial glutathione S-transferases of two fish species: Substrate specificity and biotransformation of microcystin-LR. Comp. Biochem. Physiol. C. 149, 515-523.

Sharma, V.K., 2002a. Ferrate(V) oxidation of pollutants: A premix pulse radiolysis. Radiat. Phys. Chem. 65, 349-355.

Sharma, V.K., 2002b. Potassium ferrate(VI): Environmental friendly oxidant. Adv. Environ. Res. 6, 143-156.

Sharma, V.K., 2007. Disinfection performance of Fe(VI) in water and wastewater: a review. Water Sci. Technol. 55, 225-232.

Sharma, V.K., 2010. Oxidation of inorganic compounds by ferrate (VI) and ferrate(V): one-electron and two-electron transfer steps. Environ. Sci. Technol. 44, 5148-5152.

Sharma, V.K., 2011. Oxidation of inorganic contaminants by ferrates (VI, V, and IV)-Kinetics and mechanisms: A review. J. Environ. Manage. 92, 1051-1073.

Sharma, V.K., 2013. Ferrate(VI) and ferrate(V) oxidation of organic compounds: Kinetics and mechanism. Coord. Chem. Rev. 257, 495-510.

Sharma, V.K., Anquandah, G., Kim, H., Jiang, J.Q., Zboril, R., 2013. Ferrate(VI): A green chemistry oxidant for removal of antibiotics in water. ACS Symposium Series 1123, 31-44.

Sharma, V.K., Chen, L., Marsalek, B., Zboril, R., O'Shea, K.E., and Dionysiou, D.D., 2017. Iron based sustainable greener technologies to treat cyanobacteria and microcystin-LR in water. Water Sci. Technol. Water Suppl. 17, 107-114.

Sharma, V.K., Chen, L., Zboril, R., 2016a. A review on high valent Fe^{VI} (ferrate): A sustainable green oxidant in organc chemistry and transformation of pharmaceuticals. ACS Sustainable Chem. Eng. 4, 18-34.

Sharma, V.K., Graham, N.J.D., Li, X.Z., Yuan, B.L., 2010. Ferrate(VI) enhanced photocatalytic oxidation of pollutants in aqueous TiO_2 suspensions. Environ. Sci. Pollut. Res. 17, 453-461.

Sharma, V.K., Johnson, N., Cizmas, L., McDonald, T.J., Kim, H., 2016b. A review of the influence of treatment strategies on antibiotic resistant bacteria and antibiotic resistance genes. Chemosphere 150, 702-714.

Sharma, V.K., Li, X.Z., Graham, N., Doong, R.A., 2008. Ferrate(VI) oxidation of endocrine disruptors and antimicrobials in water. J. Water Supply: Res. Technol. - AQUA. 57, 419-426.

Sharma, V.K., McDonald, T.J., Kim, H., Garg, V.K., 2015. Magnetic graphene-carbon nanotube iron nanocomposites as adsorbents and antibacterial agents for water purification. Adv. Colloid Interface Sci. 225, 229-240.

Sharma, V.K., Mishra, S.K., Nesnas, N., 2006a. Oxidation of sulfonamide antimicrobials by ferrate(VI) [$Fe^{VI}O_4^{2-}$]. Environ. Sci. Technol. 40, 7222-7227.

Sharma, V.K., Mishra, S.K., Ray, A.K., 2006b. Kinetic assessment of the potassium ferrate(VI) oxidation of antibacterial drug sulfamethoxazole. Chemosphere 62, 128-134.

Sharma, V.K., Triantis, T.M., Antoniou, M.G., He, X., Pelaez, M., Han, C., Song, W., O'Shea, K.E., De La Cruz, A.A., Kaloudis, T., Hiskia, A., Dionysiou, D.D., 2012. Destruction of microcystins by conventional and advanced oxidation processes: A review. Sep. Purif. Technol. 91, 3-17.

Sharma, V.K., Yngard, R.A., Cabelli, D.E., Clayton Baum, J., 2008. Ferrate(VI) and ferrate(V) oxidation of cyanide, thiocyanate, and copper(I) cyanide. Radiat. Phys. Chem. 77, 761-767.

Sharma, V.K., Zboril, R., 2015. Ferryl and ferrate species: Mössbauer spectroscopy investigation. Croat. Chem. Acta. 88, 363-368.

Sharma, V.K., Zboril, R., Varma, R.S., 2015. Ferrates: Greener oxidants with multimodal action in water treatment technologies. Acc. Chem. Res. 48, 182-191.

Song, W., Bardowell, S., O'Shea, K.E., 2007. Mechanistic study and the influence of oxygen on the photosensitized transformations of microcystins (cyanotoxins). Environ. Sci. Technol. 41, 5336-5341.

Song, W., De La Cruz, A.A., Rein, K., O'Shea, K.E., 2006. Ultrasonically induced degradation of microcystin-LR and -RR: Identification of products, effect of pH, formation and destruction of peroxides. Environ. Sci. Technol. 40, 3941-3946.

Song, W., Teshiba, T., Rein, K., O'Shea, K.E., 2005. Ultrasonically induced degradation and detoxification of microcystin-LR (cyanobacterial toxin). Environ. Sci. Technol. 39, 6300-6305.

Song, W., Xu, T., Cooper, W.J., Dionysiou, D.D., De La Cruz, A.A., O'Shea, K.E., 2009. Radiolysis studies on the destruction of microcystin-LR in aqueous solution by hydroxyl radicals. Environ. Sci. Technol. 43, 1487-1492.

Su, Y., Deng, Y., Du, Y., 2013. Alternative pathways for photocatalytic degradation of microcystin-LR revealed by TiO_2 nanotubes. J. Mol. Catal. A Chem. 373, 18-24.

Sukul, P., Spiteller, M., 2007. Fluoroquinolone antibiotics in the environment. Rev. Environ. Contam. Toxicol. 191, 131-162.

Sun, F., Pei, H.Y., Hu, W.R., Ma, C.X., 2012. The lysis of *Microcystis aeruginosa* in $AlCl_3$ coagulation and sedimentation processes. Chem. Eng. J. 193-194, 196-202.

Svircev, Z., Lujic, J., Marinovic, Z., Drobac, D., Tokodi, N., Stojiljkovic, B., Meriluoto, J., 2015. Toxicopathology induced by microcystins and nodularin: A histopathological review. J. Environ. Sci. Health Part C 33, 125-167.

Svrcek, C., Smith, D.W., 2004. Cyanobacteria toxins and the current state of knowledge on water treatment options: A review. J. Environ. Eng. Sci. 3, 155-185.

Szigeti, Z.M., Jámbrik, K., Roszik, J., M-Hamvas, M., Tándor, I., Beyer, D., Vasas, G., Vereb, G., Surányi, G., Máthé, C., 2010. Cytoskeletal and developmental alterations in *Ceratophyllum demersum* induced by microcystin-LR, a cyanobacterial toxin. Aquat. Bot. 92, 179-184.

Takenaka, S., 2001. Covalent glutathione conjugation to cyanobacterial hepatotoxin microcystin LR by F344 rat cytosolic and microsomal glutathione *S*-transferases. Environ. Toxicol. Pharmacol. 9, 135-139.

Teixeira, M.R., Rosa, M.J., 2005. Microcystins removal by nanofiltration membranes. Sep. Purif. Technol. 46, 192-201.

Tian, D., Zheng, W., Wei, X., Sun, X., Liu, L., Chen, X., Zhang, H., Zhou, Y., Chen, H., Zhang, H., Wang, X., Zhang, R., Jiang, S., Zheng, Y., Yang, G., Qu, W., 2013. Dissolved microcystins in surface and ground waters in regions with high cancer incidence in the Huai River Basin of China. Chemosphere 91, 1064-1071.

Tran, N.H., Chen, H., Reinhard, M., Mao, F., Gin, K.Y.H., 2016. Occurrence and removal of multiple classes of antibiotics and antimicrobial agents in biological wastewater treatment processes. Water Res. 104, 461-472.

Valério, E., Chaves, S., Tenreiro, R., 2010. Diversity and impact of prokaryotic toxins on aquatic environments: A review. Toxins. 2, 2359-2410.

Van Doorslaer, X., Dewulf, J., Van Langenhove, H., Demeestere, K., 2014. Fluoroquinolone antibiotics: An emerging class of environmental micropollutants. Sci. Total Environ. 500-501, 250-269.

Verlicchi, P., Al Aukidy, M., Zambello, E., 2015. What have we learned from worldwide experiences on the management and treatment of hospital effluent? - An overview and a discussion on perspectives. Sci. Total Environ. 514, 467-491.

Wang, H., Wang, N., Wang, B., Fang, H., Fu, C., Tang, C., Jiang, F., Zhou, Y., He, G., Zhao, Q., Chen, Y., Jiang, Q., 2016. Antibiotics detected in urines and adipogenesis in school children. Environ. Int. 89-90, 204-211.

Wang, P., He, Y.L., Huang, C.H., 2010. Oxidation of fluoroquinolone antibiotics and structurally related amines by chlorine dioxide: Reaction kinetics, product and pathway evaluation. Water Res. 44, 5989-5998.

Weirich, C.A., Miller, T.R., 2014. Freshwater harmful algal blooms: Toxins and children's health. Curr. Probl. Pediatr. Adolesc. Health Care 44, 2-24.

Wert, E.C., Korak, J.A., Trenholm, R.A., Rosario-Ortiz, F.L., 2014. Effect of oxidant exposure on the release of intracellular microcystin, MIB, and geosmin from three cyanobacteria species. Water Res. 52, 251-259.

Wood, R., 2016. Acute animal and human poisonings from cyanotoxin exposure - A review of the literature. Environ. Int. 91, 276-282.

Wood, R.H., 1958. The heat, free energy, and entropy of the ferrate ion. J. Am. Chem. Soc. 80, 2038-2041.

Woolbright, B.L., Williams, C.D., Ni, H., Kumer, S.C., Schmitt, T., Kane, B., Jaeschke, H., 2017. Microcystin-LR induced liver injury in mice and in primary human hepatocytes is caused by oncotic necrosis. Toxicon 125, 99-109.

World Health Organization, 1997. Report of the working group on chemical substances in drinking water, Geneva, 22–26 April 1997. Section 5-2 Microcystin-LR.

World Health Organization, 2014. Antimicrobial resistance-global report on surveillance. WHO/HSE/PED/AIP/2014.2, http://www.who.int/drugresistance/en/.

Wu, M.H., Que, C.J., Xu, G., Sun, Y.F., Ma, J., Xu, H., Sun, R., Tang, L., 2016. Occurrence, fate and interrelation of selected antibiotics in sewage treatment plants and their receiving surface water. Ecotoxicol. Environ. Saf. 132, 132-139.

Yan, J., Lei, M., Zhu, L., Anjum, M.N., Zou, J., Tang, H., 2011. Degradation of sulfamonomethoxine with Fe_3O_4 magnetic nanoparticles as heterogeneous activator of persulfate. J. Hazard. Mater. 186, 1398-1404.

Yang, B., Kookana, R.S., Williams, M., Ying, G.G., Du, J., Doan, H., Kumar, A., 2016. Oxidation of ciprofloxacin and enrofloxacin by ferrate(VI): Products identification, and toxicity evaluation. J. Hazard. Mater. 320, 296-303.

Yang, B., Ying, G.G., Chen, Z.F., Zhao, J.L., Peng, F.Q., Chen, X.W., 2014. Ferrate(VI) oxidation of tetrabromobisphenol A in comparison with bisphenol A. Water Res. 62, 211-219.

Yang, B., Ying, G.G., Zhao, J.L., Liu, S., Zhou, L.J., Chen, F., 2012. Removal of selected endocrine disrupting chemicals (EDCs) and pharmaceuticals and personal care products (PPCPs) during ferrate(VI) treatment of secondary wastewater effluents. Water Res. 46, 2194-2204.

Yang, X., Gan, W., Zhang, X., Huang, H., Sharma, V.K., 2015. Effect of pH on the formation of disinfection byproducts in ferrate(VI) pre-oxidation and subsequent chlorination. Sep. Purif. Technol. 156, 980-986.

Yates, B.J., Darlington, R., Sharma, V.K., 2014. High-valent iron based oxidants to treat perfluorooctanesulfonate and perfluorooctanoic acid in water. Environ. Chem. Lett. 12, 413-417.

Yu, F., Li, Y., Han, S., Ma, J., 2016. Adsorptive removal of antibiotics from aqueous solution using carbon materials. Chemosphere 153, 365-385.

Zanchett, G., Oliveira-Filho, E.C., 2013. Cyanobacteria and cyanotoxins: From impacts on aquatic ecosystems and human health to anticarcinogenic effects. Toxins 5, 1896-1917.

Zhang, Y., Shao, Y., Gao, N., Chu, W., Sun, Z., 2016. Removal of microcystin-LR by free chlorine: Identify of transformation products and disinfection by-products formation. Chem. Eng. J. 287, 189-195.

Zhang, Y., Zhang, Y., Yang, N., Liao, W., Yoshihara, S., 2013. Electrochemical degradation and mechanistic analysis of microcystin-LR. J. Chem. Technol. Biotechnol. 88, 1529-1537.

Zhou, M., Tu, W., Xu, J., 2015. Mechanisms of microcystin-LR-induced cytoskeletal disruption in animal cells. Toxicon 101, 92-100.

Zhou, Z., Jiang, J.Q., 2015a. Reaction kinetics and oxidation products formation in the degradation of ciprofloxacin and ibuprofen by ferrate(VI). Chemosphere 119, S95-S100.

Zhou, Z., Jiang, J.Q., 2015b. Treatment of selected pharmaceuticals by ferrate(VI): Performance, kinetic studies and identification of oxidation products. J. Pharm. Biomed. Anal. 106, 37-45.

Zong, W., Sun, F., Pei, H., Hu, W., Pei, R., 2015. Microcystin-associated disinfection by-products: The real and non-negligible risk to drinking water subject to chlorination. Chem. Eng. J. 279, 498-506.

Zong, W., Sun, F., Sun, X., 2013. Oxidation by-products formation of microcystin-LR exposed to UV/H_2O_2: Toward the generative mechanism and biological toxicity. Water Res. 47, 3211-3219.